

AD-A074 152

AERONAUTICAL RESEARCH LABS MELBOURNE (AUSTRALIA)

F/G 20/4

EVALUATION OF WALL INTERFERENCE EFFECTS IN A TWO-DIMENSIONAL TR--ETC(U)

FEB 79 B D FAIRLIE, N POLLOCK

UNCLASSIFIED

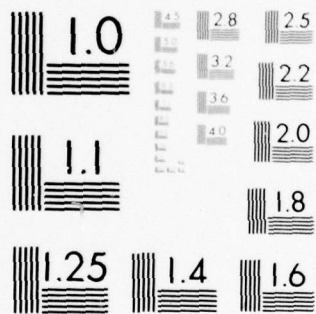
ARL/AERO-151

NL

| OF |  
AD  
A074152



END  
DATE  
FILMED  
10-79  
DDC



MICROCOPY RESOLUTION TEST CHART  
NATIONAL BUREAU OF STANDARDS-1963-A

**12 LEVEL II**



AD A 074152

**DEPARTMENT OF DEFENCE  
DEFENCE SCIENCE AND TECHNOLOGY ORGANISATION  
AERONAUTICAL RESEARCH LABORATORIES  
MELBOURNE, VICTORIA**

AERODYNAMICS REPORT 151

**EVALUATION OF WALL INTERFERENCE EFFECTS  
IN A TWO-DIMENSIONAL TRANSONIC WIND TUNNEL  
BY SUBSONIC LINEAR THEORY**

by

B. D. FAIRLIE and N. POLLOCK

**DDC  
RECEIVED  
SEP 25 1979  
B**

**DDC FILE COPY**

Approved for Public Release.



© COMMONWEALTH OF AUSTRALIA 1979

COPY No 11

FEBRUARY 1979

79 09 201 148

11 Feb 79

12 78p.

AR-001-596

DEPARTMENT OF DEFENCE  
DEFENCE SCIENCE AND TECHNOLOGY ORGANISATION  
AERONAUTICAL RESEARCH LABORATORIES

14 ARL/AERO-151

AERODYNAMICS REPORT 151

6 **EVALUATION OF WALL INTERFERENCE EFFECTS  
IN A TWO-DIMENSIONAL TRANSONIC WIND TUNNEL  
BY SUBSONIC LINEAR THEORY**

by  
10 B. D. FAIRLIE — N. POLLOCK

DDC  
RECEIVED  
SEP 25 1979  
B

SUMMARY

Results of transonic wind tunnel tests on two-dimensional aerofoils are analysed with respect to the effects of wind tunnel wall interference. The tests were conducted on two geometrically similar models of each of two aerofoil sections—the NACA 0012 and the BGK-1 sections—and covered a range of Mach numbers from 0.5 to 0.82 with model chord to tunnel height ratios of 0.125 and 0.25. Results from measurements on all models in both solid- and slotted-wall test sections are corrected for wind tunnel wall interference effects by the application of classical linearized theory. For the solid wall results, these corrections appear to produce data which are very close to being free of the effects of interference. In the case of slotted walls however, linear theory is found to significantly underestimate the magnitude of blockage interference. The introduction of an empirical blockage correction, when combined with the linear theory representation of lift-interference, enables the cross-flow characteristics of the slotted walls to be determined, and leads to a successful correction scheme for the slotted wall results. Extensive comparisons with data from other sources, both experimental and theoretical, provide further verification that the corrected results are indeed closely interference free.

POSTAL ADDRESS: Chief Superintendent, Aeronautical Research Laboratories,  
Box 4331, P.O., Melbourne, Victoria, 3001, Australia.

008 650 Lm

## CONTENTS

	Page No.
<b>LIST OF ILLUSTRATIONS</b>	
<b>NOTATION</b>	
<b>1. INTRODUCTION</b>	1
<b>2. EXPERIMENTAL DETAILS</b>	2
2.1 Section Definition	2
2.2 Model Dimensions	2
2.3 Wind Tunnel	4
2.4 Transition Fixing	4
<b>3. SUBSONIC LINEAR INTERFERENCE THEORY</b>	4
3.1 Introduction	4
3.2 Subsonic Linear Theory	4
3.2.1 Solid Blockage	6
3.2.2 Wake Blockage	7
3.2.3 Lift Interference	8
3.2.4 Blockage Velocity Gradients	8
3.3 Corrections to Measured Quantities	9
3.4 General Remarks	12
<b>4. APPLICATION OF LINEAR THEORY</b>	16
4.1 Solid Wall Results	16
4.2 Slotted Wall Results	22
<b>5. COMPARISONS WITH OTHER DATA</b>	40
5.1 Comparisons with Other Measurements	40
5.2 Comparisons with Theory	53
<b>6. DISCUSSION</b>	60
<b>7. CONCLUSIONS</b>	62

### REFERENCES

### DOCUMENT CONTROL DATA

### DISTRIBUTION

ACCESSION for		
NTIS	White Section	<input checked="" type="checkbox"/>
DDC	Buff Section	<input type="checkbox"/>
UNANNOUNCED		<input type="checkbox"/>
JUSTIFICATION _____		
BY _____		
DISTRIBUTION/AVAILABILITY CODES		
Dist. AVAIL. and/or SPECIAL		
<b>A</b>		

## LIST OF ILLUSTRATIONS

- Figure 1. Supercritical lifting aerofoil BGK-1.
2. Details of slotted working section.
  3. Definitions of slot geometries and flow models.
  4. Chen and Mears' slat model.
  5. Variation of lift curve slope with Mach number—BGK-1; corrected solid wall data.
  6. Variation of lift curve slope with Mach number—NACA-0012; corrected solid wall data.
  7. Variation of lift curve slope with Mach number—BGK-1; uncorrected solid wall data.
  8. Variation of lift curve slope with Mach number—NACA-0012; uncorrected solid wall data.
  9. Variation of pressure ratio with Mach number—NACA-0012; corrected solid wall data.
  10. Comparison of BGK-1 design pressure distributions; solid wall data.
  11. Variation of root mean square deviation with  $\beta/P$ —classical linear theory.
  12. Variation of lift curve slope with Mach number—BGK-1; corrected slotted wall data.
  13. Variation of lift curve slope with Mach number—NACA-0012; corrected slotted wall data.
  14. Variation of lift curve slope with Mach number—BGK-1; uncorrected slotted wall data.
  15. Variation of lift curve slope with Mach number—NACA-0012; uncorrected slotted wall data.
  16. Variation of pressure ratio with Mach number—NACA-0012; comparison of slotted wall data with corrected solid wall data.
  17. Variation of Mach number increment with Mach number—NACA-0012; slotted wall data.
  18. Variation of root mean square deviation with  $\beta/P$ —linear theory with empirical blockage.
  19. Variation of lift curve slope with Mach number—BGK-1; slotted wall data with empirical blockage correction.
  20. Variation of lift curve slope with Mach number—NACA-0012; slotted wall data with empirical blockage correction.
  21. Comparison of BGK-1 design pressure distributions; slotted wall data.
  22. Comparison of corrected pressure distributions—NACA-0012;  $M = 0.767$ .
  23. Comparison of corrected and uncorrected lift curves—NACA-0012;  $M = 0.767$ .
  24. Comparison of corrected lift curves—BGK-1.
  25. Comparison of pressure distributions—BGK-1;  $M = 0.705$ .

26. Comparison of pressure distributions—BGK-1;  $M = 0.748$ .
27. Comparison of pressure distributions—BGK-1;  $M = 0.765$ .
28. Uncorrected shock positions—NACA-0012;  $\alpha = 0^\circ$ .
29. Corrected shock positions—NACA-0012;  $\alpha = 0^\circ$ .
30. BGK-1 lift curve slope—comparison with other measurements.
31. Comparison of experimental design pressure distributions—BGK-1.
32. NACA-0012 lift curve slope—comparison with other measurements.
33. NACA-0012 shock position—comparison with other measurements.
34. BGK-1 lift curve slope—comparison with theory.
35. NACA-0012 lift curve slope—comparison with theory.
36. NACA-0012 shock position—comparison with theory.
37. Comparison of experimental and theoretical pressure distributions—BGK-1;  
 $M = 0.760, \alpha = 0.5^\circ$ .
38. Comparison of experimental and theoretical pressure distributions—BGK-1;  
 $M = 0.760, \alpha = 1.5^\circ$ .
39. Comparison of experimental and theoretical pressure distributions—BGK-1;  
 $M = 0.760, \alpha = 0^\circ$ .

## NOTATION

<i>A</i>	Area of aerofoil section in <i>x-z</i> plane
<i>A<sub>e</sub></i>	Effective area of aerofoil section in <i>x-z</i> plane
<i>a</i>	Width of slot (see Fig. 3)
<i>b</i>	Breadth of tunnel
<i>C<sub>DW</sub></i>	Wake drag coefficient = (drag force from wake traverse)/ $\frac{1}{2}\rho U^2 S$
<i>C<sub>D</sub></i>	Drag coefficient = (drag force)/ $\frac{1}{2}\rho U^2 S$
<i>C<sub>L</sub></i>	Lift coefficient = (lift force)/ $\frac{1}{2}\rho U^2 S$
<i>C<sub>N</sub></i>	Normal force coefficient = (normal force)/ $\frac{1}{2}\rho U^2 S$
<i>C<sub>ma</sub></i>	Pitching moment coefficient = (pitching moment about <i>c/4</i> )/ $\frac{1}{2}\rho U^2 S c$
<i>C<sub>p</sub></i>	Pressure coefficient
<i>c</i>	Aerofoil chord
<i>c<sub>1</sub>, c<sub>2</sub></i>	Constants
<i>d</i>	Mean periodic spacing of slots (see Fig. 3)
<i>E</i>	Universal empirical blockage factor
<i>F</i>	Slotted tunnel geometry factor
<i>G</i>	Ratio of corrected to uncorrected kinetic pressures
<i>H</i>	Free stream total pressure
<i>h</i>	Height of tunnel
<i>I<sub>A</sub>, I<sub>C</sub>, I<sub>G</sub>, I<sub>F</sub></i>	Integrals (see Section 3.2)
<i>K<sub>1</sub>, K<sub>2</sub></i>	Constants
<i>L</i>	Aerodynamic loading = $(p_l - p_u)/\frac{1}{2}\rho U^2$
<i>L'</i>	Lift per unit span of aerofoil
<i>l</i>	Thickness of slats
<i>M</i>	Free stream Mach number
<i>m<sub>a</sub></i>	Strength of doublet representing aerofoil displacement
<i>m<sub>s</sub></i>	Strength of source representing aerofoil wake
<i>N</i>	Effective number of full width slots
<i>n</i>	Number of measured values of Mach number
<i>P</i>	Wall porosity parameter
<i>p</i>	Local static pressure
<i>p<sub>0</sub></i>	Free stream static pressure
<i>q</i>	Dummy integration variable
<i>R<sub>e</sub></i>	Reynolds number based on <i>c</i>

$S$	Wing area ( $b \times c$ )
$T$	Free stream temperature
$t$	Aerofoil maximum thickness
$U$	Free stream velocity
$u$	Streamwise velocity induced by tunnel walls
$w$	Vertical velocity induced by tunnel walls
$x$	Streamwise co-ordinate of tunnel, origin at mid chord
$x_L$	Chordwise co-ordinate, origin at leading edge
$y$	Spanwise ordinate, origin at mid span
$z$	Aerofoil thickness co-ordinate; also vertical co-ordinate of tunnel
$\alpha$	Angle of incidence
$\beta$	Prandtl Glauert compressibility parameter = $(1 - M^2)^{-1/2}$
$\Gamma$	Circulation
$\gamma$	Ratio of specific heats, taken to be 1.4
$\Delta$	Prefix denoting correction increment
$\Delta_{rms}$	Root mean square deviation from mean curves
$\delta_0$	Lift interference parameter associated with stream direction
$\delta_1$	Lift interference parameter associated with streamline curvature
$\epsilon$	Blockage factor
$\eta$	Transformed co-ordinate (see Section 3.2)
$\theta$	Chordwise parameter (see Section 3.3)
$\mu$	Doublet strength
$\xi$	Transformed co-ordinate (see Section 3.2)
$\rho$	Free stream density
$\phi$	Perturbation velocity potential
$\phi_1$	Perturbation velocity potential due to aerofoil in unconstrained flow
$\phi^*$	Perturbation velocity potential induced by tunnel-wall constraints
$\Omega$	Ratio of ventilated-wall to closed-wall values of blockage factors

*Subscripts*

$B$	Denotes total-blockage values
$c$	Denotes closed-(solid-) wall values
$f$	Denotes free-air (i.e. corrected) values
$l$	Denotes aerofoil lower-surface values
$s$	Denotes solid-blockage values
$u$	Denotes aerofoil upper-surface values
$v$	Denotes ventilated-(slotted-) wall values
$w$	Denotes wake-blockage values

## 1. INTRODUCTION

The derivation of two-dimensional aerofoil characteristics from wind tunnel tests, especially at transonic speeds, is subject to several sources of experimental error, one of the most significant of which is wind tunnel wall interference. When an aerofoil is placed in a wind tunnel, forces and pressures measured on it differ from those which would be obtained if the model were tested under similar conditions in free air because the wind tunnel walls interfere with the flow. It is usual to make "corrections" to the measured quantities, and to Mach number and angle of incidence, so that the "corrected" results might correspond to those which would be obtained if the model were tested in free air at the "corrected" Mach number and angle of incidence. Such corrections may be reduced by using models with chords very much less than the tunnel test section height. However, in an effort to make maximum possible use of the available tunnel Reynolds number, models are generally designed with large chord to tunnel height ratios, giving rise to significant errors due to wind tunnel wall interference.

The problems in obtaining accurate two-dimensional transonic aerofoil data from wind tunnel tests, and in attempting to eliminate uncertainties in transonic two-dimensional aerofoil theory were recognised by the Commonwealth Advisory Aeronautical Research Council.\* That body endorsed<sup>1</sup> a proposal by the Co-ordinators in Aerodynamics<sup>2</sup> to "test a small number of suitable aerofoils in as many as possible of the transonic wind tunnels, throughout the Commonwealth, in which two-dimensional research is normally done". A proposal for such a research program, put forward by the United Kingdom CAARC Co-ordinator in Aerodynamics,<sup>3</sup> stated that the purpose of such a program would be "to add to our mutual knowledge and understanding of experimental techniques in a subject which is at once of great practical importance and at the same time afflicted with serious uncertainties, both theoretical and experimental".

Two basic aerofoil shapes were selected for the co-operative program. The first, the NACA-0012 section was selected to provide a "standard" symmetrical section. The second, an aerofoil designed by the numerical hodograph plane method of Bauer, Garabedian and Korn,<sup>4</sup> is an example of a modern "supercritical" section, with a reasonable extent of shock free supersonic flow on the upper surface and some degree of rear loading. This aerofoil (hereafter referred to as BGK-1) had the added advantage of having already been extensively tested at high Reynolds number in the NAE wind tunnel in Canada.<sup>5,6</sup> Since both these sections already formed part of a theoretical and experimental investigation of transonic aerofoils at ARL, with models of each either completed or being manufactured, it was decided to extend the experimental investigation to include the test program proposed in Reference 3. Results from tests in a slotted wall tunnel on two models of differing chord lengths of aerofoil BGK-17<sup>8,9</sup> and of three models of the NACA-0012 section<sup>10</sup> have been reported previously. These tests were later repeated with the slotted walls replaced with solid ones.<sup>14</sup>

The present report concentrates on the analysis of the above test results with respect to wind tunnel wall interference. For a model of fairly small chord to tunnel height ratio, the corrections can be calculated theoretically by linearized potential flow theory,<sup>11</sup> in which the changes to the stream direction and the streamline curvature are referred to as lift interference, and changes in stream velocity and longitudinal gradient are referred to as blockage interference. The lift interference arises from changes induced by the tunnel walls in the circulation or vorticity around the model and is assumed to be independent of the blockage effect, which is associated with changes in the velocity potential of a doublet and source representing the volume occupied by the aerofoil and its wake.

A major problem to be faced when applying such linear theory to a practical wind tunnel

---

\* Australia, Canada, India, New Zealand and the United Kingdom are active members of CAARC.

situation is that of correctly representing the boundary conditions at the tunnel walls. For the case of solid walls, the boundary conditions are straightforward and mathematically amenable. However, in transonic flows, porous or slotted (as is the case for the ARL transonic wind tunnel) walls are often used. Such walls are usually arranged primarily for the generation of low supersonic Mach numbers using diffuser suction, or to minimize shock reflections at high subsonic and low supersonic Mach numbers, with little attempt being made to utilize the available reduction in interference made possible by the non-solid walls. In this case the wall boundary conditions are complicated and it is usual to change the mixed boundary conditions into an equivalent homogeneous boundary condition which produces the same solution at the centre of the test section, but the correct representation remains open to question.<sup>12,13</sup> As data are available from tests in solid as well as in slotted walls, it should be possible to examine the validity of the assumption of the independence of lift and blockage interference, and hence the applicability of linear theory, separately from the physical and mathematical representation of the non-solid wall boundary condition, since the solid-wall boundary condition is straightforward.

The statement of the results of linear interference theory given in the standard references has until recently included errors, originating in the early analyses and faithfully reproduced by later authors. These errors were pointed out by Catherall.<sup>11</sup> It was therefore considered worthwhile to include a review of the major results of classical linear theory, and this is included in Section 3.

## 2. EXPERIMENTAL DETAILS

### 2.1 Section Definition

Aerofoil section BGK-1 was one of the earliest designed by Garabedian and his colleagues using their numerical hodograph method.<sup>4</sup> The section was designed to produce shock-free flow on the upper surface at  $M = 0.75$  and  $\alpha = 0^\circ$ , giving a  $C_L$  of 0.63 (inviscid) (Fig. 1). The ordinates of the aerofoil were derived from those published in Reference 5, with the exception of those close to the trailing edge, where the presence of a cusp required some modification to simplify model manufacture. These modifications involved thickening the section in the region  $0.95 \leq x_L/c \leq 1.00$  and are noted in Reference 9.

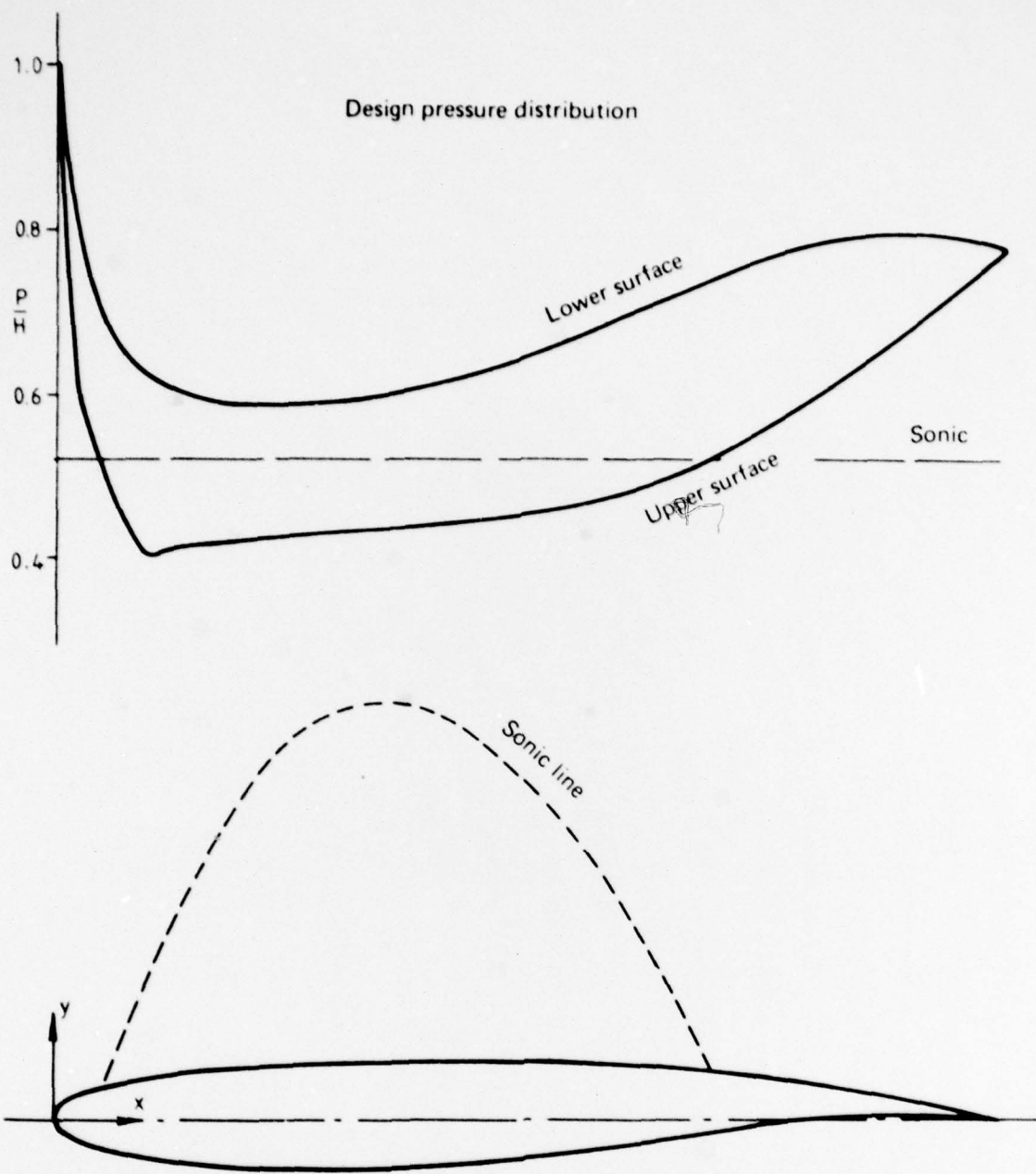
The NACA-0012 is a symmetrical section, 12% thick, with ordinates given by:

$$\frac{z}{c} = 0.6 \left\{ 0.29690 \sqrt{\frac{x_L}{c}} - 0.12600 \frac{x_L}{c} - 0.35160 \left( \frac{x_L}{c} \right)^2 + 0.28430 \left( \frac{x_L}{c} \right)^3 - 0.10150 \left( \frac{x_L}{c} \right)^4 \right\}$$

with a leading edge radius of  $0.0158c$ . The basic section has a blunt base of  $0.00252c$ . However, to avoid confusing comparisons between models arising from base pressure variations with Reynolds number, the upper and lower surfaces were linearly extended to a sharp ( $0.1$  mm thick) trailing edge. Due to this extension the actual physical chord length of the models was slightly greater than the nominal chord. The calculated force coefficients are based on the nominal chord ( $c$ ).

### 2.2 Model Dimensions

The testing of two-dimensional aerofoils in transonic wind tunnels presents conflicting requirements on model chord; a small chord, while minimizing tunnel interference effects, introduces difficulty in producing a model of sufficient strength, and limits the number of pressure orifices which can be included. A larger chord also allows greater use to be made of available tunnel Reynolds number. Model aspect ratios should also be large enough to produce sensibly two-dimensional flow conditions, at least over the central measuring section. Since one of the aims of these tests was to investigate the effects of tunnel interference, models with larger values of model chord to tunnel height ratios than would normally be tested were considered desirable, both to increase the magnitude of any interference making it easier to measure, and to investigate the limits of applicability of linearized theory. On the basis of these considerations, a maximum model chord of 203.2 mm was selected. The  $c/h$  ratio of 0.25 is within the suggested limits of applicability of linearized theory ( $c/h \leq 0.3$ ),<sup>3</sup> and the aspect ratio (2.6)



Thickness/Chord = 0,115  
 Design conditions  $M = 0,750$   $\alpha = 0^\circ$   $C_L = 0,63$

FIG. 1 SUPERCRITICAL LIFTING AEROFOIL BGK1

is sufficiently large to avoid major effects of three-dimensionality. Models of both sections with this maximum chord were therefore tested, as were models with 101.6 mm chords (giving  $c/h = 0.125$ , aspect ratio = 5.25) to provide comparative results.

### 2.3 Wind Tunnel

All tests were carried out in the ARL variable pressure transonic wind tunnel. The test section fitted for the slotted wall tests had solid side walls and longitudinally slotted top and bottom walls (open area ratio 16.5% at the model location), with dimensions at the model location of  $b = 533$  mm,  $h = 813$  mm (Fig. 2), surrounded by a plenum chamber 2540 mm in diameter. These walls are those normally used for two-dimensional testing in this tunnel. The open area ratio, which was selected primarily for the generation of low supersonic Mach numbers through diffuser suction, is known to be larger than that giving interference free subsonic test conditions. For the slotted wall tests, Mach number was derived from measurements of the pressure in the plenum chamber surrounding the test section, and in the entry to the contraction, assuming these to be the static and total pressures of the test section flow respectively. For the solid wall tests, test section total pressure was once again derived from the static pressure in the contraction entry, while test section static pressure was measured at a side wall pressure hole.<sup>14</sup>

### 2.4 Transition Fixing

The effects of transition fixing on the BGK-1 section have been studied previously.<sup>8</sup> That investigation showed the need to fix transition if gross, shock induced, laminar separations were to be avoided at Mach numbers and angles of incidence above the design conditions ( $M = 0.75$ ,  $\alpha = 0^\circ$ ). However, the use of transition fixing destroyed agreement between theory and experiment at the design condition. In spite of this problem, it was decided to conduct the slotted wall tests with transition fixed on both surfaces to avoid both shock induced laminar separations, and the misleading variations of drag and pitching moment (and to a lesser extent lift) caused by the movement of the chordwise position of transition with Mach number and angle of incidence. Also, the transition free behaviour of the section had already been the subject of a detailed investigation.<sup>7</sup>

Transition was therefore fixed on both surfaces of the BGK-1 models for the slotted wall tests. For consistency, a similar transition fixing was used for the slotted wall tests on the NACA-0012 section,<sup>10</sup> and these conditions were maintained throughout the tests in solid walls.<sup>14</sup> Surface oil flow observations indicated that at the maximum test Reynolds number for each model, boundary-layer transition was effectively produced.

## 3. SUBSONIC LINEAR INTERFERENCE THEORY

### 3.1 Introduction

In subsonic linear theory, interference is assumed to be due to three independent characteristics of the model: its lift, its displacement, and the displacement of its wake. The contributions of these three characteristics are usually<sup>11</sup> estimated by representing them as a vortex, a doublet and a source respectively, and the three corresponding modes of wall interference referred to as lift interference, solid blockage, and wake blockage. If the velocity potentials are obtained for each of these singularities in the tunnel, then the interference will be represented by interference potentials, which are the difference between the potentials in the tunnel and in free air. Evaluation of these interference potentials in the neighbourhood of the model may then be used as estimates of the interference corrections required to be made to measured quantities.

### 3.2 Subsonic Linear Theory

The linearized equation of motion for two-dimensional subsonic compressible flow is

$$\beta^2 \frac{\partial^2 \phi}{\partial x^2} + \frac{\partial^2 \phi}{\partial z^2} = 0 \quad (3.1)$$

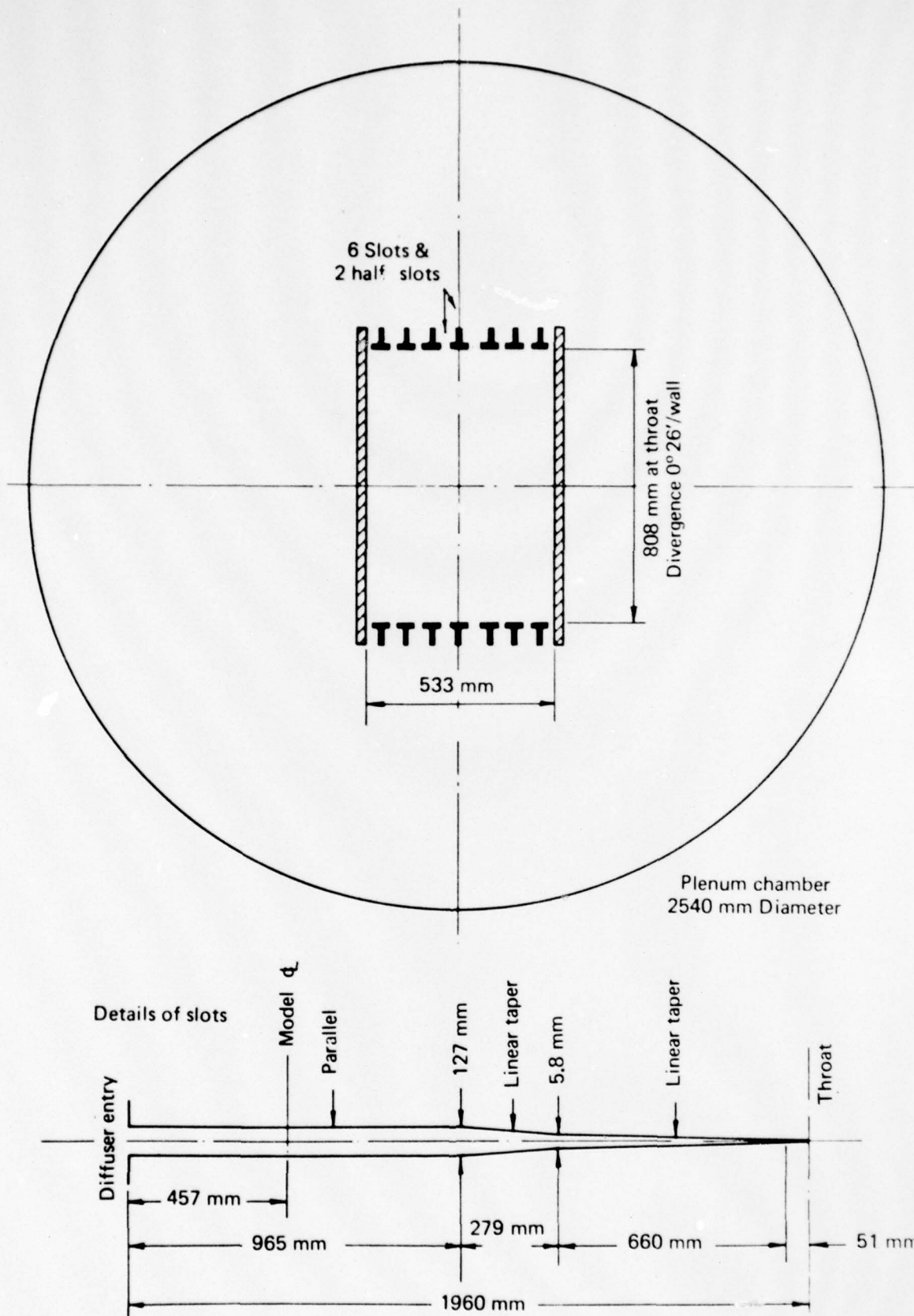


FIG. 2 DETAILS OF SLOTTED WORKING SECTION

where  $\phi$  is the perturbation velocity potential of the flow. Baldwin *et al.*<sup>15</sup> have derived a single homogeneous boundary condition for ventilated wind tunnel walls in the form

$$\left( \frac{\partial \phi}{\partial x} \pm \frac{Fh}{2} \frac{\partial^2 \phi}{\partial x \partial z} \pm \frac{1}{P} \frac{\partial \phi}{\partial z} \right)_{z=\pm \frac{h}{2}} = 0 \quad (3.2)$$

where  $P$  is a porosity parameter, and  $F$  is slot parameter given by

$$F = \frac{2d}{\pi h} \ln \operatorname{cosec} \frac{\pi a}{2d} \quad (3.3)$$

where  $a$  is the slot width and  $d$  the mean periodic slot spacing (see Fig. 3).

It should be noted that the general boundary condition (3.2) contains the special cases

- (i) solid wall— $1/P \rightarrow \infty$  or  $F \rightarrow \infty$ ;
- (ii) perforated wall— $1/P \neq 0$ ,  $F = 0$ ;
- (iii) ideal slotted wall— $1/P = 0$ ,  $F \neq 0$ ;
- (iv) open jet— $1/P = 0$ ,  $F = 0$

and hence results derived from this boundary condition will contain results applicable to all possible tunnel wall conditions.

Writing

$$\phi = \phi_1 + \phi^* \quad (3.4)$$

where  $\phi_1$  is the perturbation potential about the model in free air and  $\phi^*$  is the interference potential, then Baldwin *et al.*<sup>15</sup> and Wright<sup>16</sup> have obtained solutions for  $\phi^*$  by solving Equations (3.1) and (3.4) with the boundary condition (3.2) by a Fourier transform method. This then yields the change in stream conditions caused by the walls at the model position, given by

$$u = \frac{\partial \phi^*}{\partial x} \Big|_{x=z=0} \quad (3.5)$$

which is the blockage correction,

$$w = \frac{\partial \phi^*}{\partial z} \Big|_{x=z=0} \quad (3.6)$$

which is the upwash correction, and

$$\frac{\partial w}{\partial x} = \frac{\partial^2 \phi^*}{\partial z \partial x} \Big|_{x=z=0} \quad (3.7)$$

which is the streamline curvature correction. Each correction will now be considered in turn.

### 3.2.1 Solid Blockage

In free air, the potential due to a doublet of strength  $m_d$  is given by

$$\phi_1 = \frac{m_d}{2\pi} \left( \frac{x}{x^2 + \beta^2 z^2} \right) \quad (3.8)$$

and the strength of the doublet may be related to the size of the model with sufficient accuracy by

$$m_d = \frac{AU}{\beta} \quad (3.9)$$

where  $A$  is the cross-sectional area of the model in the  $x$ - $z$  plane. Baldwin *et al.* showed that the interference potential due to the doublet is given by

$$\phi^* = -\frac{AU}{\pi\beta^2 h} \left\{ \frac{\beta}{P} \int_0^\infty \frac{1}{I_A} \cosh(q\eta) \cos(q\xi) dq + \int_0^\infty \frac{I_C}{I_A} \cosh(q\eta) \sin(q\xi) dq \right\} \quad (3.10)$$

where

$$\left. \begin{aligned} I_C &= \left[ 1 - F^2 q^2 - \left( \frac{\beta}{P} \right)^2 \right] + \left[ \left( 1 - Fq \right)^2 + \left( \frac{\beta}{P} \right)^2 \right] e^{-2q} \\ I_A &= \left( \cosh q + Fq \sinh q \right)^2 + \left( \frac{\beta}{P} \right)^2 \sinh^2 q \end{aligned} \right\} (3.11)$$

with

$$\eta = \frac{2z}{h}$$

$$\xi = \frac{2x}{\beta h}$$

Differentiating (3.10) and setting  $x = z = 0$  gives

$$u_s = -\frac{AU}{\pi\beta^3 h^2} \int_0^\infty \frac{I_C}{I_A} q \, dq \quad (3.12)$$

for the additional stream velocity at the model position due to the walls. Allowing  $F \rightarrow \infty$  gives the solid wall result

$$u_{sc} = \frac{\pi AU}{6 \beta^3 h^2} \quad (3.13)$$

### 3.2.2 Wake Blockage

For a two-dimensional source of strength  $m_s$

$$\phi_s = \frac{m_s}{2\pi\beta} \ln(x^2 + \beta^2 z^2)^{1/2} \quad (3.14)$$

and the strength of the source may be related to the model wake by

$$m_s = \frac{1}{2} U c C_D \quad (3.15)$$

where  $C_D$  is the drag coefficient of the model. The interference potential is then given by

$$\begin{aligned} \phi^* &= -\frac{U c C_D}{4\pi\beta} \left\{ \frac{\beta}{P} \int_0^\infty \frac{1}{I_A} \left[ \cosh(q\eta) \sin(q\xi) - \sin q \right] \frac{dq}{q} \right. \\ &\quad \left. - \int_0^\infty \frac{I_C}{I_A} \left[ \cosh(q\eta) \cosh(q\xi) - \cos q \right] \frac{dq}{q} \right\} \end{aligned} \quad (3.16)$$

where  $I_A$  and  $I_C$  are as defined in (3.11). Differentiating and setting  $x = z = 0$  yields

$$u_w = -\frac{U C_D c \beta}{4\pi\beta^2 h P} \int_0^\infty \frac{1}{I_A} dq \quad (3.17)$$

for the additional stream velocity at the model position due to wake blockage. Once again, allowing  $F \rightarrow 0$  gives the solid wall result

$$u_{wc} = \frac{U C_D c}{4\pi\beta^2 h} \quad (3.18)$$

It should be noted that the expressions (3.17) and (3.18) are different from those derived by Wright,<sup>16</sup> which included an error. This error, which was pointed out by Catherall<sup>17</sup> has been corrected in the above equations.

### 3.2.3 Lift Interference

In free air the potential due to a two-dimensional vortex at the origin is given by

$$\phi_1 = -\frac{\Gamma}{2\pi} \tan^{-1}\left(\frac{\beta z}{x}\right) \quad (3.19)$$

The circulation,  $\Gamma$ , about the model is related to the model lift per unit width by

$$L' = \rho U \Gamma = \frac{1}{2} \rho U^2 C_{Lc} \quad (3.20)$$

and the interference potential may be written as

$$\phi^* = -\frac{\Gamma}{2\pi} \left\{ \frac{\beta}{P} \int_0^\infty \frac{1}{I_F} \sinh(q\eta) \cos(q\xi) \frac{dq}{q} + \int_0^\infty \frac{I_G}{I_F} \sinh(q\eta) \sin(q\xi) \frac{dq}{q} \right\} \quad (3.21)$$

where

$$\left. \begin{aligned} I_G &= \left[ (1 - Fq) (\sinh q + Fq \cosh q) - \left(\frac{\beta}{P}\right)^2 \cosh q \right] e^{-q} \\ I_F &= (\sinh q + Fq \cosh q)^2 + \left(\frac{\beta}{P}\right)^2 \cosh^2 q \end{aligned} \right\} \quad (3.22)$$

Differentiating and setting  $x = z = 0$  yields the upwash velocity, given by

$$w = -\frac{\Gamma \beta}{\pi h P} \int_0^\infty \frac{1}{I_F} dq = -\frac{C_{Lc} U}{2\pi h} \left(\frac{\beta}{P}\right) \int_0^\infty \frac{1}{I_F} dq \quad (3.23)$$

and the streamwise gradient of the upwash velocity or the streamline curvature at the origin is given by

$$\frac{\partial w}{\partial x} = -\frac{2\Gamma}{\pi \beta h^2} \int_0^\infty \frac{I_G}{I_F} q dq = -\frac{C_{Lc} U}{\pi \beta h^2} \int_0^\infty \frac{I_G}{I_F} q dq \quad (3.24)$$

Again allowing  $F \rightarrow \infty$ , gives the solid wall result

$$w_c = 0 \quad (3.25)$$

and

$$\left(\frac{\partial w}{\partial x}\right)_c = \frac{\pi C_{Lc} U}{24 \beta h^2} \quad (3.26)$$

Once again the expressions (3.23) and (3.24) are different from those derived by Wright due to an error in the analysis also pointed out by Catherall.

### 3.2.4 Blockage Velocity Gradients

The variation in longitudinal velocity due to both solid and wake blockage given by Equations (3.12) and (3.17) is not symmetrical forward and aft of the aerofoil mid-chord. This gives rise to longitudinal velocity gradients (at the origin) by

$$\frac{\partial u_s}{\partial x} = \frac{4AU \beta}{\pi \beta^3 h^3 P} \int_0^\infty \frac{1}{I_A} q^2 dq \quad (3.27)$$

for the solid blockage term, and

$$\frac{\partial u_w}{\partial x} = -\frac{UC_{Dc}}{2\pi \beta^3 h^2} \int_0^\infty \frac{I_C}{I_A} q dq \quad (3.28)$$

for the wake blockage term. These longitudinal velocity gradients give rise to longitudinal

bouyancy forces on the model which would be absent in free air. Balance measurements of model drag would record this bouyancy force and would therefore have to be corrected in order to correspond to free-air values. However, if model drag is obtained by wake traverse measurements downstream of the model, no bouyancy corrections need be applied. Since no balance drag measurements were undertaken in the present tests, these terms will not be considered further.

### 3.3 Corrections to Measured Quantities

As shown in Section 3.2.3, lift interference induces an upwash velocity  $w$  which varies along the tunnel and necessitates corrections to the model incidence, loading, and lift and pitching moment coefficients. The correction to incidence,  $\Delta\alpha$ , represents the interference upwash at the aerofoil mid-chord, and the remaining corrections allow for the residual upwash distributed over the aerofoil. Since the representative vortex must be placed at the aerofoil's centre of pressure, and the mid-chord is approximately at a distance  $c \left( \frac{1}{4} + \frac{C_m}{C_L} \right)$  downstream, then the correction to incidence will be

$$\Delta\alpha = \frac{w}{U} + \frac{c}{U} \frac{\partial w}{\partial x} \left( \frac{1}{4} + \frac{C_m}{C_L} \right) \quad (3.29)$$

or

$$\Delta\alpha = \frac{c C_L}{h} \delta_0 + \frac{c^2}{\beta h^2} \delta_1 \left( \frac{1}{4} C_L + C_m \right) \quad (3.30)$$

where

$$\left. \begin{aligned} \delta_0 &= \frac{hw}{UcC_L} \\ \text{and} \\ \delta_1 &= \frac{\beta h^2}{UcC_L} \frac{\partial w}{\partial x} \end{aligned} \right\} \quad (3.31)$$

The choice of  $\Delta\alpha$  is such that the residual loading correction,  $\Delta L$ , vanishes at the aerofoil leading edge, and the increment to be added to the measured loading is

$$\Delta L = -2 \left( \frac{c}{h} \right)^2 \frac{\delta_1}{\beta^2} C_L \sin \theta \quad (3.32)$$

where  $\theta$  is a parameter used to describe the chordwise distance aft of the leading edge of the aerofoil,

$$x - x_L = \frac{c}{2} (1 - \cos \theta) \quad (3.33)$$

The incremental correction to lift is obtained by integrating  $\Delta L$  along the aerofoil chord, giving

$$\Delta C_L = -\frac{\pi}{2} \left( \frac{c}{h} \right)^2 \frac{\delta_1}{\beta^2} C_L \quad (3.34)$$

and the incremental correction to pitching moment is obtained by integrating

$$\{\Delta L(x_L + 0.25c - x)\}$$

along the aerofoil chord giving

$$\begin{aligned} \Delta C_m &= \frac{\pi}{8} \left( \frac{c}{h} \right)^2 \frac{\delta_1}{\beta^2} C_L \\ &= -\frac{\Delta C_L}{4} \end{aligned} \quad (3.35)$$

It should be noted that the values of lift and pitching moment coefficients appearing in Equations (3.30), (3.34) and (3.35) are uncorrected and based on the uncorrected kinetic pressure,  $\frac{1}{2}\rho U^2$ .

The doublet and source representing the aerofoil displacement and that of its wake give rise to changes in longitudinal velocity due to solid and wake blockage respectively. These two blockage components can be added together to give a total blockage factor

$$\frac{u}{U} = \frac{u_w}{U} + \frac{u_s}{U} \quad (3.36)$$

or

$$\frac{u}{U} = \epsilon_B = \epsilon_s + \epsilon_w \quad (3.37)$$

where

$$\epsilon_B = \frac{1}{U} \frac{\partial \phi^*}{\partial x}$$

It is usual to express the values of  $\epsilon_s$  and  $\epsilon_w$  for the general ventilated wall case by factoring the solid-wall blockage factors by the quantities  $\Omega_s$  and  $\Omega_w$  respectively. The total blockage factor can then be written

$$\epsilon_B = \Omega_s \epsilon_{sc} + \Omega_w \epsilon_{wc} \quad (3.38)$$

where  $\epsilon_{sc}$  and  $\epsilon_{wc}$  are the solid wall values of  $\epsilon_s$  and  $\epsilon_w$  and  $\Omega_s$  and  $\Omega_w$  are the ratios of solid wall to general ventilated wall blockage factors. Thus  $\Omega_s = \Omega_w = 1$  for the solid wall case. From Equation (3.13),

$$\epsilon_{sc} = \frac{\pi A}{6\beta^3 h^2} \quad (3.39)$$

and from Equation (3.18),

$$\epsilon_{wc} = \frac{1}{4} \left( \frac{c}{h} \right) \frac{C_D}{\beta^2} \quad (3.40)$$

where, if drag measurements are made by the wake traverse method,  $C_D$  is the uncorrected drag coefficient based on the uncorrected kinetic pressure  $\frac{1}{2}\rho U^2$ . Garner *et al.*<sup>11</sup> point out that improved agreement with experimental results is obtained if  $\epsilon_{sc}$  and  $\epsilon_{wc}$  are modified on the basis of more elaborate theories. Thus  $\epsilon_{sc}$  contains a factor to account for the effect of incidence, and the cross-sectional area is multiplied by an empirical factor,

$$\epsilon_{sc} = \frac{\pi A}{6\beta^3 h^2} \left[ 1 + 1.2\beta \left( \frac{t}{c} \right) \right] \left[ 1 + 1.1 \left( \frac{c}{t} \right) x^2 \right] \quad (3.41)$$

The expression for  $\epsilon_{wc}$  contains an extra compressibility factor which then gives a compressibility factor between  $\beta^{-2}$  and  $\beta^{-3}$ , thus

$$\epsilon_{wc} = \frac{1}{4} \left( \frac{c}{h} \right) \frac{[1 + 0.4M^2]}{\beta^2} C_D \quad (3.42)$$

and this expression has been found to lead to better agreement with experiment at high subsonic Mach numbers.

Because blockage changes the stream longitudinal velocity, the static pressure, density and static temperature of the stream will also change. The incremental corrections to be added to the undisturbed stream values to allow for these changes, and the associated corrections to flow quantities derived from them are as follows:

$$\frac{u}{U} = \frac{\Delta U}{U} = \epsilon_B \quad (3.37)$$

$$\frac{\Delta p_0}{p_0} = -1.4M^2 \epsilon_B \quad (3.43)$$

$$\frac{\Delta p}{\rho} = -M^2 \epsilon_B \quad (3.44)$$

$$\frac{\Delta M}{M} = (1 + 0.2M^2) \epsilon_B \quad (3.45)$$

$$\frac{\Delta(\frac{1}{2}\rho U^2)}{\frac{1}{2}\rho U^2} = (2 - M^2) \epsilon_B \quad (3.46)$$

It is now possible to correct aerodynamic coefficients measured in the tunnel, and based on uncorrected kinetic pressure, to free-air values. This process can be considered in two steps:

(i) adding to the measured  $C_L$  and  $C_m$  values the lift-interference corrections  $\Delta C_L$  and  $\Delta C_m$ ; and

(ii) multiplying the results by  $G$ , the ratio of uncorrected to corrected kinetic pressure.

The free-air values of aerodynamic coefficients, based on the corrected kinetic pressure are then given by:

$$(C_L)_f = (C_L + \Delta C_L)G \quad (3.47)$$

$$(C_m)_f = (C_m + \Delta C_m)G \quad (3.48)$$

$$(C_D)_f = C_D G \text{ (for wake traverse)} \quad (3.49)$$

where

$$G = \frac{\frac{1}{2}\rho U^2}{\frac{1}{2}\rho U^2 + \Delta(\frac{1}{2}\rho U^2)} = \frac{1}{1 + (2 - M^2)\epsilon_B} \quad (3.50)$$

When comparing results from tests on two or more models or from tests in differing wall configurations, corrected values of both Mach number and angle of incidence must agree for the comparison to be valid. In practice, this severely limits the number of cases available for comparison. One method of overcoming this limitation is to use zero lift lift curve slope as the basis for comparison, in which case the only requirement is that comparisons be made at the same corrected Mach number. It is therefore useful to combine the separate corrections to lift coefficient and angle of incidence into a single correction to lift curve slope. Assuming that, in a small region around zero lift, the lift curve is approximately linear, i.e.

$$C_L \approx K_1 \alpha + c_1 \quad (3.51)$$

then the lift curve slope may be written as

$$\left. \frac{\partial C_L}{\partial \alpha} \right|_{C_L=0} = \frac{C_{L2} - C_{L1}}{\alpha_2 - \alpha_1} = K_1 \quad (3.52)$$

and the lift curve slope corrected to free-air conditions as

$$\left( \left. \frac{\partial C_L}{\partial \alpha} \right|_{C_L=0} \right)_f = \frac{C_{L2f} - C_{L1f}}{\alpha_{2f} - \alpha_{1f}} = K_{1f} \quad (3.53)$$

Now

$$\alpha_f = \alpha + \Delta \alpha$$

and

$$C_{L,f} = (C_L + \Delta C_L)G$$

Substituting into (3.53) we obtain

$$\left( \left. \frac{\partial C_L}{\partial \alpha} \right|_{C_L=0} \right)_f = \frac{[(C_{L2} - C_{L1}) + (\Delta C_{L2} - \Delta C_{L1})] G}{(\alpha_2 - \alpha_1) + (\Delta \alpha_2 - \Delta \alpha_1)}$$

Now

$$\Delta C_{L2} - \Delta C_{L1} = \frac{\partial(\Delta C_L)}{\partial C_L} (C_{L2} - C_{L1})$$

and

$$\Delta\alpha_2 - \Delta\alpha_1 = \frac{\partial(\Delta\alpha)}{\partial\alpha}(\alpha_2 - \alpha_1)$$

Therefore

$$\left(\frac{\partial C_L}{\partial\alpha}\right)_{C_L=0} = \frac{(C_{L2} - C_{L1})\left(1 + \frac{\partial(\Delta C_L)}{\partial C_L}\right)G}{(\alpha_2 - \alpha_1)\left(1 + \frac{\partial(\Delta\alpha)}{\partial\alpha}\right)} \quad (3.54)$$

From (3.30) we have

$$\Delta\alpha = \frac{c}{h}\delta_0 C_L + \left(\frac{c}{h}\right)^2 \frac{\delta_1}{\beta} \left(\frac{C_L}{4} + C_m\right)$$

Assuming that the pitching moment coefficient varies linearly with incidence in the region of the zero lift point, i.e.

$$C_m \approx K_2\alpha + c_2 \quad (3.55)$$

then

$$\frac{\partial(\Delta\alpha)}{\partial\alpha} = \frac{c}{h}\delta_0 K_1 + \left(\frac{c}{h}\right)^2 \frac{\delta_1}{\beta} \left(\frac{K_1}{4} + K_2\right) \quad (3.56)$$

Also, from (3.34)

$$\frac{\partial(\Delta C_L)}{\partial C_L} = -\frac{\pi}{2} \left(\frac{c}{h}\right)^2 \frac{\delta_1}{\beta^2} \quad (3.57)$$

Substituting (3.56) and (3.57) into (3.54) we obtain

$$\left(\frac{\partial C_L}{\partial\alpha}\right)_{C_L=0} = \frac{\partial C_L}{\partial\alpha} \Big|_{C_L=0} \times \left\{ \frac{\left[1 - \frac{\pi}{2} \left(\frac{c}{h}\right)^2 \frac{\delta_1}{\beta^2}\right]G}{\left[1 + \frac{c}{h}\delta_0 K_1 + \left(\frac{c}{h}\right)^2 \frac{\delta_1}{\beta} \left(\frac{K_1}{4} + K_2\right)\right]} \right\} \quad (3.58)$$

This expression takes into account both blockage and lift interference and thus enables lift curve slopes to be directly compared, the only further requirement being that the individual lift curve slopes be compared at their corrected Mach numbers.

### 3.4 General Remarks

The theory of wind tunnel wall interference correction is still far from complete. The basic deficiency in the application of subsonic theory to ventilated wall test sections is an inadequate knowledge of the wall boundary conditions and a lack of understanding of the viscous loss characteristics across the walls. This makes it difficult to apply classical wall correction theory and expect the same accuracy that has been realized for solid walls or for open jets. If the wall boundary conditions for ventilated test sections could be specified as satisfactorily as those for solid walls or for open jets, ventilated wall corrections would be subject to the same limitations that have always been present in the classical correction methods. These limitations arise from the first order linearized approach to the problem and to the modelling of the situation by three independent corrections. This gives rise to the implication, for example, that since there is streamline curvature, a warped model should be tested to simulate the uniform unbounded flow situation, and that the model warpage should be changed with each angle of attack. However, the wall loss characteristic problem is more fundamental to the ventilated wall case since it precludes the confident application of classical methods.

Consider the slot parameter,  $F$ , defined by Equation (3.3). It was pointed out by Davis and Moore,<sup>10</sup> and later by Berndt and Sørensen,<sup>12</sup> that if the slots have finite thickness,  $l$  (see Fig.3), then  $F$  is given by

$$F = \frac{2d}{h} \left\{ \frac{1}{\pi} \ln \operatorname{cosec} \frac{\pi a}{2d} + \frac{l}{a} \right\} \quad (3.59)$$

More recently Barnwell<sup>20</sup> has generalized the flat slat formulation so that variations involving slots with sidewalls and separation in the plenum can be treated. He derived an expression for  $F$  for the case in which the flow separated on the plenum side of the slots as follows:

$$F = \frac{2d}{h} \left\{ \frac{1}{\pi} \ln \left( \frac{2 + \pi d}{4\pi a} \right) \right\} \quad (3.60)$$

and for the case of slots with sidewalls (see Fig. 3)

$$F = \frac{2d}{h} \frac{1}{\pi} \ln \left( \frac{d}{2a} \right) \quad (3.61)$$

It can be shown that the differences in the values of  $F$  derived from Equations (3.3), (3.60) or (3.61) are relatively small if the slot width to slot spacing ratio  $a/d$  is small. However, these differences, due to the uncertainty of the exact nature of the wall boundary condition, can become quite large in the case of a tunnel wall with only a few relatively wide slots.

In Reference 21 Chen and Mears develop a model in which the slots are represented by bodies which are generated by doublet rods of constant strength as shown in Figure 4. The boundary of each body is the dividing streamline between the outside flow and the flow associated with the doublet rod. The slot width and slot spacing are again designated as  $a$  and  $d$ , and the distance between the doublet rods is designated as  $D$ . Barnwell<sup>20</sup> has pointed out a mistake in the analysis of Chen and Mears in that they equated the distance between the rods,  $D$ , with the slot width  $a$ . These distances are obviously not equal since there must be a small space between the end of the rod and the dividing streamline as indicated in Figure 4a so that the fluid which is emitted in front of the rod by the source half of each doublet can flow around the end and into the sink half of the doublet at the rear. This error led to an order of magnitude difference in the values of  $F$  for small values of  $a/d$  and to some doubt as to the validity of the approach when compared with the classical approach leading to (3.3).

Chen and Mears analysis leads to an expression for  $F$  of

$$F = \frac{d}{h} \left( 1 - \frac{D}{d} \right) \frac{\cos \left( \frac{\pi D}{d} \right) + \cosh \left( \frac{\pi l}{d} \right)}{\sin \left( \frac{\pi D}{d} \right)} \quad (3.62)$$

where in this case  $l$  is the centreline thickness of the slat. The rod gap  $D$  is unknown and must be determined iteratively by fixing  $d$  and  $l$  and assuming a value for  $D$ . The value of  $a$  is then obtained from the equation for the stream function describing the slat shape:

$$\sin \left\{ \frac{\pi}{2} \left( \frac{D}{d} + \frac{a}{d} \right) \right\} = \sin \left\{ \frac{\pi}{2} \left( \frac{D}{d} - \frac{a}{d} \right) \right\} \exp \left\{ \frac{\pi}{\mu} \frac{d}{d} \left( 1 - \frac{a}{d} \right) \right\} \quad (3.63)$$

where  $\mu$  is related to the doublet strength and is given by

$$\mu = d \frac{\cos \left( \frac{\pi D}{d} \right) + \cosh \left( \frac{\pi l}{d} \right)}{\sin \left( \frac{\pi D}{d} \right)} \quad (3.64)$$

The slat shapes developed by Chen and Mears' approach are plotted in Figure 4b for several values of centre-line thickness. It is apparent that the effective thickness of the slat cannot be reduced below about  $\frac{1}{2}$ . For this reason, the usefulness of the doublet-rod model in its present form is limited. More control could be exerted over the effective thickness of the slat if the doublet strength could be varied along the length of the rod. However, the model does indicate<sup>20</sup> that the value of  $F$  is more sensitive to the shape of the slat than to whether or not the flow separates on the plenum side of the slat.

A more serious problem in the specification of the wall boundary condition arises with the

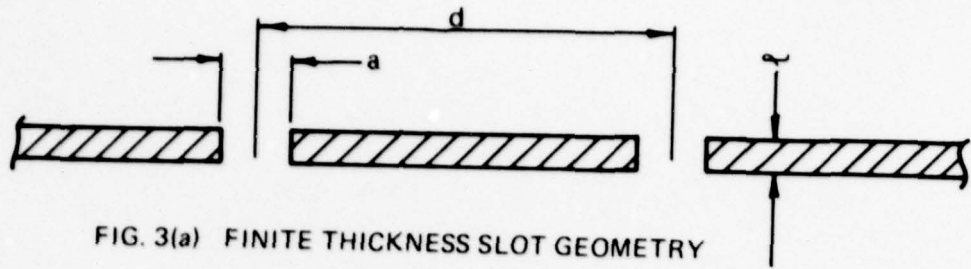


FIG. 3(a) FINITE THICKNESS SLOT GEOMETRY

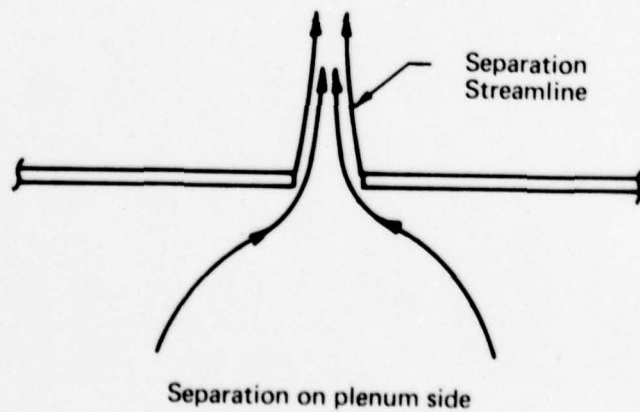
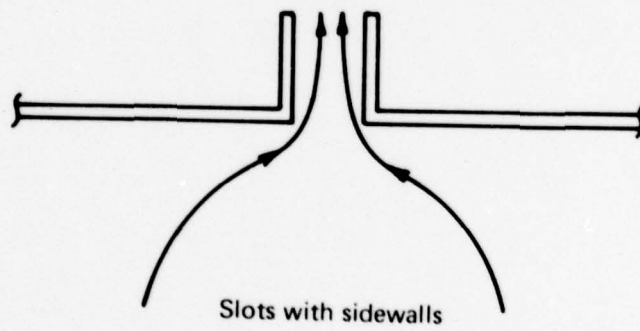
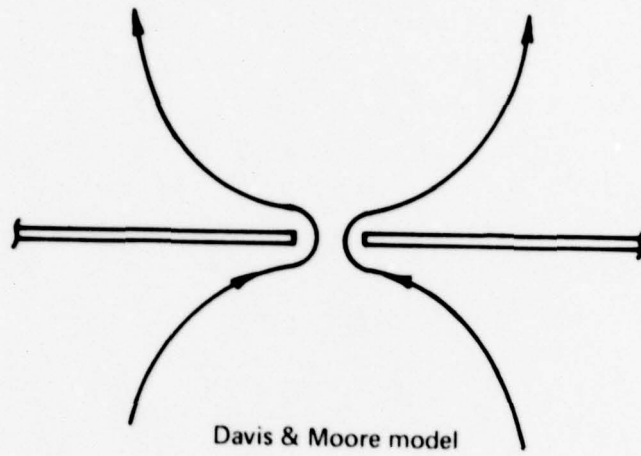
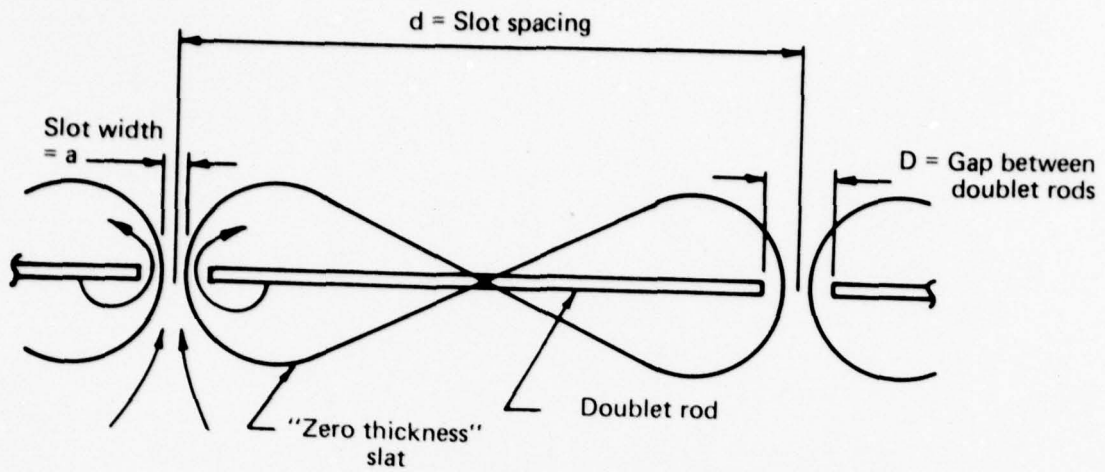
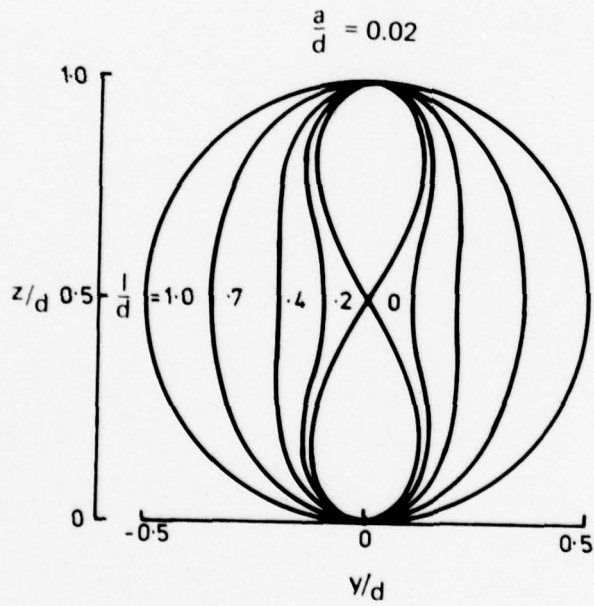


FIG. 3(b) SLOT FLOW MODELS



(a) Chen and Mears model of slat



(b) Possible slat shapes

FIG. 4 CHEN AND MEARS' SLAT MODEL

term to take account of viscous effects in the slots. The constant "porosity",  $P$ , in Equation (3.2) is assumed to be determined by the wall geometry and the free-stream Mach number, although unlike the slot parameter,  $F$ , there is no method for computing it *a priori*. This term is analogous to the term expressing the linearized pressure drop across a porous wall. The basis for using such a characteristic for slotted walls is however, even more tenuous than the basis for using it for porous walls, slotted walls departing even further from the physical basis (i.e. Darcy's law for flow through dense porous media). It has been suggested by several workers<sup>12</sup> that the viscous loss characteristic of slotted walls may be better represented by a quadratic term rather than a linear one, especially in cases where the cross-flow velocities are large.

The whole area of slotted wall boundary conditions is further complicated by the presence of the wall boundary layers, no account of which is taken by representations such as (3.2). The total cross-sectional area of the wall boundary-layers may well approach or even exceed the cross-sectional area of the model. It is therefore possible that to a large extent the fluid entering the slots could be low momentum boundary-layer air, rather than free-stream air. The slot flow is then bound to be less efficient in maintaining a pressure difference between the test section and the plenum chamber. These considerations also apply to any region where the slot flow passes into the test section from the plenum chamber with its more or less stagnant air. For the case where there is vanishing longitudinal flux in the slot region, there will be a negligible pressure difference and the wall will appear to the test section flow as a free-jet boundary at the plenum pressure.

It is clear then, that the flow properties of slotted walls may well be rather complicated, very likely more complicated than consistent with the simplifying assumptions made in the homogeneous boundary conditions of classical interference theory presented in the previous section. Some attempts<sup>12</sup> have been made to examine the situation with a view to obtaining a better representation of the boundary conditions, but these await further experimental verification before the use of their more complicated forms can be justified. Meanwhile the use of the classical forms of boundary condition will continue, but the accuracy of the resulting corrections will be open to doubt and will certainly be less than that achieved for the solid wall or open jet cases.

#### 4. APPLICATION OF LINEAR THEORY

##### 4.1 Solid Wall Results

The results of tests on both models of NACA-0012 and BGK-1 in the solid wall test section have been analysed in accordance with linear interference theory presented in the previous section. Lift-curve slope at zero lift was used as a basis for comparison, the data being corrected by the application of Equation (3.58). For the solid-wall case, the lift interference parameters  $\delta_0$  and  $\delta_1$  are given explicitly by (3.31), with  $\delta_0$  going to zero. The blockage factors  $\epsilon_{sc}$  and  $\epsilon_{uc}$  are given by (3.41) and (3.42). No wake drag measurements were undertaken for the solid wall tests, and the value of drag coefficient in (3.42) was therefore obtained from the results of the slotted wall tests at the corresponding uncorrected Mach numbers and attitudes. Since wake blockage accounts for less than 10% of the total blockage factor, this should not give rise to any significant errors.

The corrected values of lift-curve slope are plotted in Figure 5 for BGK-1 and in Figure 6 for the NACA-0012. Results from tests on the two models of each section shape now show satisfactory agreement, although scatter is still evident in the results for the BGK-1 section, especially at supercritical Mach numbers. The corrected data generally fall within  $\pm 2\%$  of the common curve, compared with differences of about 10% for the uncorrected data (see Figs. 7 and 8). An analysis of the expected errors in the value of lift curve slope (on the basis of typical experimental errors in angle of incidence of  $\pm 0.02^\circ$  and in lift coefficients of  $\pm 0.002$ , and lift curve slopes being derived from the slope of the lift curve over an angle of incidence of  $4^\circ$ ) indicates that they would be of the order of  $\pm 2\%$ —the same order as the scatter between corrected results.

Further evidence of the success of linear theory in correcting the data obtained in the solid wall tests is provided by the zero lift NACA-0012 results. Figure 9 presents the variation of pressure ratio with Mach number for one particular chordwise position ( $x/c = 0.3$ ). Corrected data from both models of the NACA-0012 are plotted and the data are seen to define a single curve with very little scatter.

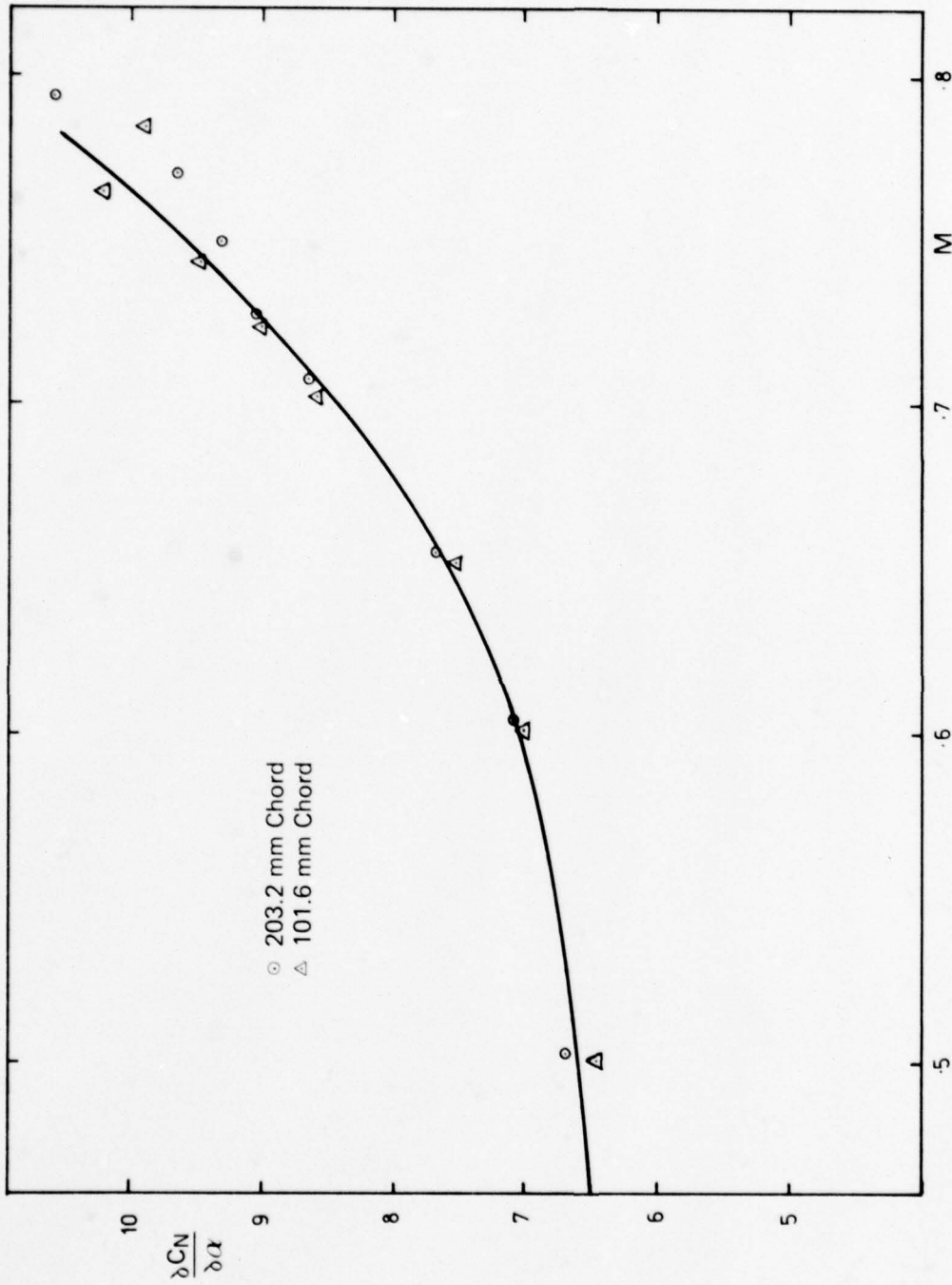


FIG. 5 VARIATION OF LIFT CURVE SLOPE WITH MACH NUMBER - BGK-1;  
CORRECTED SOLID WALL DATA

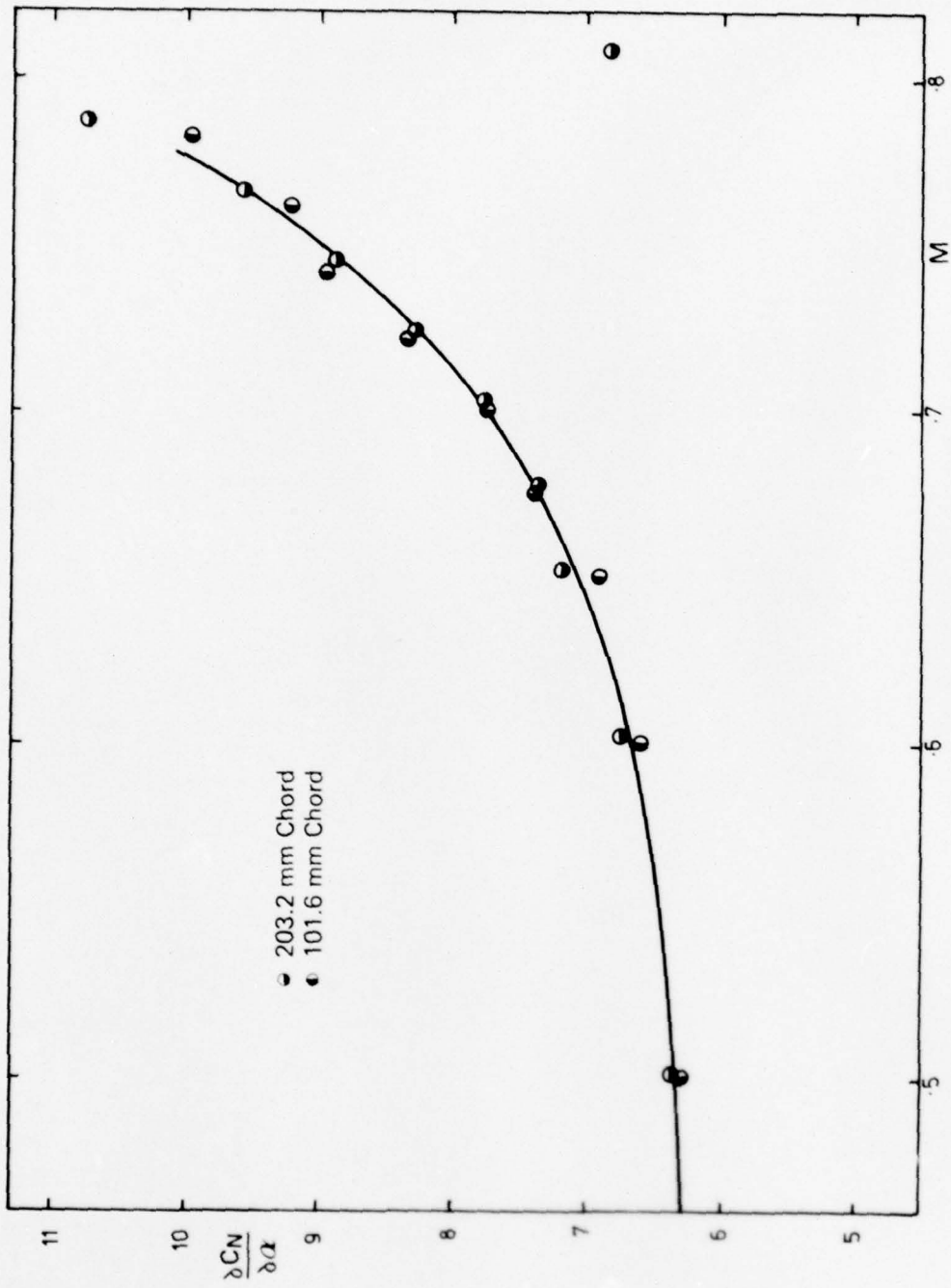


FIG. 6 VARIATIONS OF LIFT CURVE SLOPE WITH MACH NUMBER - NACA-0012;  
CORRECTED SOLID WALL DATA

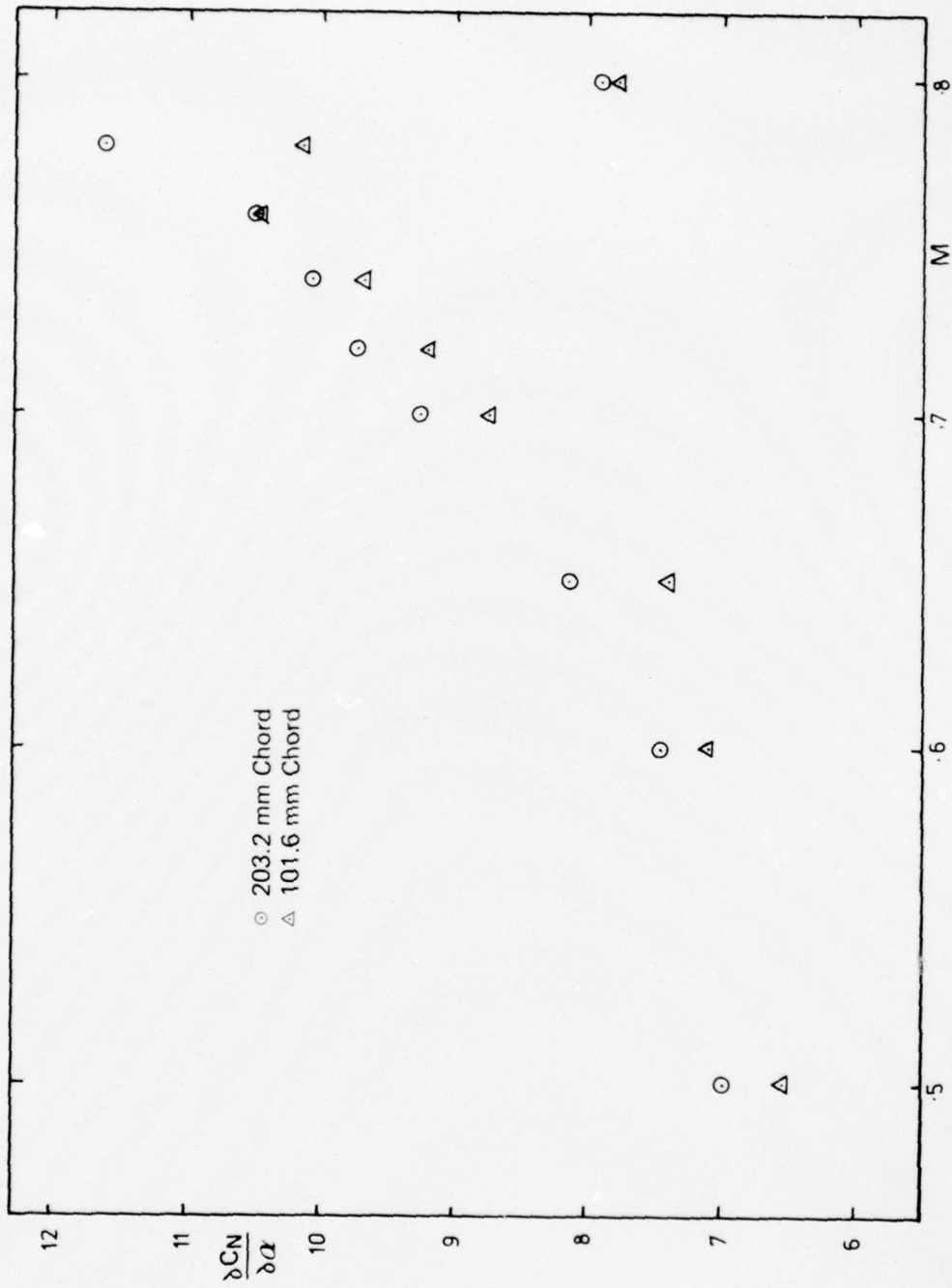


FIG. 7 VARIATION OF LIFT CURVE SLOPE WITH MACH NUMBER - BGK-1;  
 UNCORRECTED SOLID WALL DATA

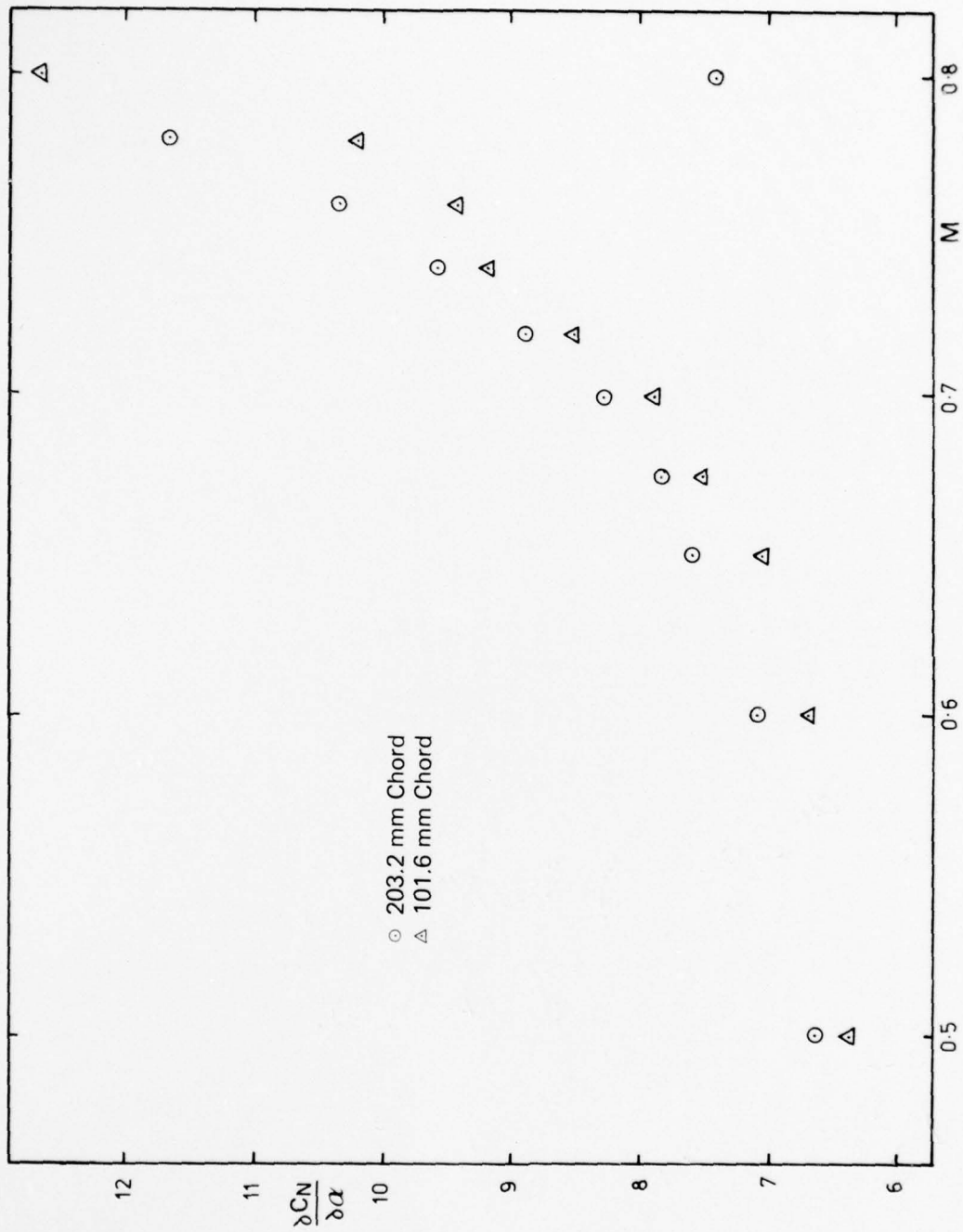


FIG. 8 VARIATION OF LIFT CURVE SLOPE WITH MACH NUMBER - NACA-0012;  
UNCORRECTED SOLID WALL DATA

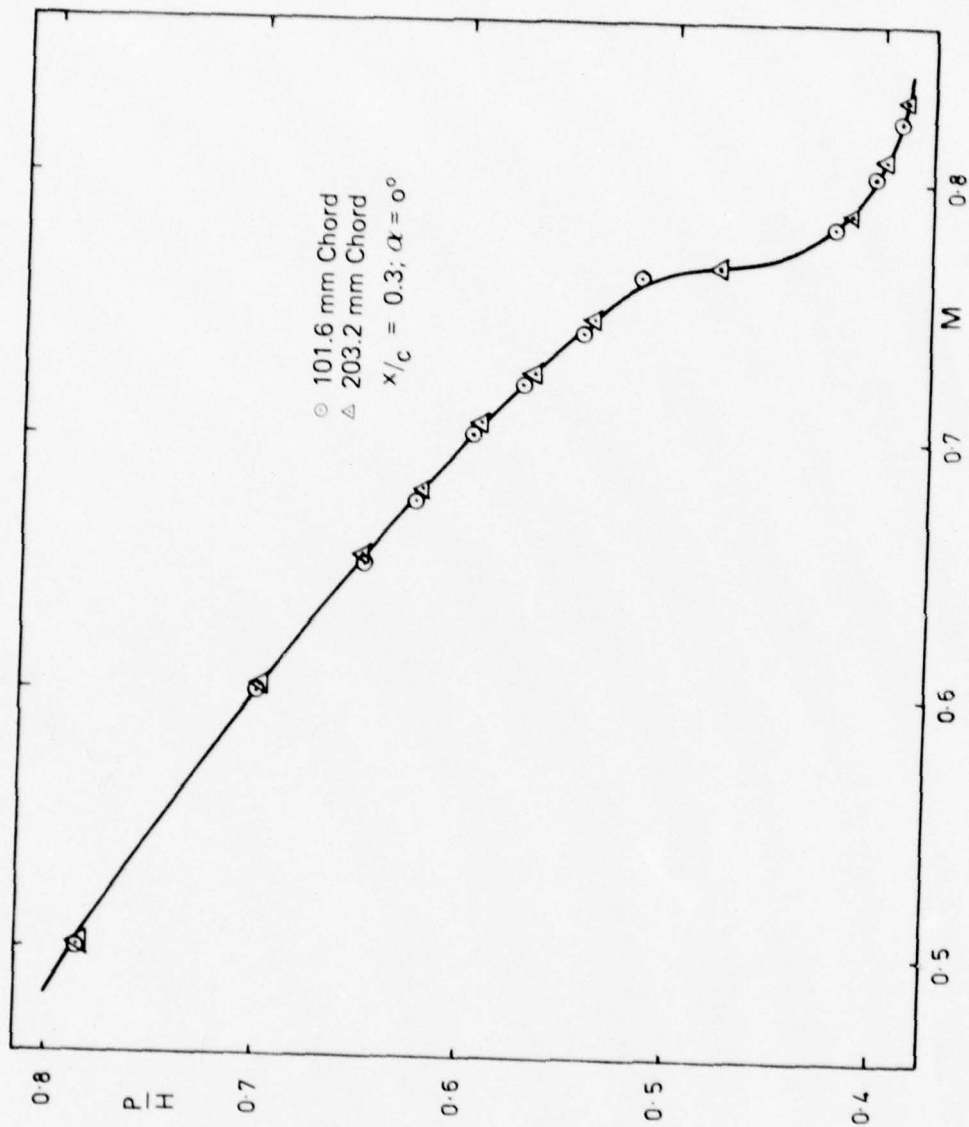


FIG. 9 VARIATION OF PRESSURE RATIO WITH MACH NUMBER - NACA-0012;  
CORRECTED SOLID WALL RESULTS

As suggested in Reference 7, the existence of a design pressure distribution for the BGK-1 section also provides a convenient reference point for the study of wind tunnel wall interference. The experimental design distributions have been found to be quite sensitive to small changes in  $M$  and  $\alpha$ , and such a reference point would appear to be well defined. If the results could be made free of interference effects, the conditions at which the design pressure distribution was obtained for each model should be the same (since viscous effects should be in the same order for both) although this condition would not be expected to agree with that found from inviscid theory. Applying linear theory to the BGK-1 design pressure distribution results from the solid wall tests we obtain the corrected design point conditions as tabulated below.

$c$ (mm)	Uncorrected				Corrected			
	$M$	$\alpha$	$C_N$	$C_m$	$M$	$\alpha$	$C_N$	$C_m$
101.6	0.753	0.60°	0.544	-0.115	0.755	0.60°	0.538	-0.113
203.2	0.748	0.55°	0.560	-0.124	0.755	0.56°	0.536	-0.118

Again the agreement between the two models is excellent. The existence of a single design condition relevant to both models is further supported by the close agreement between the experimental design pressure distributions, as shown in Figure 10.

Overall, the solid wall data corrected by linear theory shows very satisfactory agreement. It is therefore to be expected that the corrected results will provide fairly close to interference free data.

#### 4.2 Slotted Wall Results

In the slotted wall case, the tunnel walls are characterized by two non-dimensional parameters— $F$  which is a unique function of the geometry of the slots, and  $P$  (the "porosity factor")—usually considered as the ratio  $\beta/P$ , which appears in the full homogeneous boundary condition (3.2) to allow for viscous effects in the slots. The parameter  $F$  is fairly easily determined, the only problem being whether to take the finite thickness of the slats into account.  $P$  or  $\beta/P$  on the other hand must be determined empirically and its definition is the basic problem encountered in the application of subsonic linear theory to slotted wall wind tunnels.

Considering firstly the slot geometry parameter  $F$ , from Equation (3.3)

$$F = \frac{2d}{\pi h} \ln \operatorname{cosec} \frac{\pi a}{2d}$$

For the slotted test section walls used in the present tests

$$a = 12.7 \text{ mm}$$

$$b = 533 \text{ mm}$$

$$h = 808 \text{ mm}$$

and

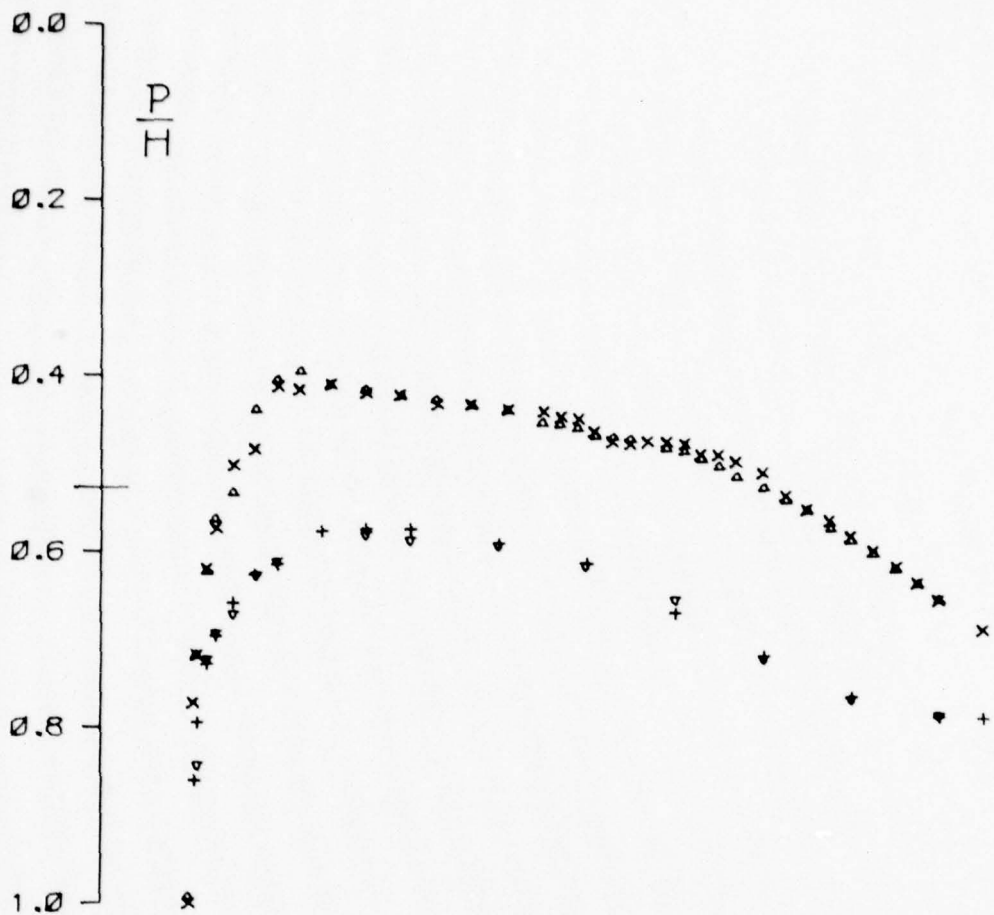
$$d = b/N = 76.1 \text{ mm } (N = 7)$$

giving

$$F = 0.0810.$$

If the finite thickness of the slats ( $l = 2.54 \text{ mm}$ ) is taken into account, then from Equation (3.59) we obtain  $F = 0.119$ .

Turning now to the viscous flow parameter  $\beta/P$ , there are three classes of methods, all basically experimental, which have been used for its determination. They are:



+ x BGK-1 2Ø3.2MM CHORD SOLID WALLS CORRECTED  
M= .755 AL= 0.56 CN= 0.536 CM=-0.118 R= 1.653

v Δ BGK-1 1Ø1.6MM CHORD SOLID WALLS CORRECTED  
M= .755 AL= 0.60 CN= 0.538 CM=-0.113 R= 0.832

FIG. 10 COMPARISON OF BGK-1 DESIGN PRESSURE DISTRIBUTIONS;  
SOLID WALL DATA

direct measurement;  
 indirect measurement;  
 comparison of measurements.

Direct measurement consists of the calibration of actual or sample wind tunnel walls by the measurement of the pressure drop across the wall for various cross flow velocities and free stream Mach numbers. This method is more suitable for use with perforated walls, and has been extensively used for this purpose at the Arnold Engineering Development Centre (AEDC).<sup>22</sup>

A method of indirect measurement, originating at the National Lucht-en Ruimtevaart-laboratorium (NLR),<sup>23</sup> consists of an aerofoil drag balance method in which all non-interference drag contributions are either measured or calculated, and are then compared to the drag obtained from wake rake measurements. The "porosity factor"  $\beta/P$  may then be obtained for each Mach number and angle of attack by subtraction. This method suffers from the disadvantages of requiring unrealistically accurate measurements of profile drag to be obtained from aerofoil surface pressure measurements and the difficulty of accurately estimating skin-friction drag.

The methods allowing the determination of  $\beta/P$  from comparative measurements usually consist of either testing a single aerofoil model in a test section in which the wall conditions may be varied from closed, through several wall permeabilities, to a condition comparable to that of an open jet, or of testing two or more geometrically similar models of the same aerofoil section in a single ventilated-wall test section. Such methods, because of their straightforward application, are by far the most popular.

The approach adopted here will also be one of comparative measurements, but because of the unusual set of test results available, the approach will be somewhat different from that usually followed. In the previous section it was shown that the solid wall results, corrected according to linear interference theory, provide a set of measurements close to being free of the effects of interference. The approach will be to accept these measurements as being truly "interference free" and to use them to, in effect, calibrate the slotted walls in finding the applicable value of  $\beta/P$ . The basis for comparison will be the variation of corrected solid wall lift curve slope (at zero lift) with Mach number, and then to attempt to find a value of  $\beta/P$  which minimizes the deviations of the corrected slotted wall lift curve slopes from these "interference free" measurements. For this purpose "mean curves" shown on Figures 5 and 6 have been drawn as lines of best fit to the corrected solid wall data. To quantify the agreement between the slotted wall data and these mean curves, we define a root mean square deviation ( $\Delta_{rms}$ ) given by

$$\Delta_{rms} = \left( \frac{\sum_0^n (K_r - K_{cf})^2}{n} \right)^{1/2} \quad (4.1)$$

where  $K_{cf}$  are the corrected solid wall lift curve slopes taken from the mean curve, and  $K_r$  are the slotted wall lift curve slopes, the summation being taken over the  $n$  values of Mach number at which measurements were made for each model of each aerofoil section. Care was taken to ensure that the value of  $K_{cf}$  was interpolated from the mean curves to correspond to the corrected Mach number of the slotted wall values  $K_r$ . Each model of each aerofoil section was treated separately to ensure that any trends due to either varying chord or aerofoil section would be apparent.

As for the solid wall results, the lift curve slopes were corrected by the application of Equation (3.58). In this case, however, the interference parameters  $\delta_0$  and  $\delta_1$  given by (3.31) now become functions of  $F$  and  $\beta/P$  and are found by substituting from (3.23) and (3.24) into (3.31). Similarly the blockage factor,  $\epsilon_B$ , which determines  $G$  (the ratio of corrected to uncorrected kinetic pressure), is related to  $F$  and  $\beta/P$  via Equations (3.12), (3.17) and (3.37).

The variation of the root mean square deviation  $\Delta_{rms}$  with  $\beta/P$  is shown in Figure 11 for the four aerofoil models. The values of  $\beta/P$  giving the minimum deviation for each model are also noted on the figure. Although there is some variation in this value between the models, notably for the 101.6 mm chord NACA-0012 model, the results indicate a single value of  $\beta/P$ , appropriate to the slotted walls used, with a value of about 0.4. It is interesting to note the steeper slopes about the minima obtained for both the larger chord models. This is indicative of the greater dependence of the larger chord model results on  $\beta/P$  due to the presence of increased interference effects.

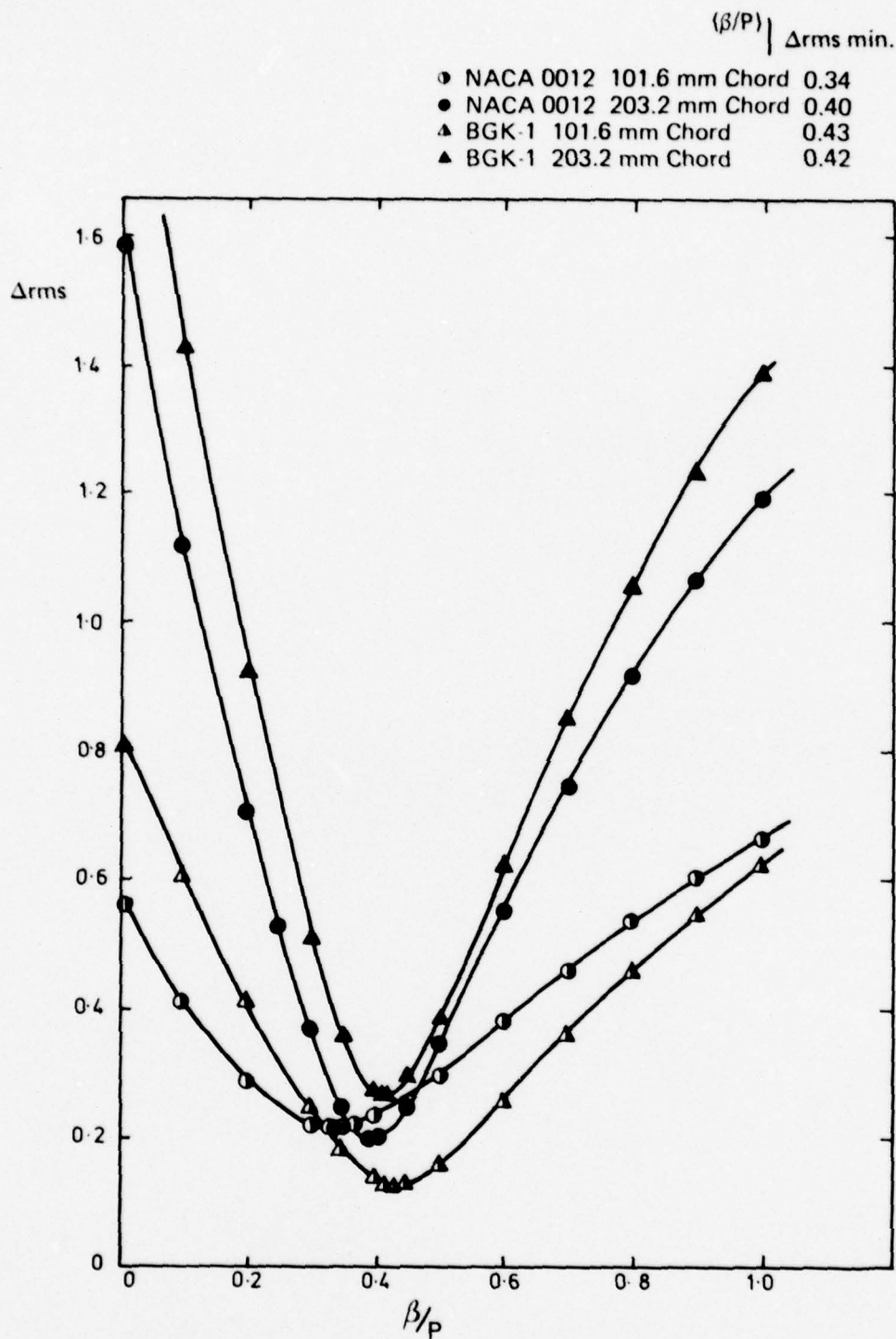


FIG. 11 VARIATION OF ROOT MEAN SQUARE DEVIATION WITH  $\beta/P$  — CLASSICAL LINEAR THEORY

These calculations were repeated with the value of  $F$  (0.119) taking into account the finite thickness of the slats. The indicated value of  $\beta/P$  differed by only a few per cent from the original value (0.4) and the value of  $F$  was therefore retained at 0.081 for all future work.

Corrected lift curve slopes were then calculated using linear theory with the value of  $\beta/P$  held constant at 0.40. These corrected values are plotted in Figure 12 for the BGK-1 section and in Figure 13 for the NACA-0012 together with the mean curves of the corrected solid wall results for comparison. Apart from the low Mach number range for the BGK-1 section, the slotted wall results now fall within  $\pm 2$  to  $\pm 3\%$  of the corrected solid wall curves. Considering that the increase in lift curve slope over the uncorrected results (which are shown in Figures 14 and 15 for comparison) amounts to between 25% and 50% for the 203.2 mm chord models and between 15% and 25% for the 101.6 mm chord models, this agreement is remarkably good.

Once again, the zero lift NACA-0012 results provide a useful check on the blockage corrections in the form of pressure ratio ( $p/H$ ) variation with Mach number at constant chordwise position. If we again take the corrected solid wall data as being interference free, and provided that a given pressure at a fixed point on the model represents a given flow on the model, i.e. provided the blockage effect produces no distortion at the model and can be applied as a correction to longitudinal velocity, then the differences,  $\Delta M$ , on horizontal intercepts between the corrected solid wall curve and the uncorrected slotted wall curve give the blockage effects on Mach number for the slotted walls. A typical plot, for  $x/c = 0.03$  is shown in Figure 16. From this plot, at a Mach number of 0.75 we see that  $\Delta M$  is approximately  $-0.009$ , compared with  $-0.002$  predicted by linear theory. Linear theory clearly underestimates the blockage effect by a significant amount, and this is true throughout the Mach number range.

By plotting these  $\Delta M$ s against Mach number we may obtain an estimate of the actual blockage effects on Mach number as a function of Mach number for the slotted walls. If similar curves are plotted for various chordwise positions a check can be made for the existence of significant flow distortions, since in that case it would be expected that the shape of these curves would vary in an ordered manner with chordwise position. Such a series of results are plotted in Figure 17, and although significant scatter is present, the scatter is largely random, the result of experimental errors rather than any trend due to significant flow distortion, supporting the assumption that blockage can be allowed for by a simple correction to free-stream velocity. Also plotted on the figure are the curves predicted by linear theory for the case of a slotted wall with  $\beta/P = 0.40$  and an open jet. It is evident that even the open jet case underestimates the blockage by a factor of four or five. This would suggest that the present slotted walls, at least as far as blockage is concerned, are more "open" than an open jet. Similar results have been found by Pearcey *et al.*<sup>24</sup> and some possible reasons for this discrepancy will be discussed in a later section.

Classical linear theory suggests that the variation with Mach number of the differences shown in Figure 17 should be of the form

$$\frac{\Delta M}{M} = \left(1 + 0.2M^2\right) \frac{e}{\beta^3} \quad (4.2)$$

where  $e$  is an empirical blockage factor. This empirical blockage factor therefore replaces  $\epsilon_B$  in Equation (3.45) and embraces the solid blockage and wake blockage, where it exists, both now factored by  $1/\beta^3$ . Again following classical theory, we will assume that  $e$  is related to the dimensions of the test section and model by

$$e = E \frac{A_e}{h^2} \quad (4.3)$$

where  $A_e$  is the effective model cross-sectional area given by (see Equation (3.41))

$$A_e = A \left(1 + 1.2\beta \frac{t}{c}\right) \quad (4.4)$$

and  $E$  should be a constant depending only on the properties of the particular test-section walls. Equation (4.2) is plotted in Figure 17, and the value of  $E$  giving the closest agreement with the data is about  $-1.25$ . Unfortunately, the data from the 101.6 mm chord model of the NACA-0012, which could have provided an independent check on the value of  $E$  from a similar process, contained too much experimental scatter to allow any meaningful deductions. (It should be

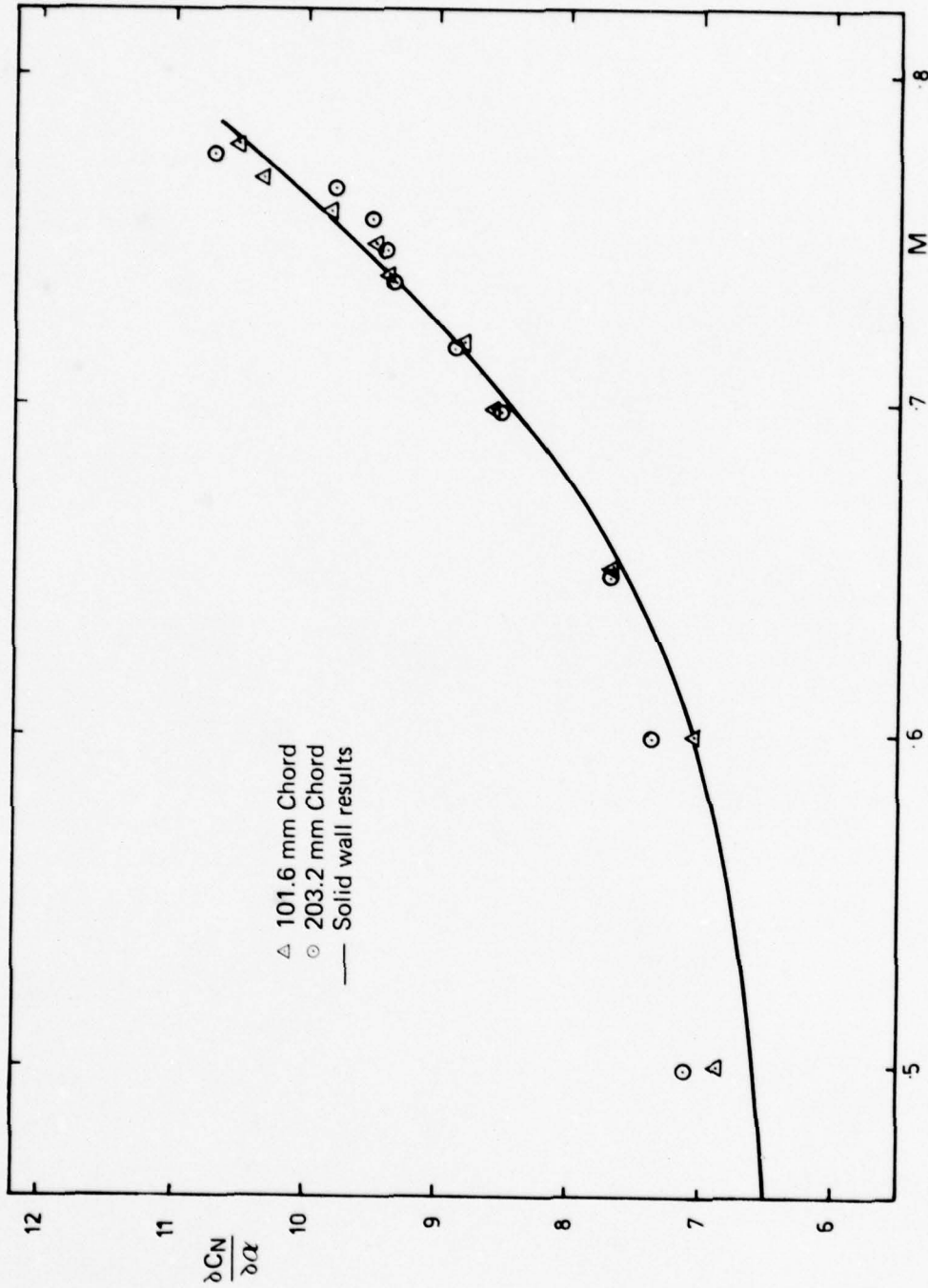


FIG. 12 VARIATION OF LIFT CURVE SLOPE WITH MACH NUMBER - BGK-1;  
CORRECTED SLOTTED WALL DATA

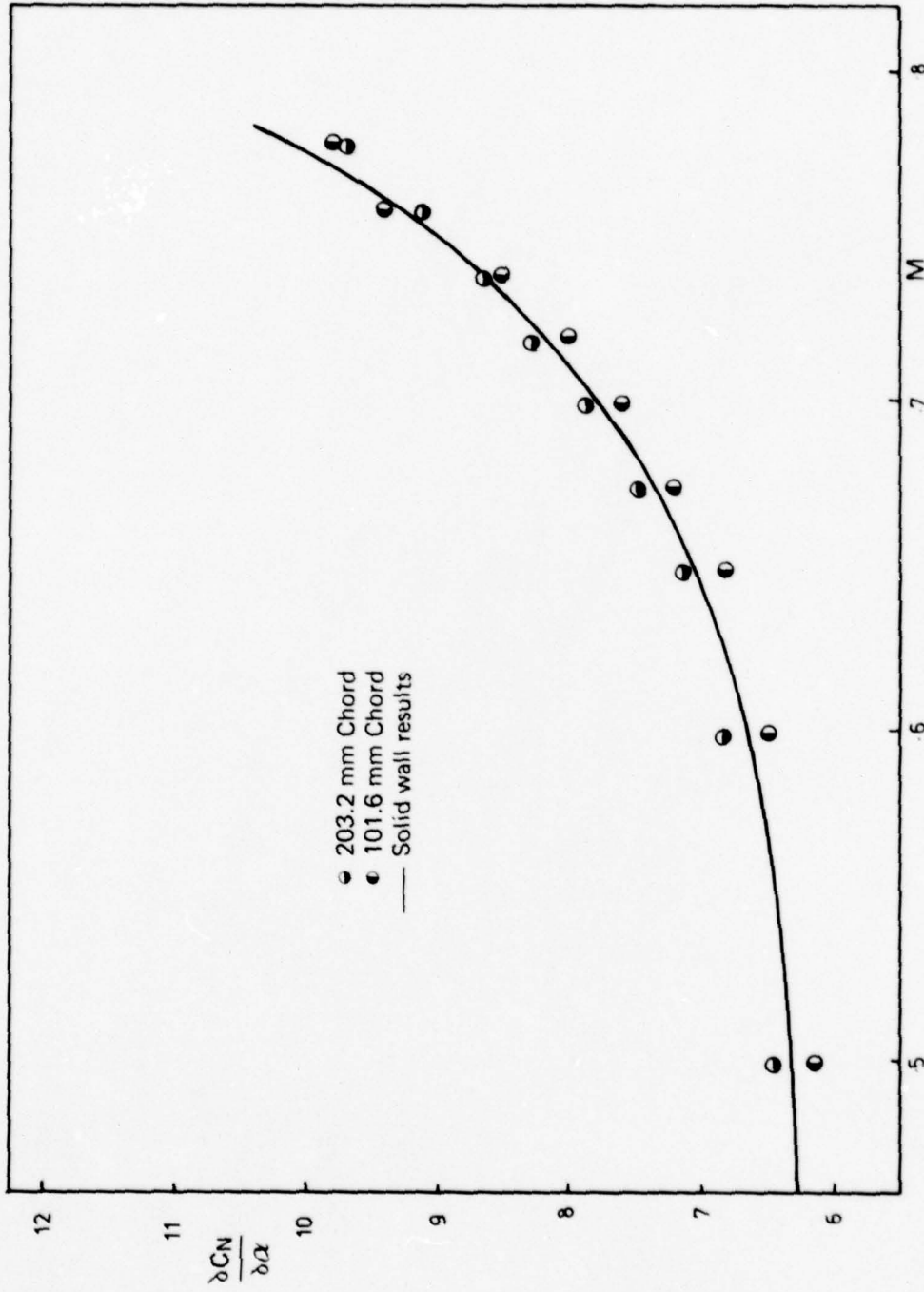


FIG. 13 VARIATION OF LIFT CURVE SLOPE WITH MACH NUMBER - NACA-0012;  
CORRECTED SLOTTED WALL DATA

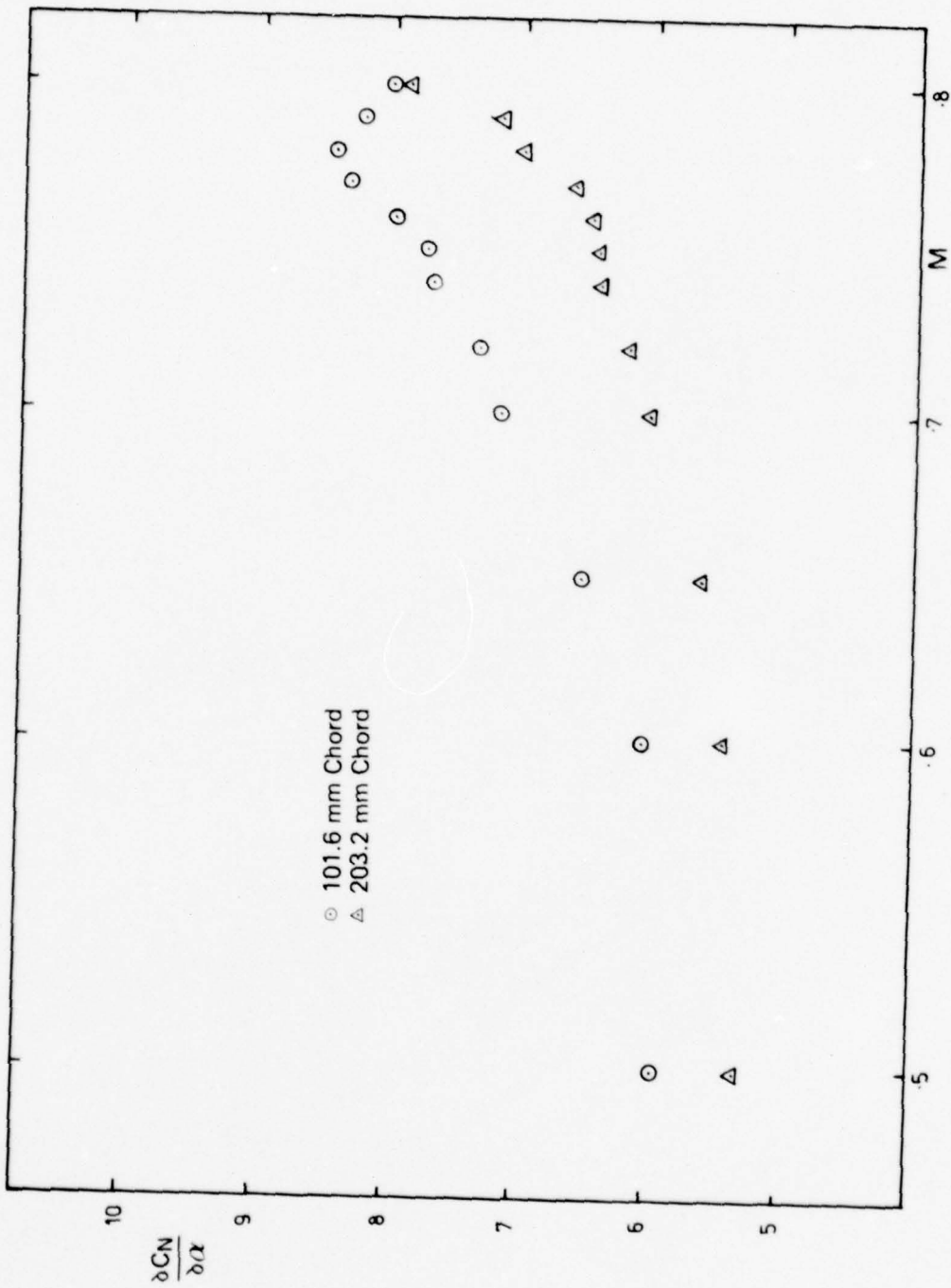


FIG. 14 VARIATION OF LIFT CURVE SLOPE WITH MACH NUMBER - BGK.1;  
UNCORRECTED SLOTTED WALL DATA

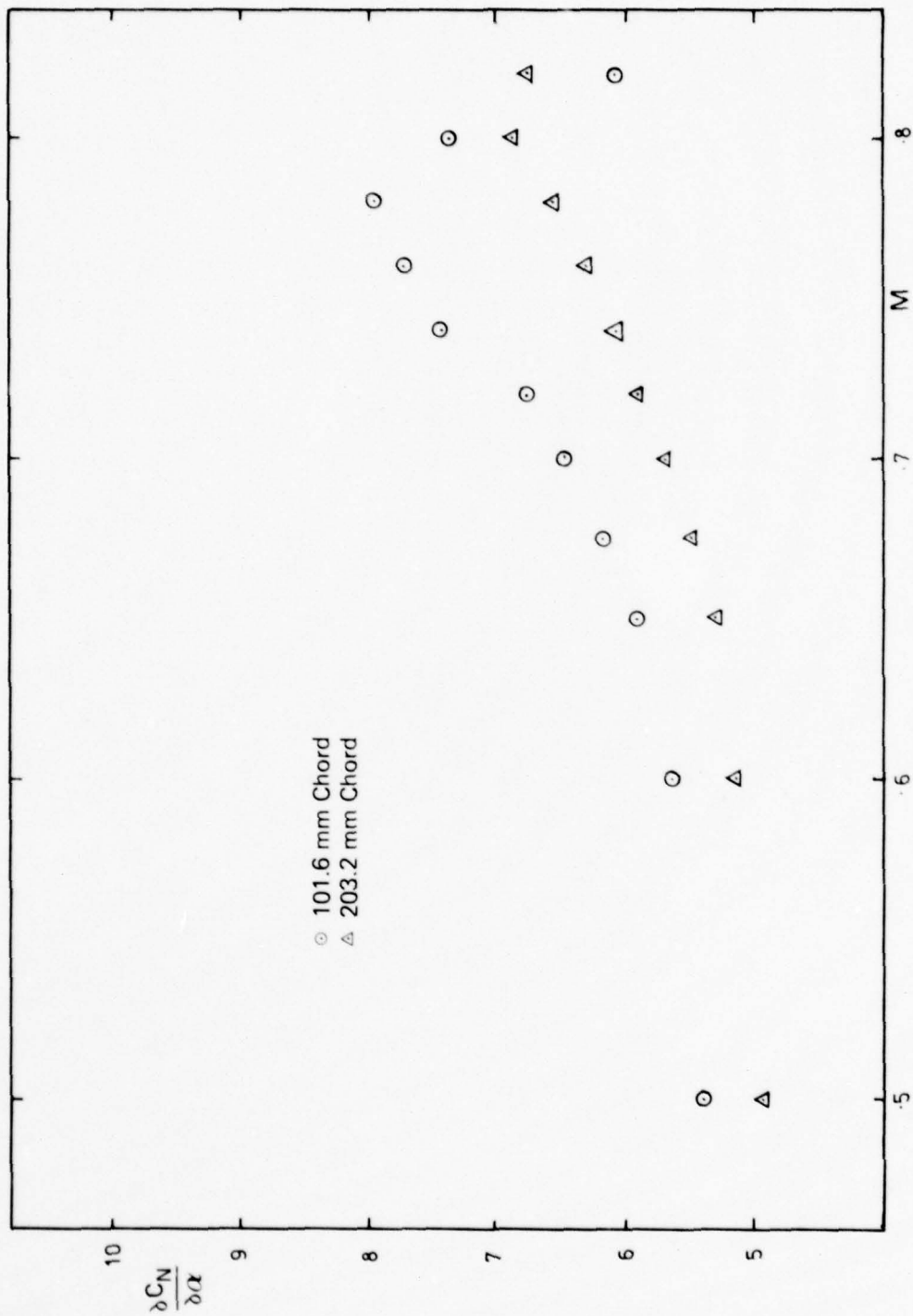


FIG. 15 VARIATION OF LIFT CURVE SLOPE WITH MACH NUMBER - NACA-0012;  
UNCORRECTED SLOTTED WALL DATA

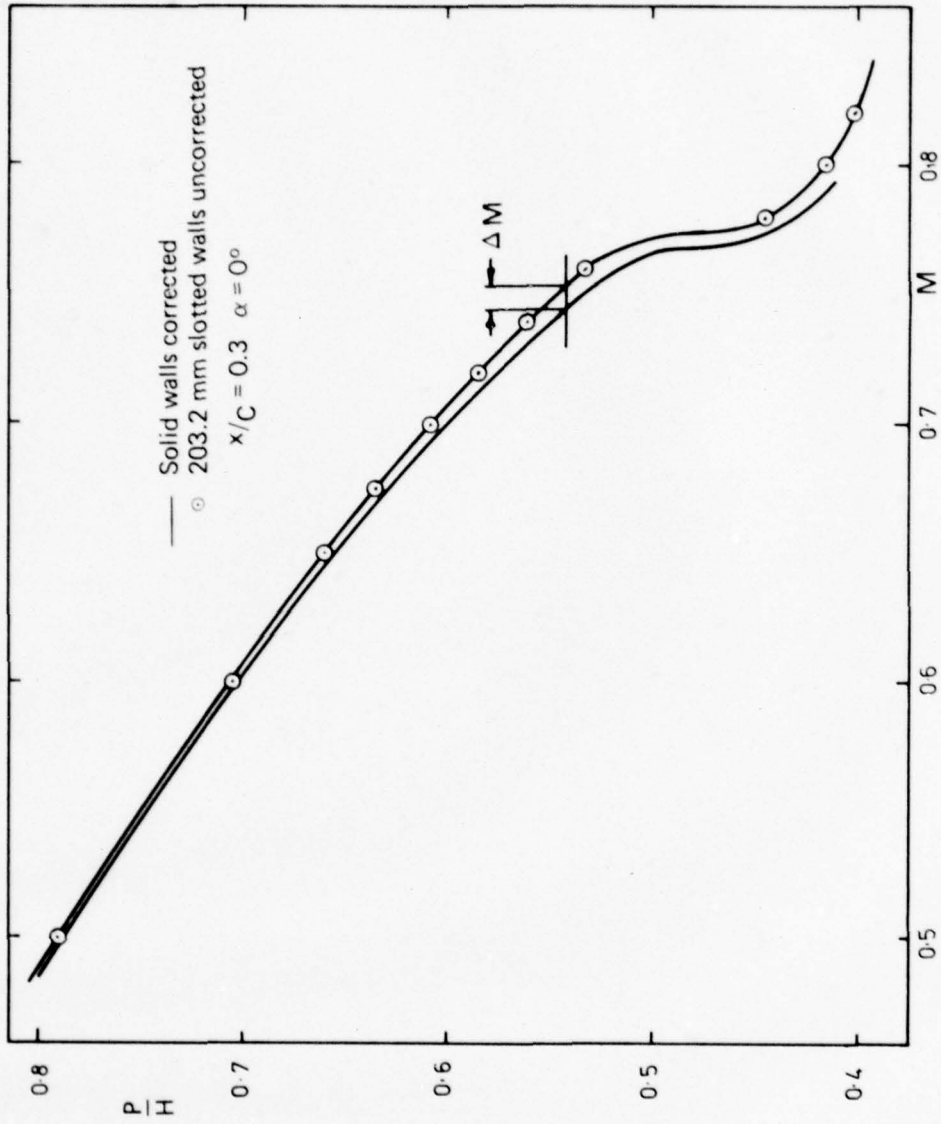


FIG. 16 VARIATION OF PRESSURE RATIO WITH MACH NUMBER - NACA-0012; COMPARISON OF SLOTTED WALL DATA WITH CORRECTED SOLID WALL DATA

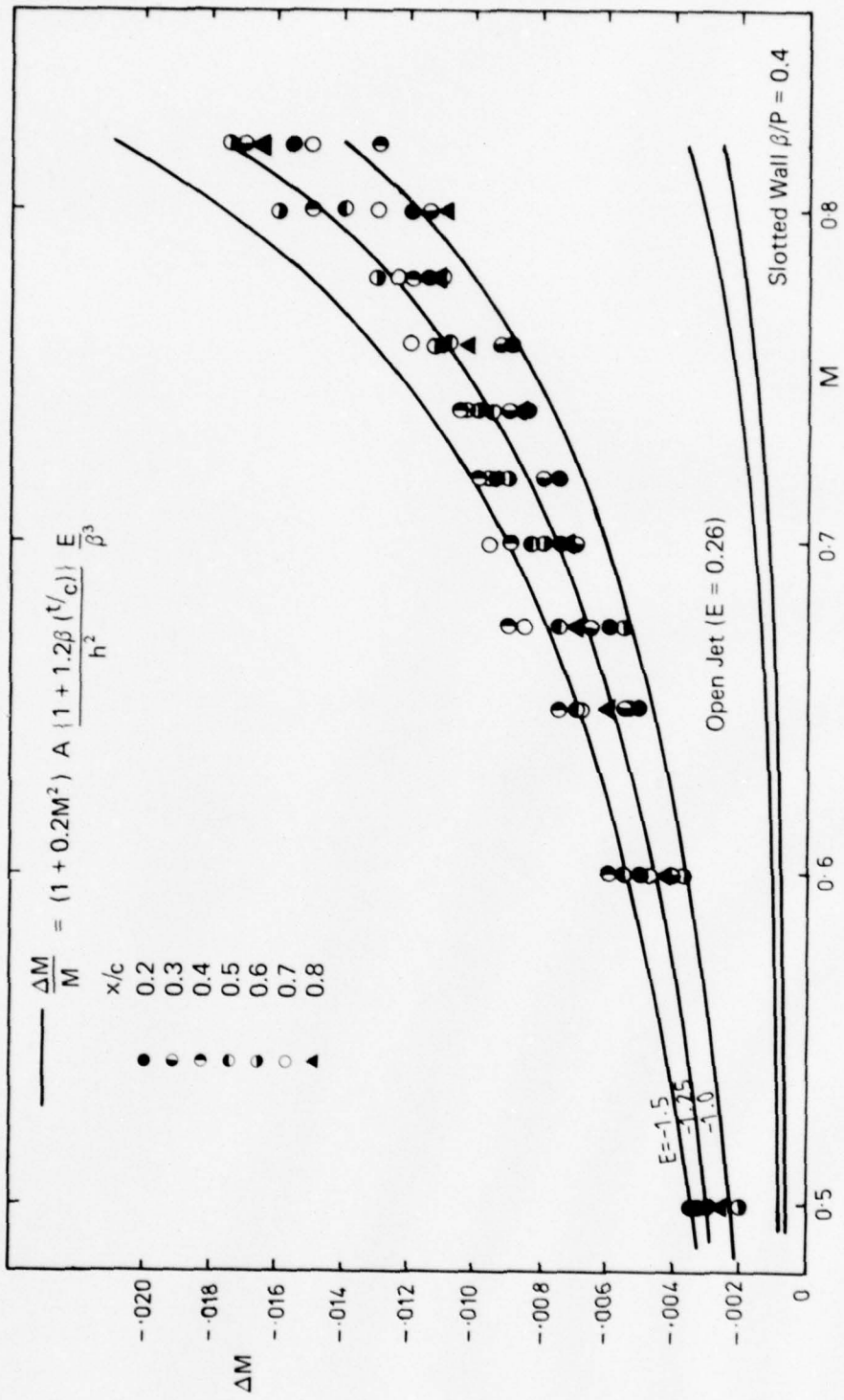


FIG. 17 VARIATION OF MACH NUMBER INCREMENT WITH MACH NUMBER - NACA-0012; SLOTTED WALL DATA

noted that the  $\Delta M$ s predicted from Equation (4.2) would be a factor of 4 smaller than those of the 203.2 mm chord model.) It is worth noting that values of  $E$  corresponding to solid walls and to slotted walls with a value of  $\beta/P$  of 0.4 (calculated by assuming the value of wake blockage relevant to a Mach number of 0.75) are 0.50 and -0.17 respectively, and for the case of an open jet (where the wake blockage is zero) the value of  $E$  is -0.26. It is seen that the empirical value of  $E$ , -1.25, is almost 5 times the open jet value.

This empirical blockage correction, in the form of Equation (4.2), may be combined with the normal linear theory for lift interference to form a "semi-empirical" correction scheme for the slotted wall results. The results of the application of this scheme to correct the zero-lift lift curve slopes are shown in Figure 18 where the root mean square deviations from the means of the corrected solid wall results are plotted against  $\beta/P$ . Although there is somewhat more scatter in the values of  $\beta/P$  giving minimum deviation, plots of the corrected lift curve slopes shown in Figures 19 and 20, using an average value of  $\beta/P$  of 0.51, show similar scatter to those corrected by complete linear theory.

As for the solid wall results, the experimentally determined design pressure distributions found for the BGK-1 section may again be used as a check on the validity of the corrections. The design point data, obtained from Reference 7 have been corrected by the application of the "semi-empirical" scheme developed above, with  $E = -1.25$  and  $\beta/P = 0.51$ . (The values of lift interference parameters  $\delta_0$  and  $\delta_1$  obtained with such a scheme are -0.16 and -0.05 respectively.) The corrected slotted wall results, together with the corrected solid wall results for comparison, are tabulated below.

Wall type	c (mm)	Uncorrected				Corrected			
		M	$\alpha$	$C_N$	$C_m$	M	$\alpha$	$C_N$	$C_m$
Slotted	101.6	0.763	1.40°	0.529	-0.112	0.758	0.77°	0.536	-0.113
	203.2	0.784	1.70°	0.506	-0.122	0.760	0.50°	0.533	-0.129
Solid	101.6	0.753	0.60°	0.544	-0.115	0.755	0.60°	0.538	-0.113
	203.2	0.748	0.55°	0.560	-0.124	0.755	0.56°	0.536	-0.118

Again the agreement between the two models is quite good, as is the agreement between the corrected results from both solid and slotted wall tests. The agreement between the pressure distributions for the experimental design condition of each model, plotted in Figure 21, is not as good as that between the two solid wall distributions. Evidence of a loss of lift from a decrease in lower surface pressure is apparent for the 203.2 mm chord model up to mid chord, with an increase in lift from higher upper surface suction apparent thereafter. This behaviour is consistent with the presence of significant streamline curvature for this model. It is surprising that such an effect should be visible in the slotted wall results and not in those from the solid walls, since the relative magnitudes of the lift interference parameter  $\delta_1$ , which characterizes streamline curvature, would indicate that the streamline curvature in solid walls should be more than double that in the slotted walls. This could be interpreted to mean that the streamline curvature in the slotted walls is seriously underestimated by linear theory, but the amount of data presently available does not allow any firm conclusion to be made. To ensure that this effect was not limited to the results from the BGK-1 section, a similar comparison was sought from the NACA-0012 section results. Such a comparison is complicated by the necessity of finding two sets of results with the same corrected values of Mach number and incidence. Two such cases (for  $M_f = 0.767$ ), are plotted in Figure 22, and although not to the same extent as in the BGK-1 case, evidence of streamline curvature is indeed present, masked somewhat by the slightly higher corrected incidence and hence slightly higher lift for the slotted wall result. The agreement in corrected Mach number for these two cases also provides an opportunity for the comparison of the corrected variation of lift coefficient with incidence. Figure 23 shows quite good agreement between the results from

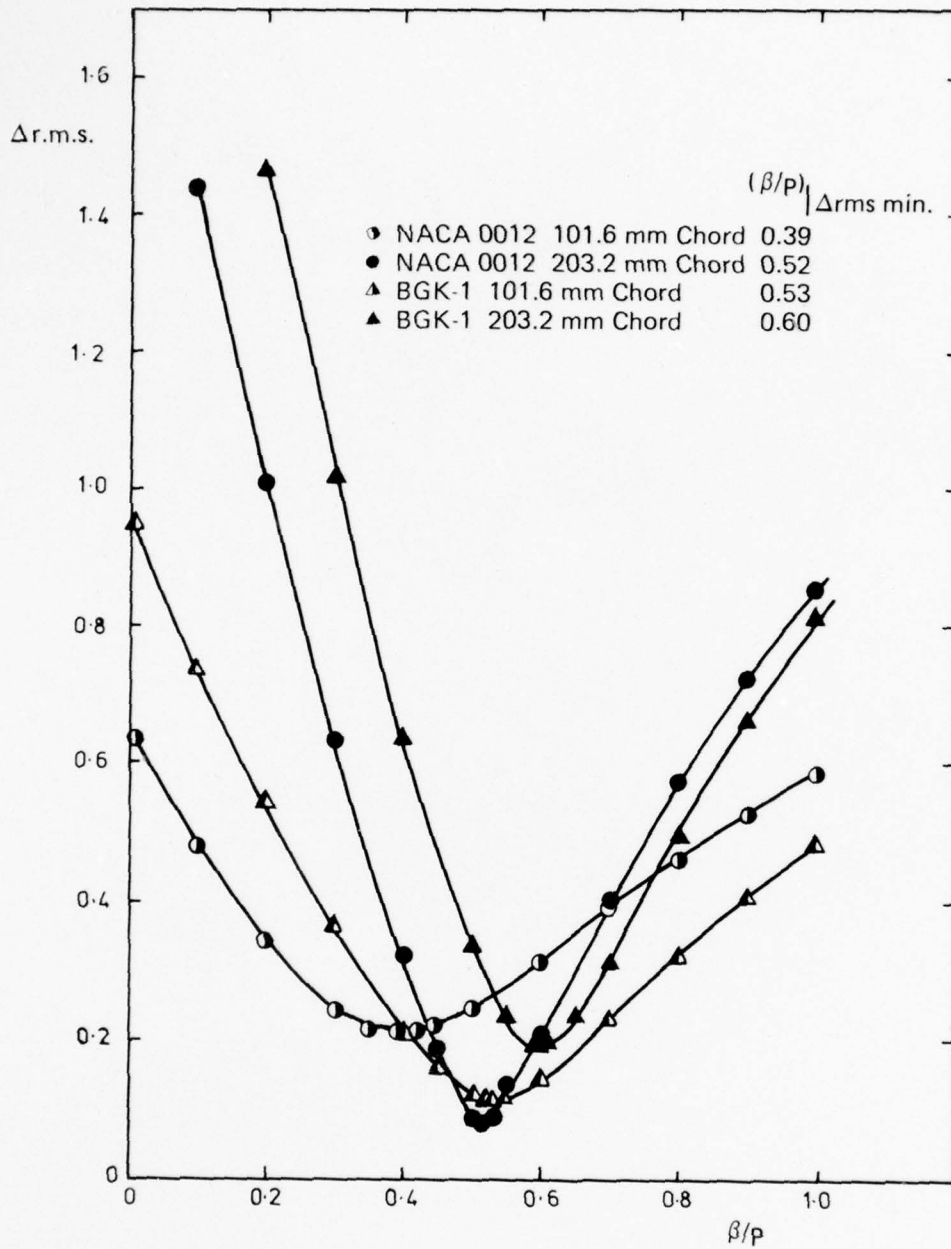


FIG. 18 VARIATION OF ROOT MEAN SQUARE DEVIATION WITH  $\beta/p$ ; LINEAR THEORY WITH EMPIRICAL BLOCKAGE

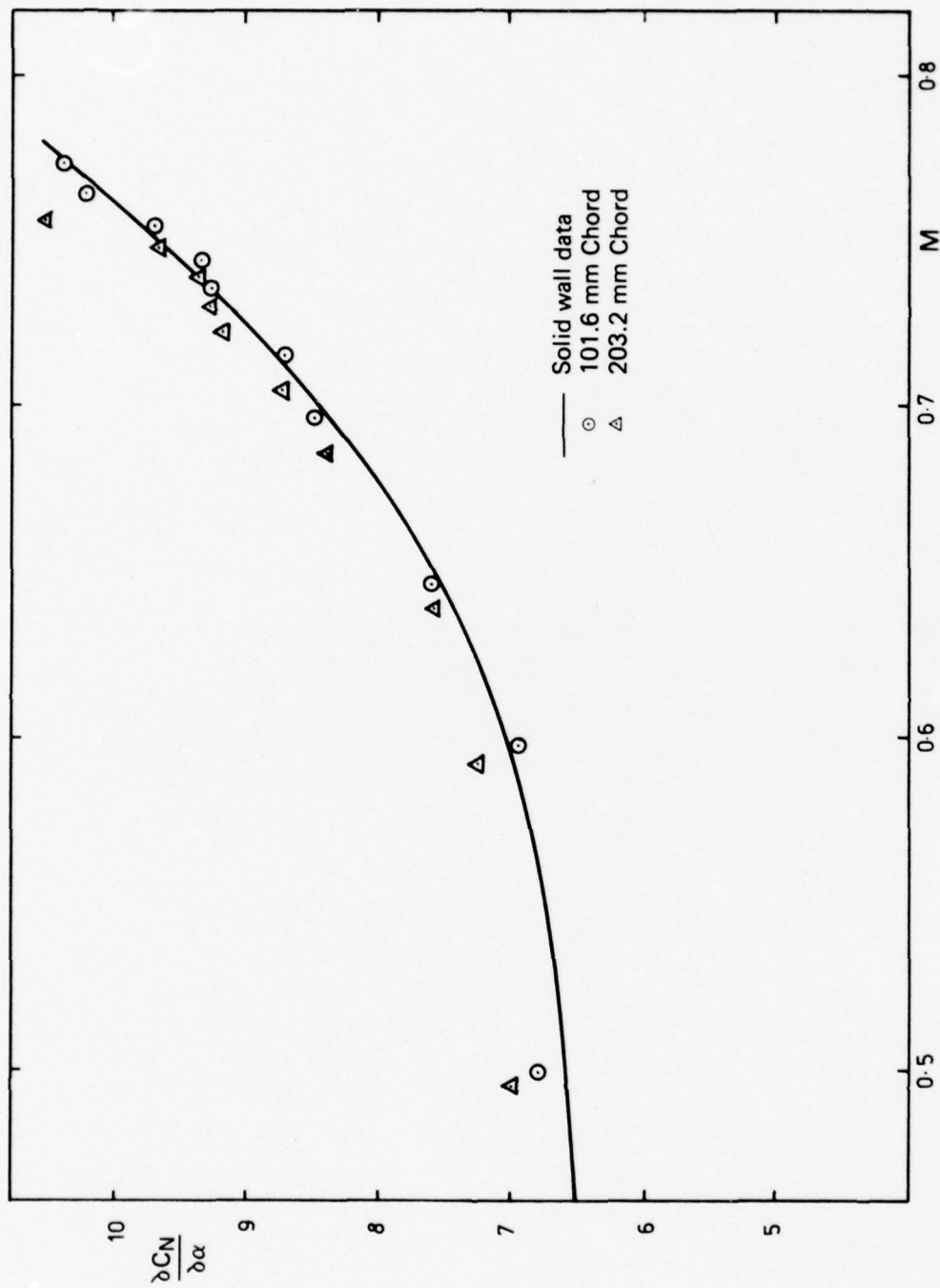


FIG. 19 VARIATION OF LIFT CURVE SLOPE WITH MACH NUMBER - BGK-1;  
SLOTTED WALL DATA WITH EMPIRICAL BLOCKAGE CORRECTION

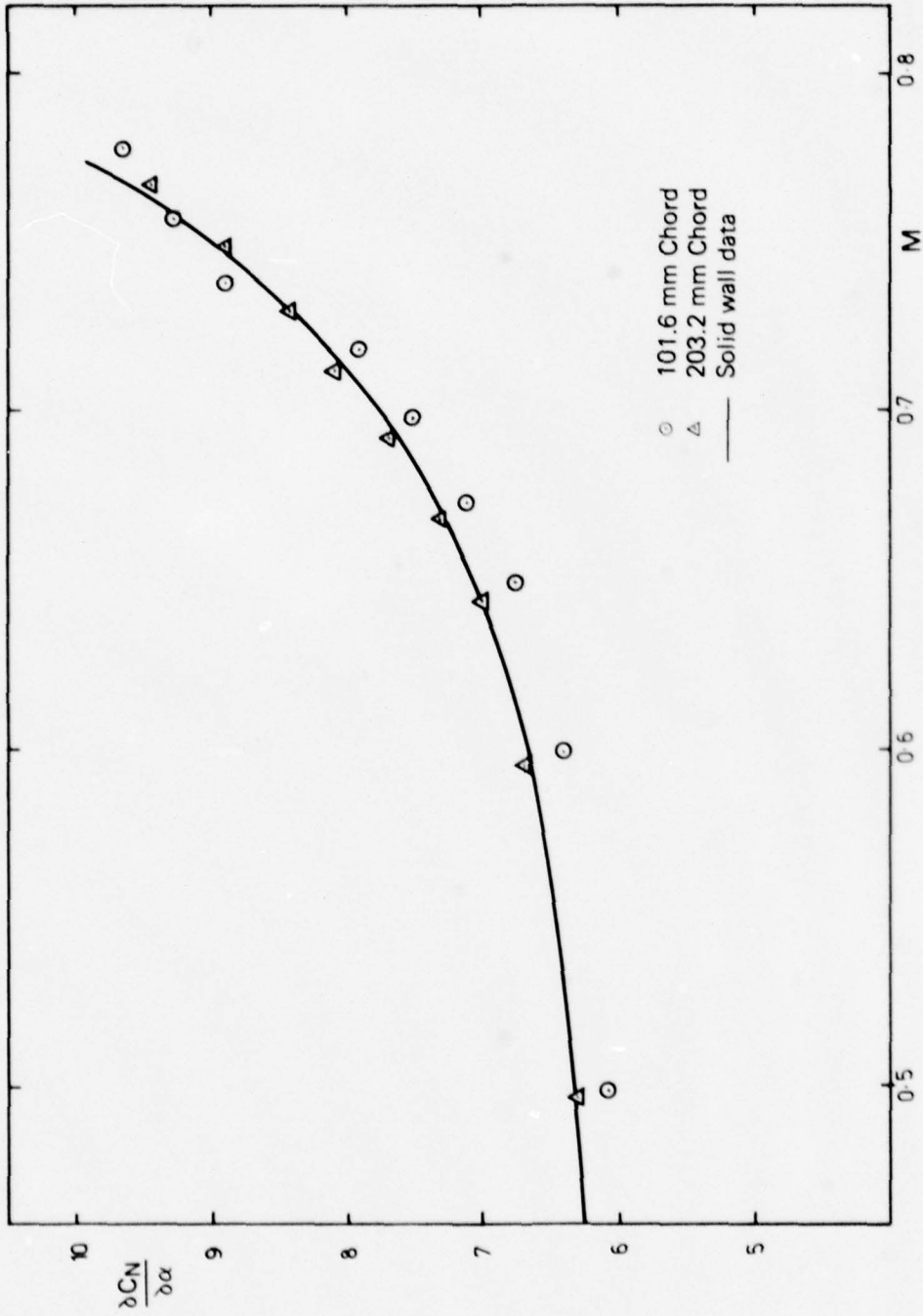
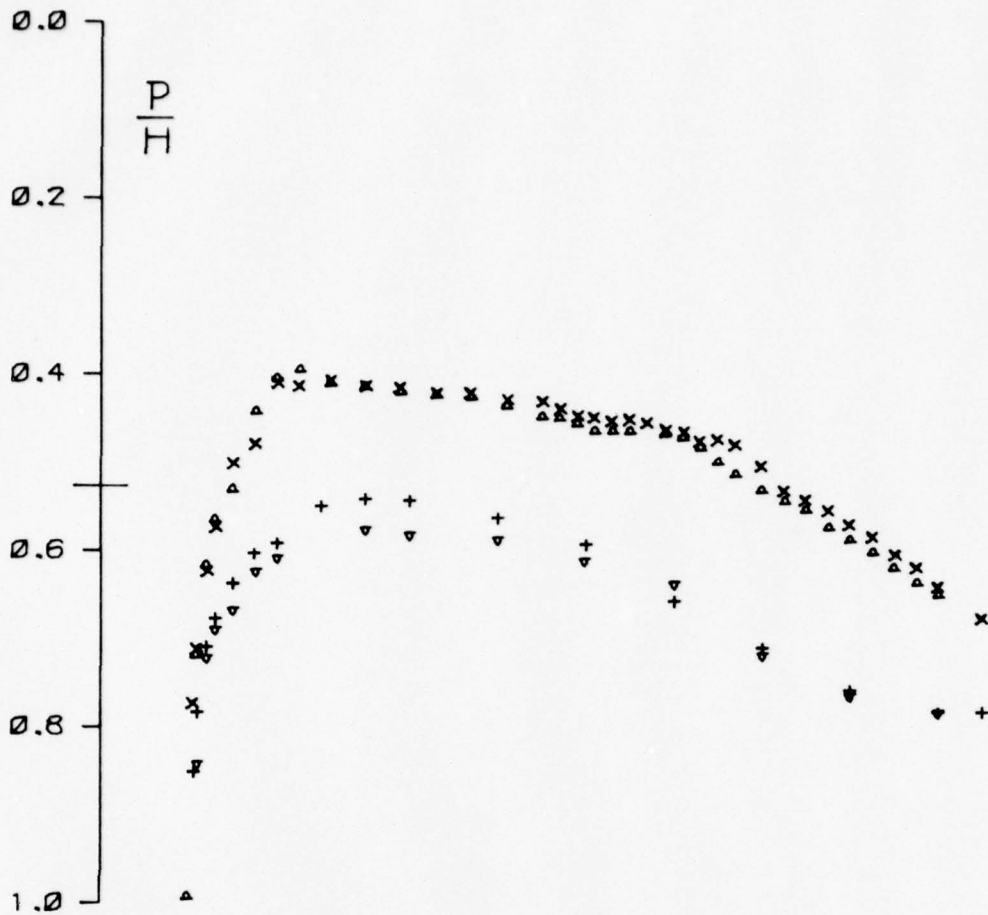


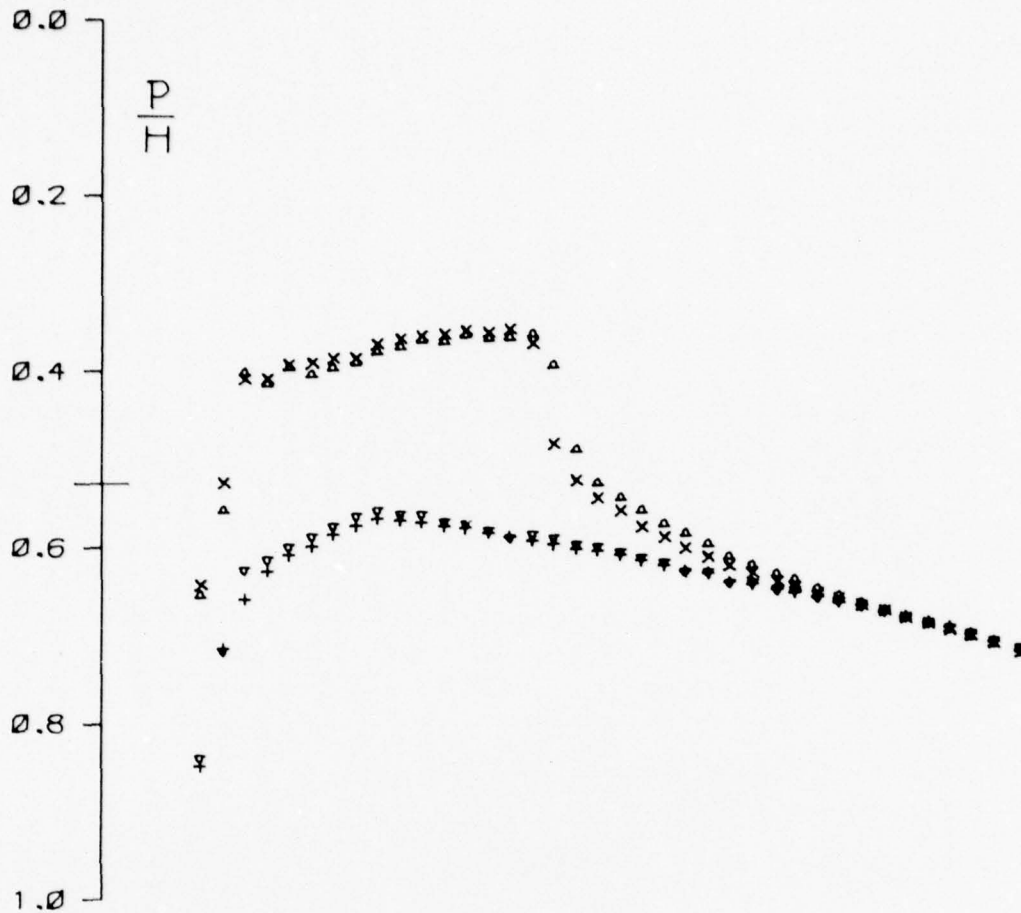
FIG. 20 VARIATION OF LIFT CURVE SLOPE WITH MACH NUMBER - NACA-0012;  
SLOTTED WALL DATA WITH EMPIRICAL BLOCKAGE CORRECTION



+ x BGK-1 203.2MM CHORD SLOTTED WALLS CORRECTED  
M= .760 AL= 0.50 CN= 0.533 CM=-0.129 R= 1.648

∇ Δ BGK-1 101.6MM CHORD SLOTTED WALLS CORRECTED  
M= .758 AL= 0.77 CN= 0.536 CM=-0.113 R= 0.791

FIG. 21 COMPARISON OF BGK-1 DESIGN PRESSURE DISTRIBUTION;  
SLOTTED WALL DATA



+ x NACA 0012 203.2MM CHORD SLOTTED WALLS CORRECTED  
M= .767 AL= 2.19 CN= 0.342 CM= 0.005 R= 1.609

v Δ NACA 0012 203.2MM CHORD SOLID WALLS CORRECTED  
M= .767 AL= 2.06 CN= 0.331 CM= 0.002 R= 1.597

FIG. 22 COMPARISON OF CORRECTED PRESSURE DISTRIBUTIONS -  
NACA-0012; M = 0.767

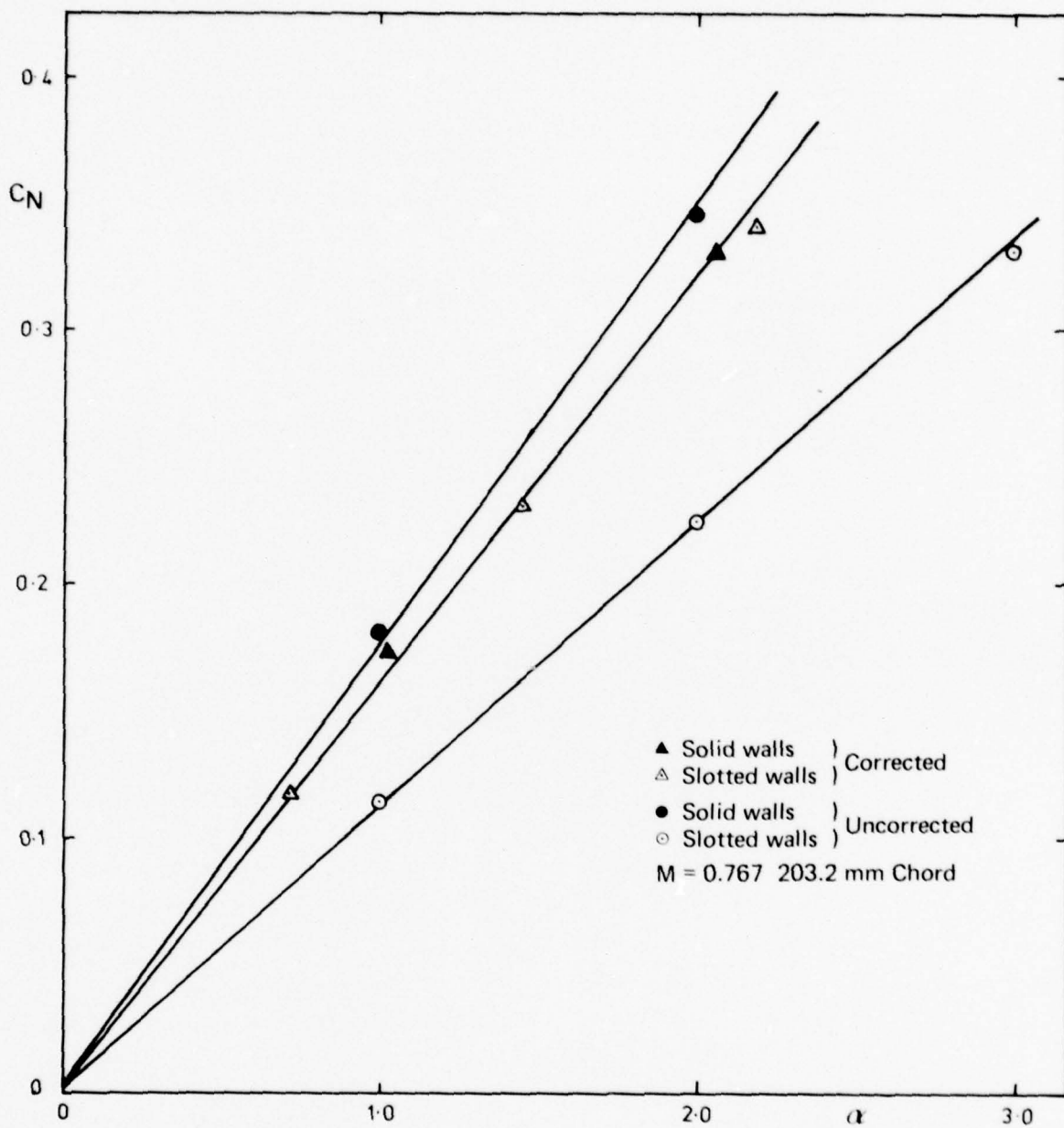


FIG. 23 COMPARISON OF CORRECTED AND UNCORRECTED LIFT CURVES - NACA-0012; M = 0.767

solid and slotted wall tests. The uncorrected curves are also included for comparison. Several similar opportunities for comparison of corrected lift curves are available from the BGK-1 data. Unfortunately no cases exist where the corrected Mach numbers agree between tests on models of different chords. Corrected lift curves for those cases where corrected Mach numbers are closely in agreement are plotted in Figure 24. Again the agreement is quite good. Fortunately each case provides one pair of results for which the corrected angles of incidence are very nearly identical. The pressure distributions corresponding to these pairs are compared in Figures 25, 26 and 27. The agreement between the pressure distributions with a corrected Mach number of 0.705 (Fig. 25) is quite remarkable, the shape and extent of the short supersonic region being reproduced very accurately. The comparison of Figure 26 is interesting, since the conditions of the comparison—a Mach number just below the experimentally determined design value and an angle of incidence just above—are in a region in which the shape of the pressure distributions are found to be extremely sensitive to small changes in Mach number and angle of incidence.<sup>7-9</sup> The agreement obtained in this case significantly increases confidence in the belief that the corrections are producing truly interference free results. The final pair (Fig. 27), for a significantly supercritical Mach number (0.765), again show excellent agreement (considering the small difference in angle of incidence). The fact that classical interference theory, which is not valid under supercritical conditions, still produces such good agreement in this case is, perhaps, one of the more surprising results of the investigation.

As a final check on the validity of the interference corrections, the chordwise position of the upper surface shock on the NACA-0012 at zero incidence may be used. Figure 28 shows the shock positions (arbitrarily defined as the mid-point of the surface pressure rise) for both models of the NACA-0012 in both solid and slotted walls, plotted against uncorrected Mach number. Although there is significant scatter present, there are obvious trends towards increasing deviations with increases in both model size and Mach number. In Figure 29 the shock locations are replotted against Mach number corrected by the application of classical theory to the solid wall results, and Equations (4.2) and (4.3) with  $E = -1.25$  to the slotted wall results. The results are now seen to collapse fairly well to a common curve. It may be argued that if the solid wall results are truly interference free, then such a collapse is inevitable from the method used to determine the value of  $E$ . Nevertheless, such a result is a further indication of the validity of the corrections.

In summary, the application of the complete classical linear interference theory to the slotted wall results leads to fair agreement in lift curve slopes, indicating a value of  $\beta/P$  of 0.4. Linear theory, however, badly underestimates the magnitude of the blockage effects leading to corrected Mach numbers in error by up to  $-0.01$ . The introduction of a semi-empirical blockage correction, while retaining the linear theory formulation of lift interference, leads to a similar scatter in the corrected lift curve slopes for a value of  $\beta/P$  of 0.51. Evidence from several sources indicates that such a semi-empirical approach leads to corrected data which are very nearly free from the effects of wind tunnel wall interference.

## 5. COMPARISONS WITH OTHER DATA

### 5.1 Comparisons with Other Measurements

A considerable volume of test data has become available in recent years for both the aerofoil sections considered in the present tests. These data provide a useful source of verification for the corrections applied to the data in the present tests. For the BGK-1 section, two major sources of data are available from tests conducted at the NRC in Canada<sup>5,6</sup> and from the ARA<sup>25</sup> in the United Kingdom. The NRC tests were conducted in the NAE  $15'' \times 60''$  two-dimensional test facility, with the top and bottom walls of the tunnel having 6% porosity for the earlier tests,<sup>5</sup> and 20.5% porosity for the later tests. For both series of tests the model chord was  $10''$  giving a chord to height ratio ( $c/h$ ) of 0.167. No corrections for blockage (believed to be small) or lift interference have been applied to the results. The great advantage of this facility is its high Reynolds number capability (averaging  $21 \times 10^6$  for the present tests), but this is obtained at the expense of aspect ratio, the aspect ratio of the present aerofoil being only 1.5. Sidewall suction is applied in the vicinity of the model in order to maintain two-dimensional flow over

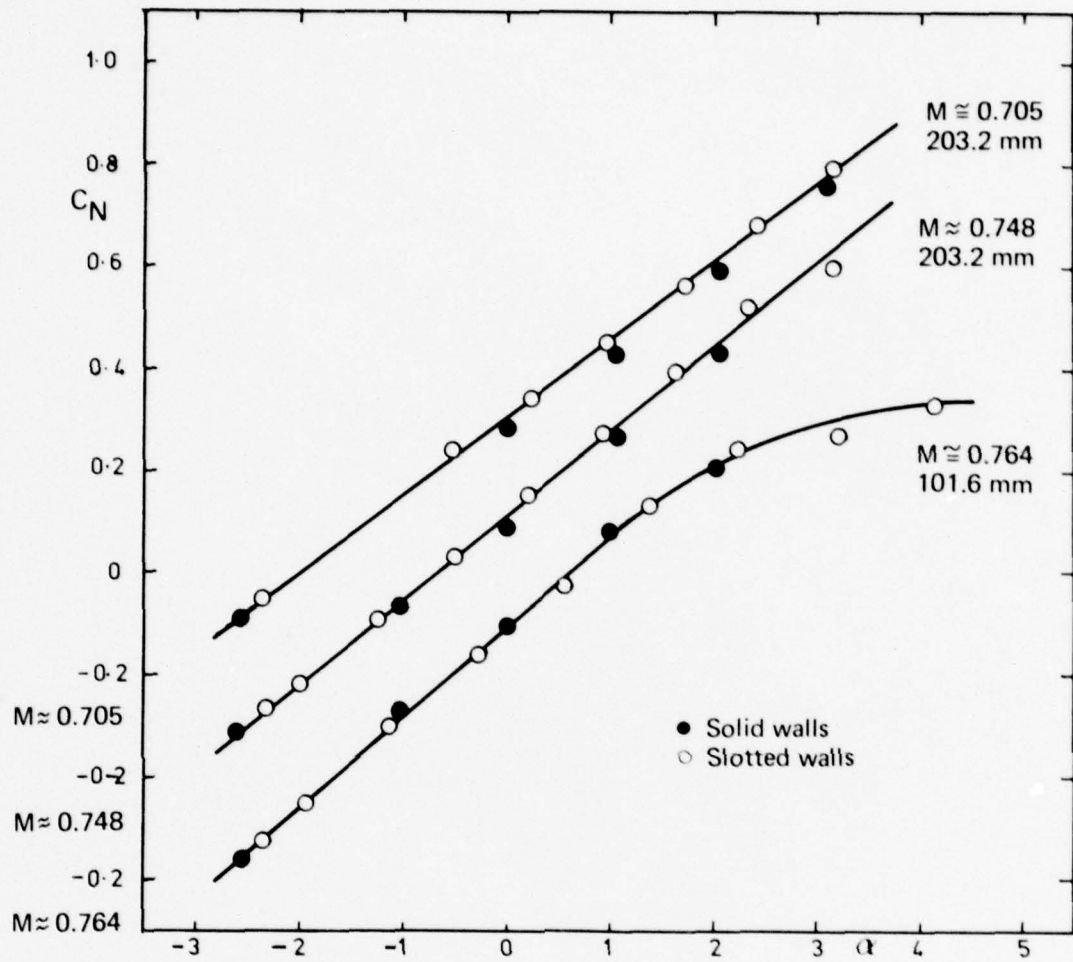
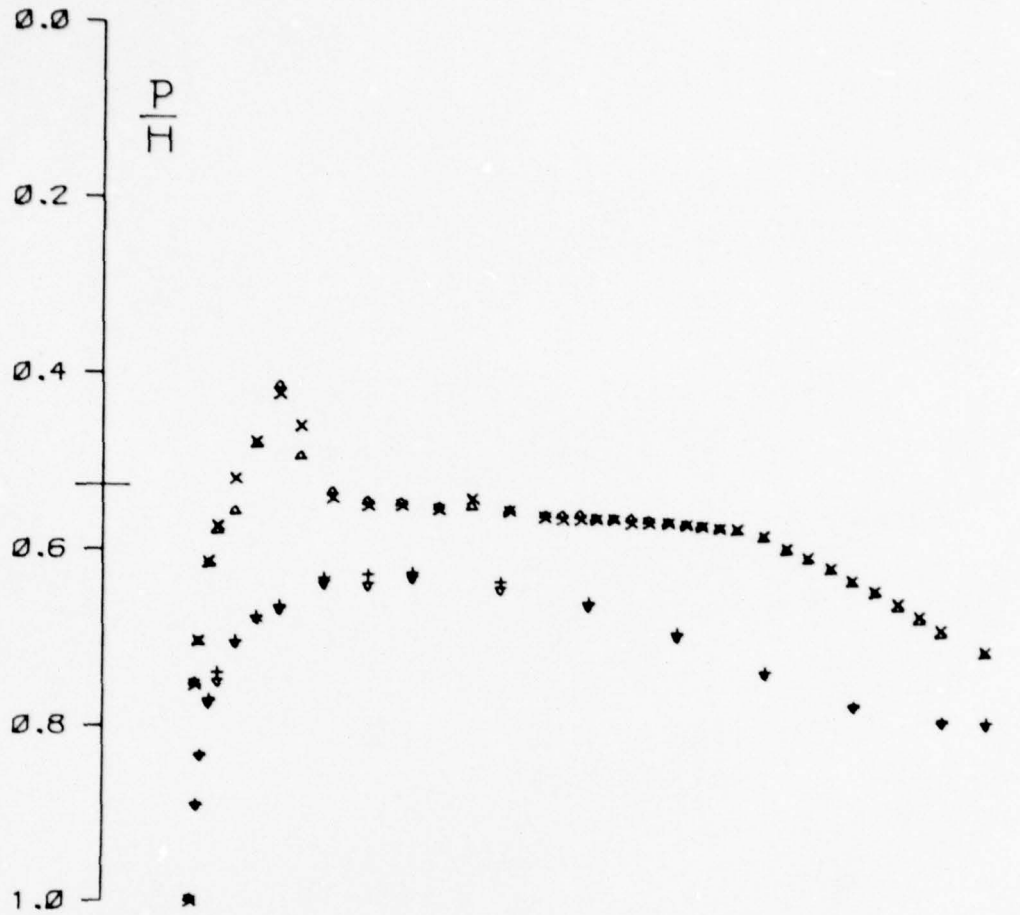


FIG. 24 COMPARISON OF CORRECTED LIFT CURVES - BGK-1



+ x BGK-1 203.2MM CHORD SLOTTED WALLS CORRECTED  
M= .705 AL= 0.97 CN= 0.451 CM=-0.093 R= 1.689

v Δ BGK-1 203.2MM CHORD SOLID WALLS CORRECTED  
M= .706 AL= 1.01 CN= 0.435 CM=-0.088 R= 1.632

FIG. 25 COMPARISON OF PRESSURE DISTRIBUTIONS - BGK-1;  
M = 0.705

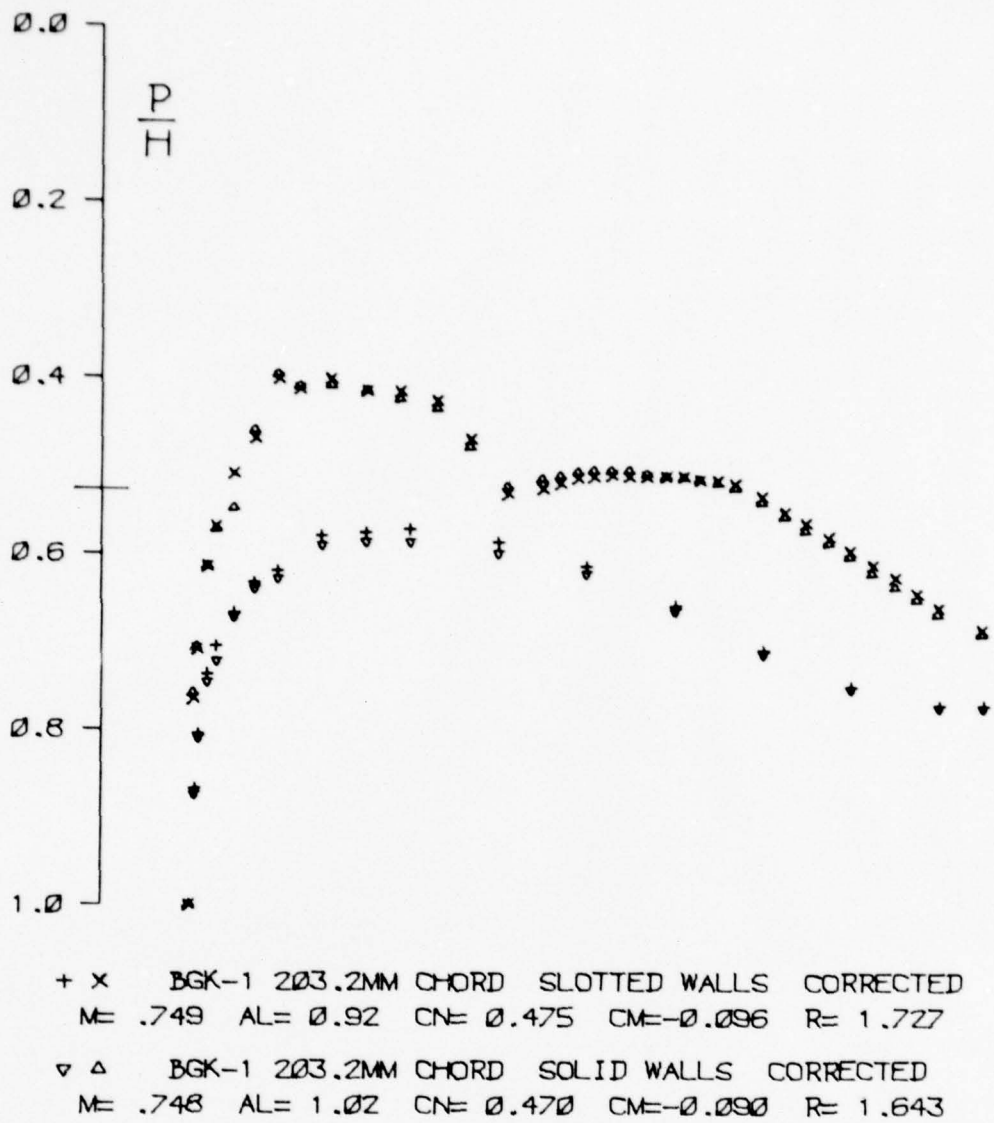
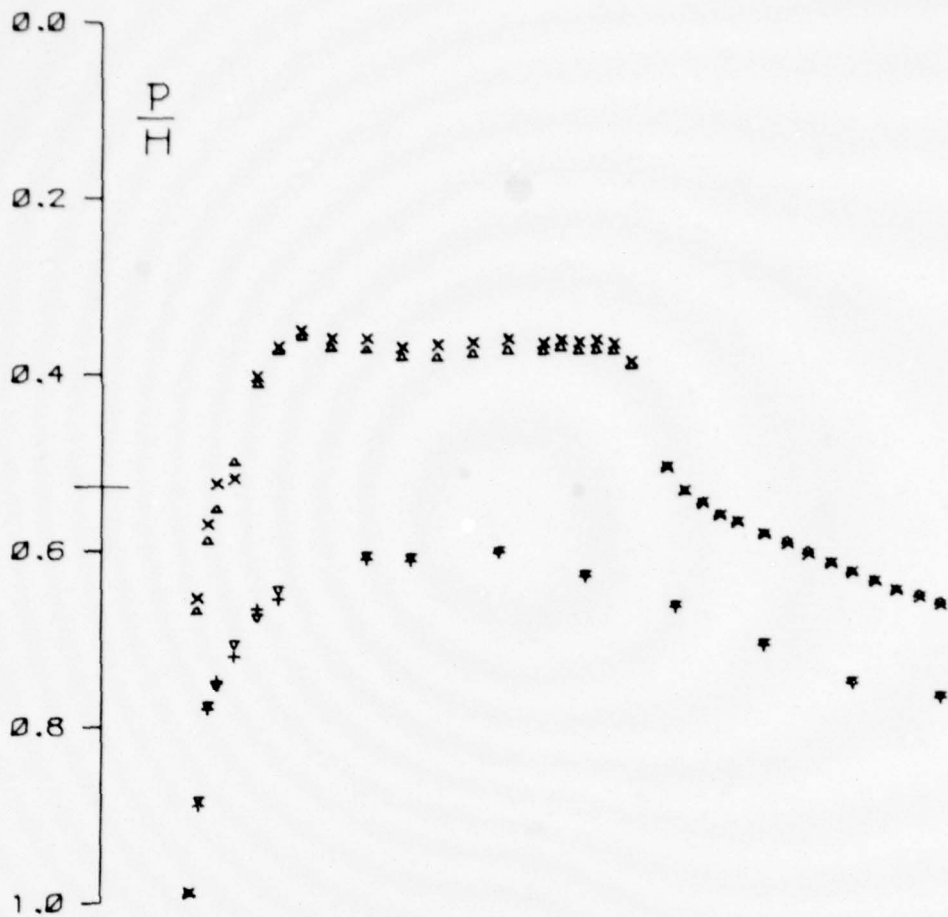


FIG. 26 COMPARISON OF PRESSURE DISTRIBUTIONS - BGK-1;  
 M = 0.748



+ x BGK-1 101.6MM CHORD SLOTTED WALLS CORRECTED  
M= .765 AL= 2.25 CN= 0.641 CM=-0.090 R= 0.819

▽ △ BGK-1 101.6MM CHORD SOLID WALLS CORRECTED  
M= .764 AL= 2.01 CN= 0.604 CM=-0.085 R= 0.807

FIG. 27 COMPARISON OF PRESSURE DISTRIBUTIONS - BGK-1;  
M = 0.765

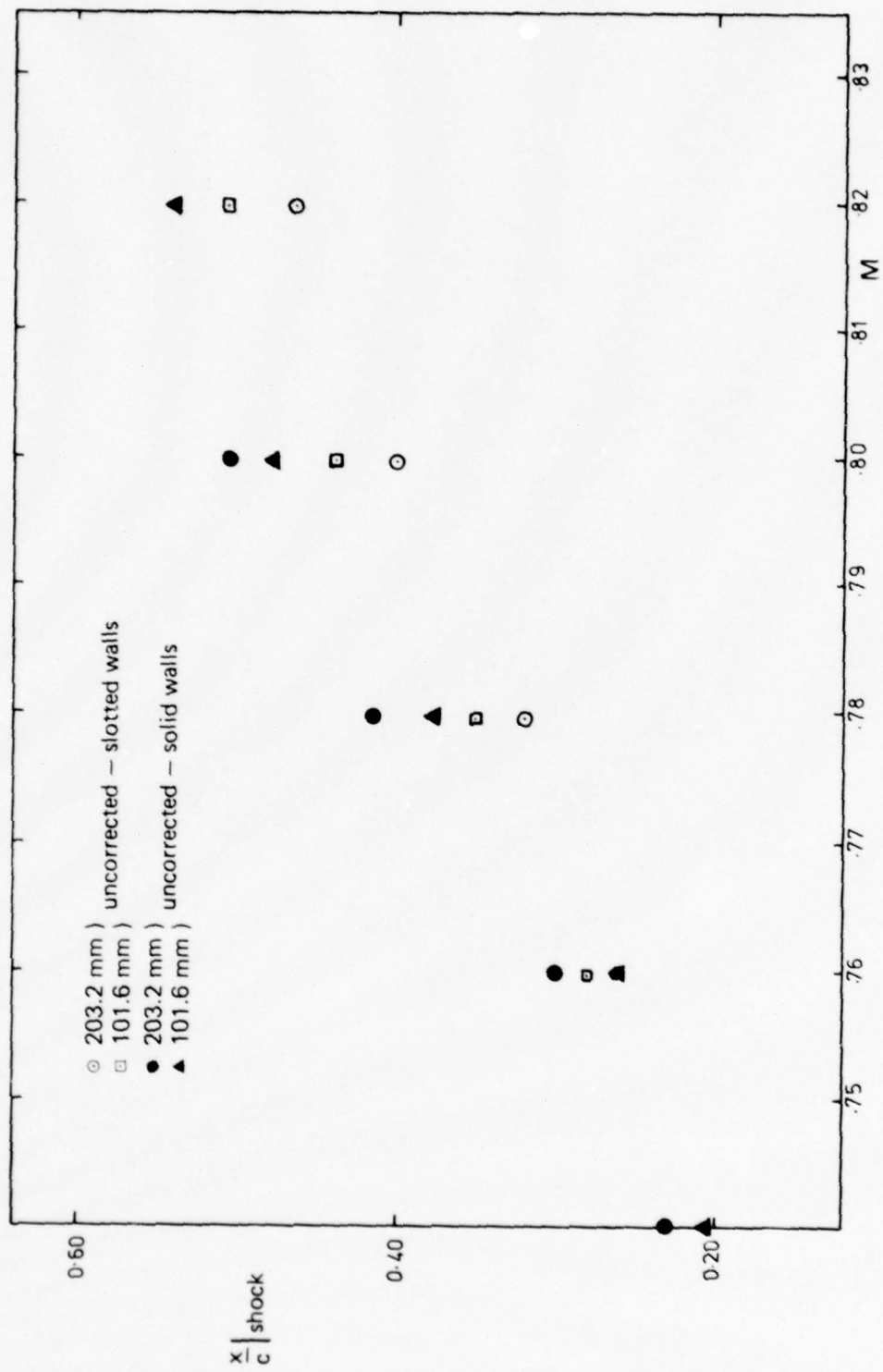


FIG. 28 UNCORRECTED SHOCK POSITIONS - NACA-0012;  $\alpha = 0^\circ$

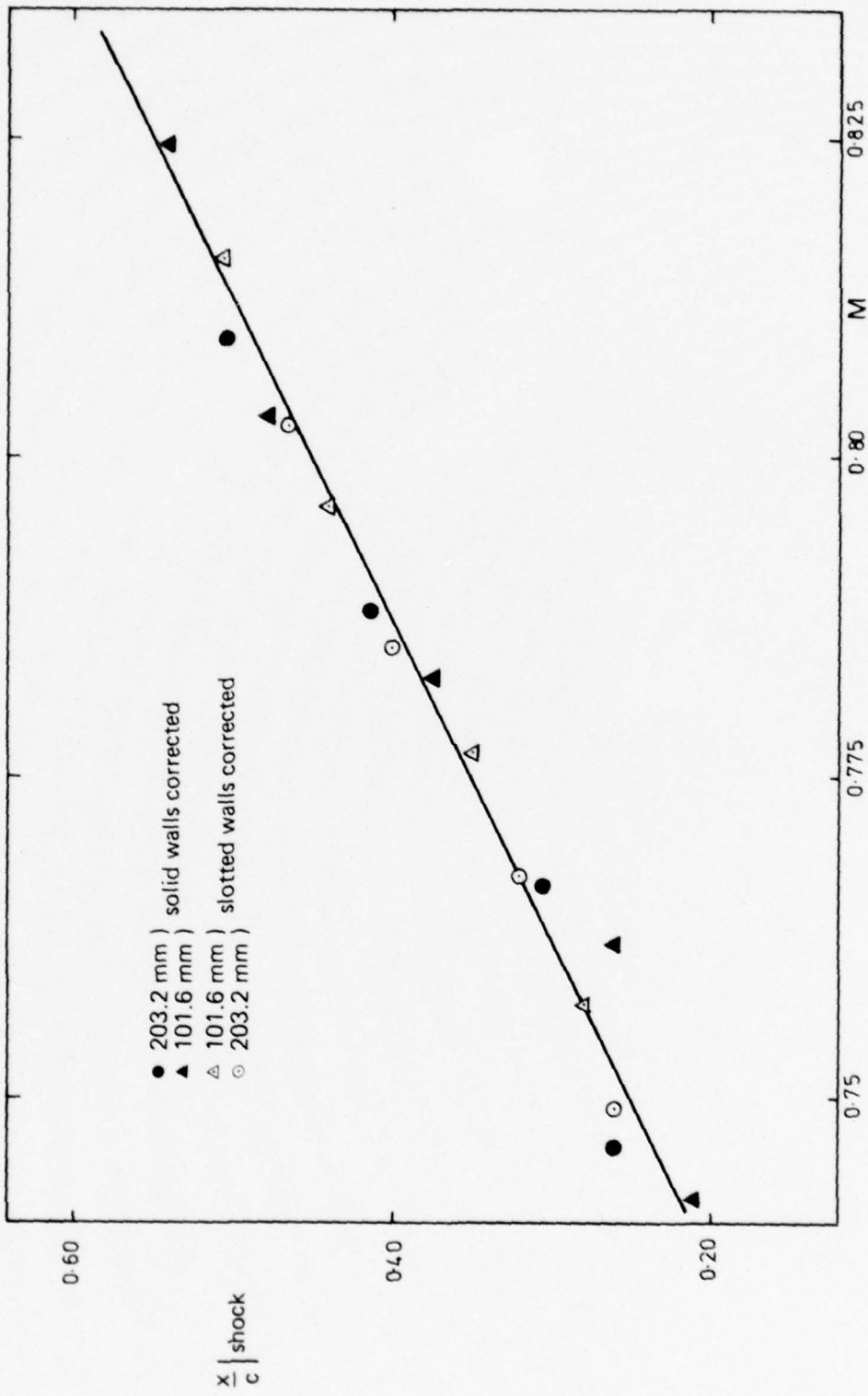


FIG. 29 CORRECTED SHOCK POSITIONS - NACA-0012;  $\alpha = 0^\circ$

the entire model, the amount of applied suction being determined on the basis of flow visualization and experience from previous tests. However, there remains the question of how two-dimensional the flow actually is, especially in the presence of shock waves and associated boundary-layer separation.

The ARA tests were conducted in its 18"  $\times$  8" two-dimensional facility. This facility has slotted top and bottom walls giving an open area ratio of 3.2%. Blockage effects in this tunnel are considered to be zero but lift interference corrections were applied in the normal manner with  $\delta_0 = -0.03$  and  $\delta_1 = +0.11$ . The model tested had a chord of 5" and a span of 8" giving a chord to height ratio of 0.278 and an aspect ratio of 1.6. The Reynolds number based on section chord was maintained at  $6 \times 10^6$  for the majority of the tests, dropping to  $4 \times 10^6$  at a Mach number of 0.5. Unlike the NRC tests which were conducted with natural transition, transition was fixed on both surfaces at 7 to 8% of chord.

Figure 30 shows a comparison of the variation of lift curve slope with Mach number between the corrected data of the present tests, and the results from the NRC and ARA tests. The agreement on the whole is quite good with the ARA results falling generally above those of the present tests as would be expected from their higher test Reynolds number. The NRC results would be expected to lie farther above again on the basis of the much higher Reynolds number. The fact that they do not seems to indicate either a need for the application of lift interference corrections in a direction applicable to an open jet, or a loss of lift due to a lack of two-dimensionality.

Figure 31 shows a comparison of the slotted wall design pressure distribution for the 203.2 mm chord model of BGK-1 with a similar pressure distribution from the ARA tests. This ARA distribution was chosen on the basis that it exhibited the closest agreement with the design distribution. The Mach numbers (corrected in the case of the present data) agree exactly, whereas the corrected angles of incidence and lift coefficients are somewhat different. Whether these differences are due to the differences in test Reynolds number or to incorrect corrections for the effects of lift interference (in one or both cases) is at this stage unclear. Once again a relative loss of lift in the upstream region of the lower surface is apparent for the present 203.2 mm tests, indicating the presence of significant streamline curvature. This effect will be more apparent in this case since the magnitude of the factor  $\delta_1$  for the ARA tests is similar to that of the present tests though of opposite sign.

For the case of the NACA-0012 aerofoil there are rather more recent test results available for comparison. Once again results are available from the NAE tunnel of the NRC.<sup>26</sup> For these tests a model of 300 mm chord was used, giving chord Reynolds numbers up to  $40 \times 10^6$ . With an aspect ratio of only 1.27 the effect of the level of sidewall suction on the two-dimensionality of the flow was quite severe. The final suction rate was chosen as that which produced a straight separation front rather than using the normal NAE criterion of surface streamlines being parallel to the freestream direction over the complete span. The justification for the use of this suction rate (about half the rate satisfying their normal criterion) is stated as being "firstly because the pressure distribution at this suction level appeared to match pressure data measured at ONERA, and secondly, because the straight as opposed to the curved separation front was felt to be important in the context of two-dimensional simulation."<sup>26</sup> The data are considered to be free of blockage interference but corrections have been applied for lift interference based on both theoretical (classical linear theory) and empirical (streamwise momentum balance) grounds. The results quoted here are limited to those corrected by the application of linear theory.

A very useful series of tests were conducted on the NACA-0012 section at Calspan in 1973.<sup>27</sup> These tests were conducted in the Calspan 8'  $\times$  8' tunnel with slotted top and bottom walls giving an open area ratio of 22.5%. The model had a chord of 6" giving a chord to height ratio of 0.063, and the results would therefore be expected to be close to interference free. Calculations with linear theory at Calspan indicated that the effects of blockage would amount to less than 0.1% and those of lift interference to less than 2%, the interference being of the open jet type. The model had a span of 48" and was fitted with end plates, giving a claimed effective aspect ratio of 72. This should ensure the complete absence of three-dimensional effects. No corrections were applied to the data, and the chord Reynolds number was maintained at  $1 \times 10^6$ .

Further results are available from tests at the NPL<sup>28</sup> in their 36"  $\times$  14" transonic tunnel.

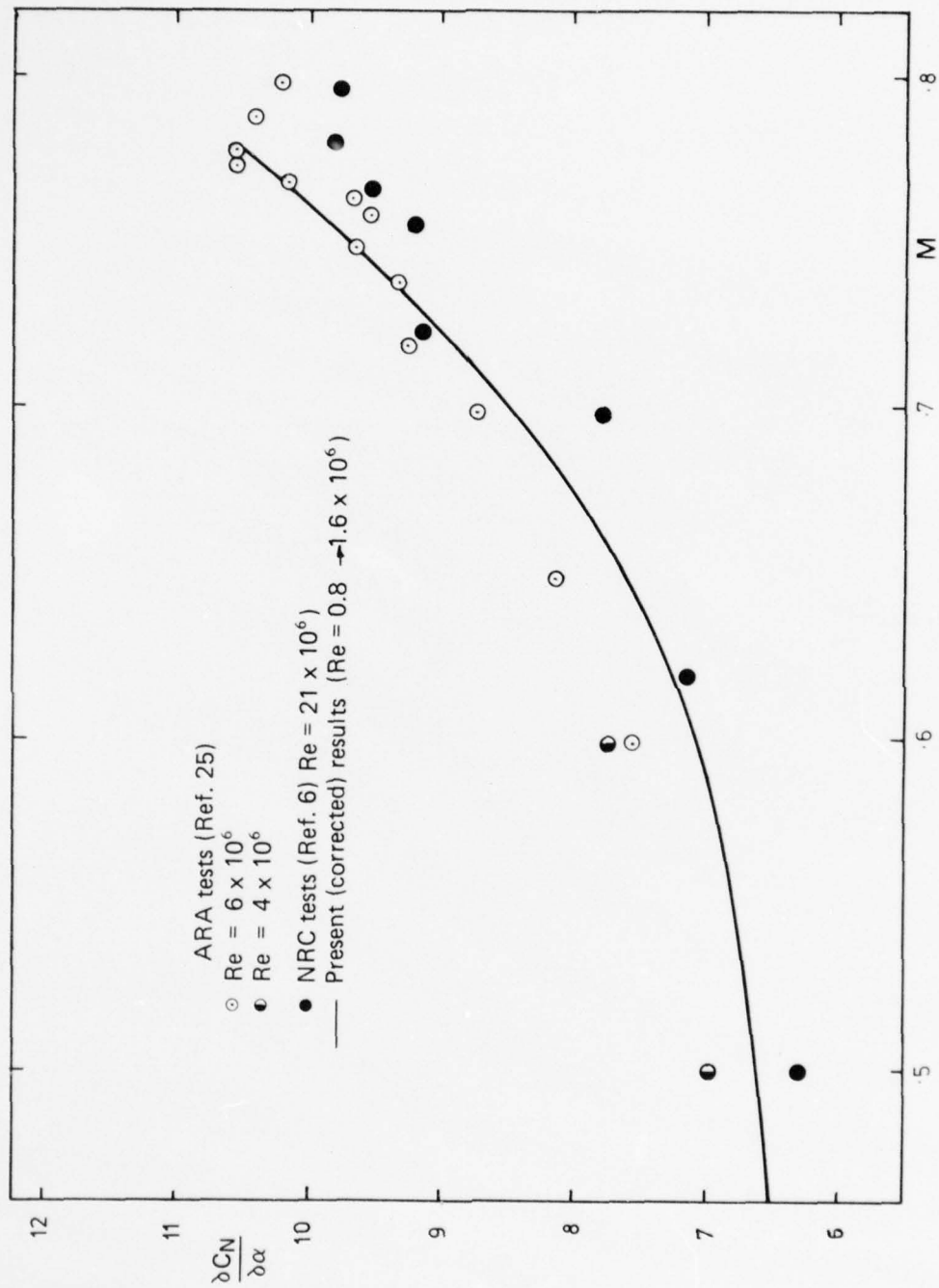
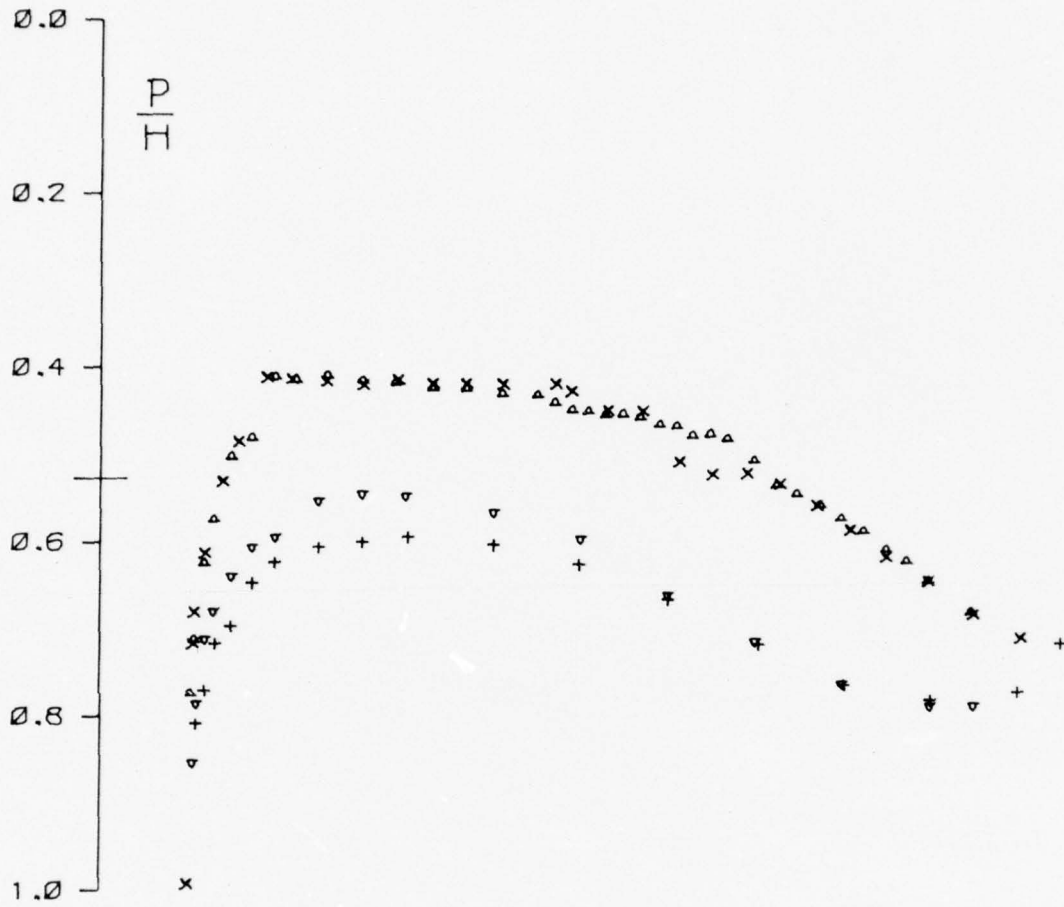


FIG. 30 BGK-1 LIFT CURVE SLOPE -- COMPARISON WITH OTHER MEASUREMENTS



+ x BGK-1 A.R.A. DATA CORRECTED  
M= .760 AL= 1.08 CN= 0.584 CM= 0.000 R= 6.000

▽ Δ BGK-1 203.2MM CHORD SLOTTED WALLS CORRECTED  
M= .760 AL= 0.50 CN= 0.533 CM=-0.129 R= 1.648

FIG. 31 COMPARISON OF EXPERIMENTAL DESIGN PRESSURE DISTRIBUTIONS - BGK-1

These tests were conducted with a 10" chord model ( $c/h = 0.28$ ) of 14" span (aspect ratio 1.4). The tunnel was equipped with slotted top and bottom walls with an open area ratio of 33%. The original report<sup>28</sup> claimed that the conditions for these tests were "close to those giving blockage-free and lift-interference-free results, and no corrections for wall constraint have been applied". Lately however, Collyer<sup>29</sup> has stated that this is now believed to be incorrect, in that although there is substantial experimental evidence to suggest that the conditions are indeed blockage-free, lift interference is significant, and gives values for the standard lift-interference parameters  $\delta_0$  and  $\delta_1$  ( $-0.088$  and  $+0.068$  respectively). The test Reynolds number varied from  $1.7 \times 10^6$  at  $M = 0.3$  to  $3.75 \times 10^6$  at  $M = 0.85$ .

The final source of experimental data on the NACA-0012 is some French tests conducted by ONERA in the S3 tunnel at Modane and in the R1 tunnel at Chalais-Meudon.<sup>30</sup> The tests in the R1 tunnel, with working section dimensions 200 mm  $\times$  70 mm, were conducted with porous top and bottom walls with the porosity varying between 0% (solid walls) and 12.5%. Three models were tested with chords of 60, 80 and 100 mm respectively ( $c/h = 0.30, 0.40$  and  $0.50$ ), with all models spanning the 70 mm tunnel dimension (giving aspect ratios of 1.17, 0.87 and 0.70). From comparisons of zero lift shock positions for the three models tested in walls of four different porosities, it was determined that the walls with 12.5% porosity gave blockage free conditions. The value of  $\beta/P$  calculated from linear theory to be relevant to the condition of zero solid blockage ( $\beta/P = 1.28$  for perforated walls) was taken as the correct value for the 12.5% porosity walls and used to determine lift-interference parameters. The S3 tunnel has test-section dimensions of 780 mm  $\times$  560 mm and was fitted with porous top and bottom walls of 9% porosity for these tests. The model tested had a chord of 210 mm, giving a chord to tunnel height ratio of 0.27, and completely spanned the tunnel (giving an aspect ratio of 2.67). On the basis of equality of zero incidence drag on three models of the NACA-0012 section of differing chords, it had been determined that the 9% porosity gives a condition close to zero blockage. Determination of porosity factor and hence lift-interference parameters had not been carried out at the time of the tests. The Reynolds number for the tests in the S3 tunnel varied between  $2 \times 10^6$  and  $10 \times 10^6$  and in the R1 tunnel between  $3 \times 10^6$  and  $6 \times 10^6$ .

Figure 32 shows a comparison of lift curve slopes between the corrected data of the ARL tests and data gathered from the various other sources. As for the BGK-1 results, the overall agreement is quite good, but several points merit further comment. Firstly, the NPL results, when corrected for lift interference in the manner suggested by Collyer,<sup>29</sup> fall well away from the main body of points, whereas the uncorrected data are in general agreement. This suggests that the statement of the original report<sup>28</sup> that the results were close to being free of lift interference may not be greatly in error. Secondly the large range in Reynolds number covered by these tests (from  $1 \times 10^6$  to greater than  $40 \times 10^6$ ) does not produce the significant differences in lift curve slope that might be expected. Since all the high Reynolds number results were obtained from tests at low values of aspect ratio, loss of lift due to three-dimensional effects is one possible explanation. Finally, it is noticeable that the NRC results suffer from a distinct loss of lift at the higher Mach numbers. Again this can probably be put down to a lack of two-dimensionality especially in the region aft of the shock. Indeed, the author of the NRC report, in discussing those results, suggests that it may perhaps have been better to use the higher suction rates, corresponding to a more two-dimensional streamline pattern overall, in order to avoid this problem. He comments that, in comparison with the ONERA data, the NAE measurements exhibit a quicker pressure recovery aft of the shock, leading to a distinct loss of lift.

Zero lift shock positions are compared in Figure 33. Again the agreement between the present corrected results and the other measurements is generally quite good. The expected effect of increasing Reynolds number—the shock location moving slowly towards the trailing edge—is not generally visible, except to some extent in the NPL results at higher Mach number and in the opposed direction in the Calspan results. The sensitivity<sup>26</sup> of shock location to suction rate in the NRC tests could be responsible for at least part of the more forward shock position, but like the ONERA R1 tunnel tests, a general lack of aspect ratio is likely to be the major factor. The extremely low aspect ratios of the R1 tunnel tests (1.17 to 0.70) are strongly reflected in the extreme forward shock locations.

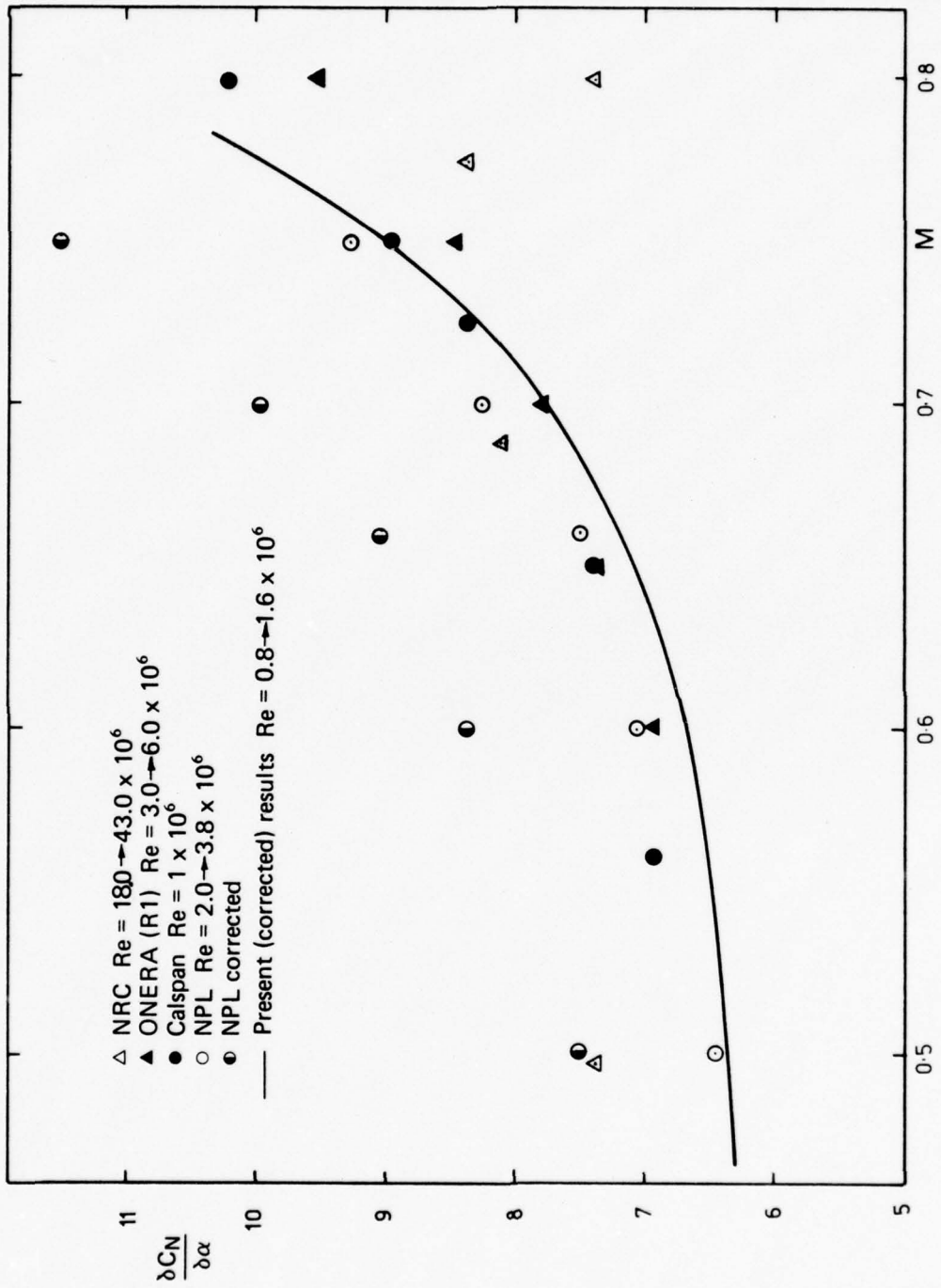


FIG. 32 NACA-0012 LIFT CURVE SLOPE -  
COMPARISON WITH OTHER MEASUREMENTS

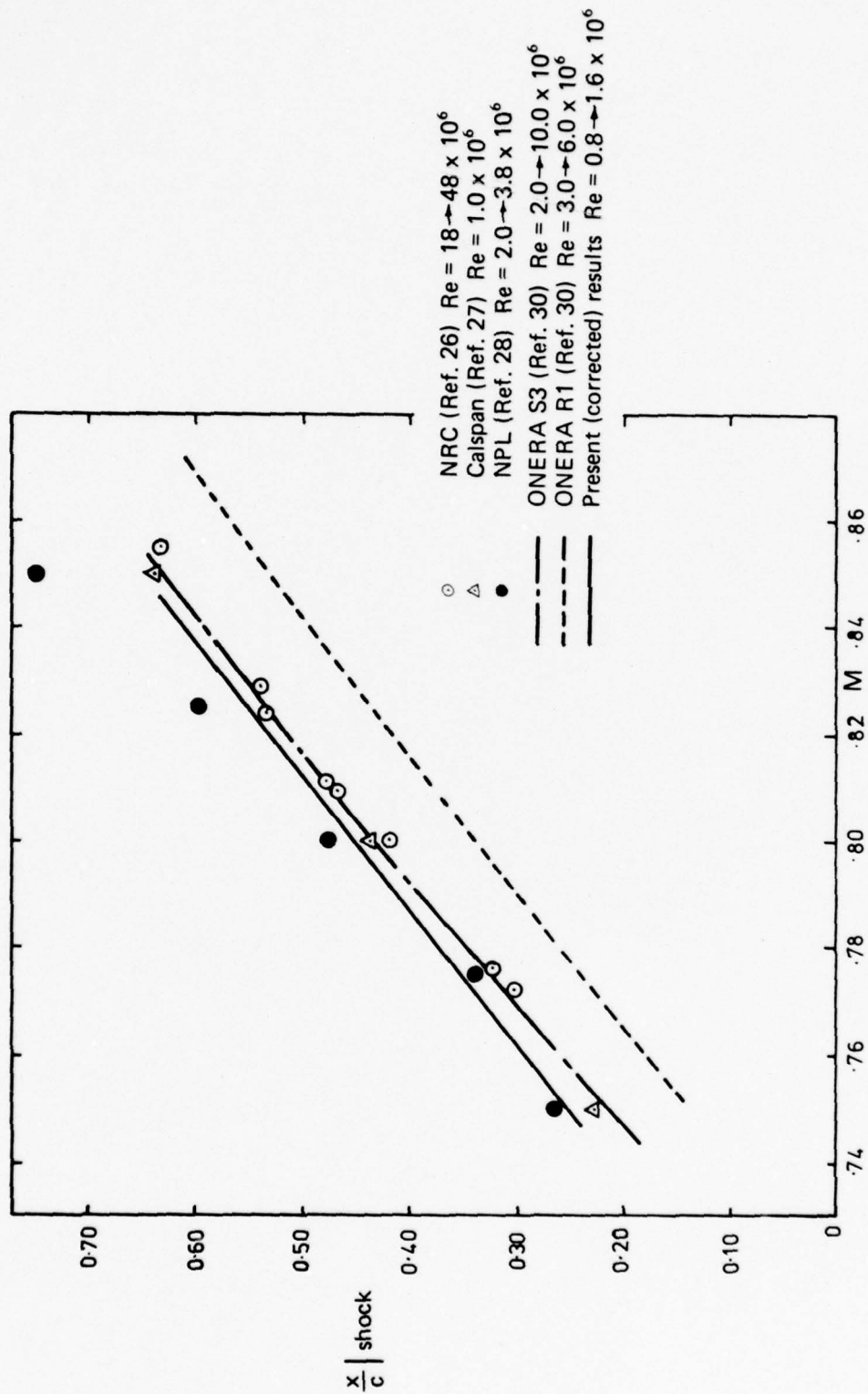


FIG. 33 NACA-0012 SHOCK POSITION - COMPARISON WITH OTHER MEASUREMENTS

## 5.2 Comparisons with Theory

In recent years there have been impressive advances in theoretical methods for predicting the pressure distribution, lift and drag for steady inviscid flow past lifting aerofoils at high subsonic and transonic speeds. This development began with the proposal by Murman and Cole<sup>31</sup> of a method for the iterative solution of the transonic small perturbation equations. The method was further developed by Garabedian and Korn<sup>4,32</sup> who used a conformal transformation due to Sells<sup>33</sup> combined with an iterative solution of the exact irrotational, isentropic equations in a manner similar to that used by Murman and Cole. It was recognized, however, that in the range of Mach numbers considered, and in the range of Reynolds numbers in which aerofoils are designed to operate, the effects of viscosity are of great importance, and hence several attempts have recently been made to develop theoretical models which include these effects.<sup>29,34-36</sup> Of these methods, only those developed at the RAE<sup>29,36</sup> make any attempt to correctly take account of the effects of the thickness and curvature of the aerofoil wake, as well as the displacement effect of the aerofoil boundary layers.

The verification of these various theoretical methods still awaits the provision of experimental measurements which are truly two-dimensional and free from the effects of wind-tunnel wall interference, and this was indeed one of the reasons for the initiation of the CAARC program.<sup>3</sup> Computer programs are now readily available for calculating inviscid flows, but unfortunately this is not yet the case for the more recently developed viscous theories. Comparisons of these theories with experimental results are therefore limited to the relatively few cases which have been reported in the literature.

Figure 34 compares corrected lift curve slope data from the present tests with inviscid theory. As expected, the inviscid theory greatly over-estimates lift curve slope, being approximately 20% greater than the corrected data throughout the range of Mach number. Unfortunately no comparable results are available from viscous theories for this section. In the case of the NACA-0012 section, however, results of theoretical viscous calculations are available from the methods of Firmin<sup>36</sup> (quoted by Lock<sup>3</sup>) and Collyer,<sup>29</sup> and these, together with an inviscid solution, are compared with the corrected data in Figure 35. Once again, the inviscid solution overestimates the lift curve slope, in this case by an average of 25%, the difference increasing slightly with Mach number. With the effects of viscosity included, the difference between theory and experiment is reduced to about 15%. The results from Collyer's theory, which would be expected to be more accurate (due to its utilization of the exact equations to represent the inviscid part of the flow) than that of Firmin (which uses the transonic small perturbation equations), show the greater difference. However, the results shown in Figure 35 are for a Reynolds number of  $3.5 \times 10^6$  compared to an average Reynolds number of the experimental results of  $1.2 \times 10^6$ . The difference in lift curve slope due to this change in Reynolds number, on the basis of published results<sup>3</sup> from Firmin's theory, would amount to about 4%. In fact, correcting Collyer's results in this manner produces quite good agreement between the two theories, but there still remains a difference of more than 10% between theory and the corrected experimental results.

Figure 36 compares zero lift shock positions predicted by inviscid theory for the NACA-0012 with those of the corrected experimental results. Also included is a single point available from Collyer's theory. The agreement between theory and experiment is again quite good. This type of comparison is, however, not strictly valid. The governing equations used in the inviscid theory (and in the viscous theory for the inviscid part of the flow) are isentropic and irrotational, and hence the compression jumps which evolve as approximations to shock waves, are only approximations to the true Rankine-Hugoniot shock jumps. Furthermore, shock waves are smeared over several mesh spacings, and differences in shock positions between non-conservative schemes (as used here) and the fully conservative relaxation schemes are significant. (See for example Bailey<sup>37</sup> or Murman<sup>38</sup> for their discussion of these points.)

Among the published results for the BGK-1 section from Collyer's theory, there are fortunately several cases in which Mach numbers and angles of incidence are sufficiently close to the corrected experimental values for direct comparison of pressure distributions. Three cases are shown in Figures 37 to 39. The first is the experimentally determined design point for the 203.2 mm model. The second is for the same Mach number, but at higher incidence, and shows the appearance of a fairly strong shock. Finally, at an incidence lower than the design value,

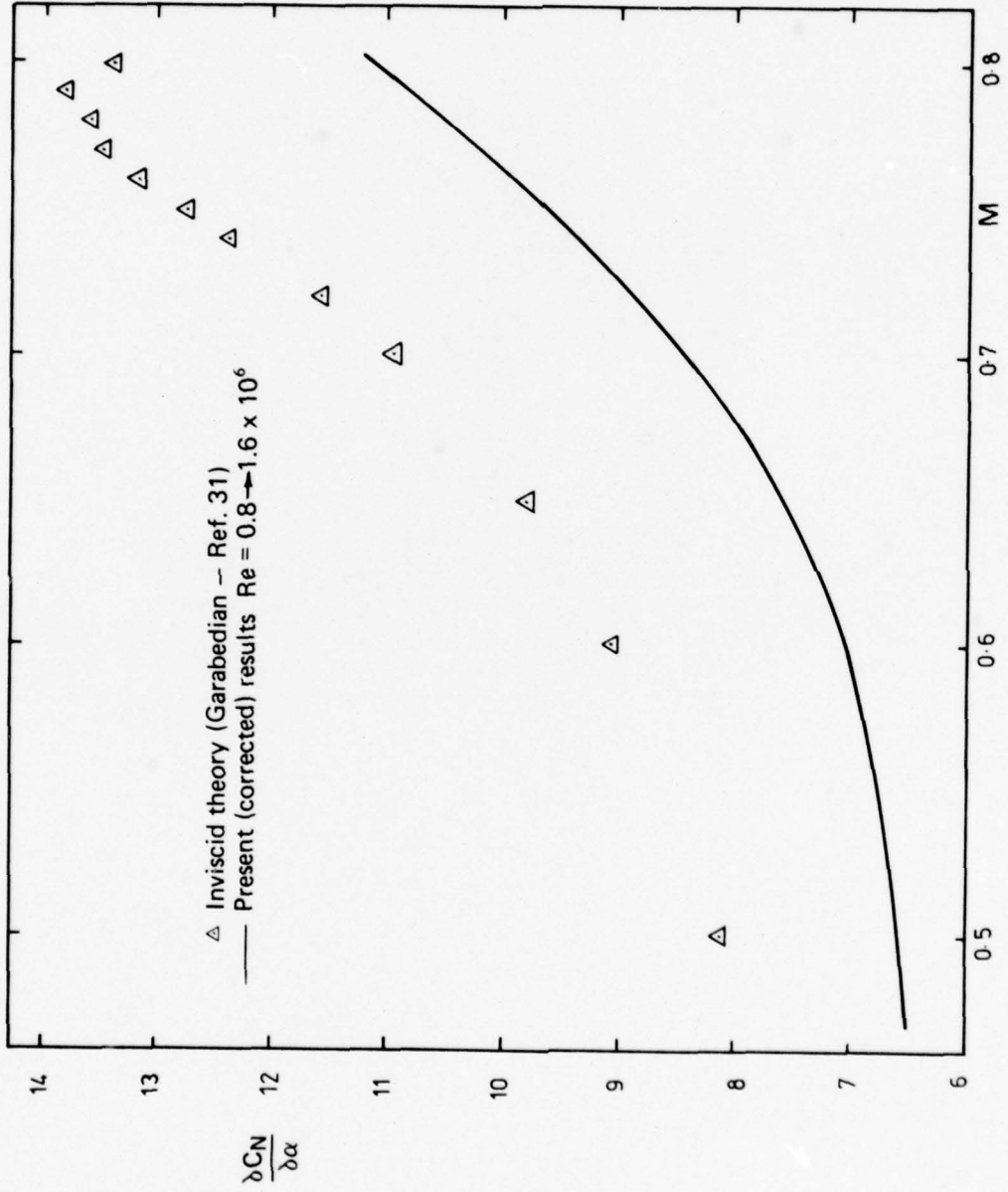


FIG. 34 BGK-1 LIFT CURVE SLOPE - COMPARISON WITH THEORY

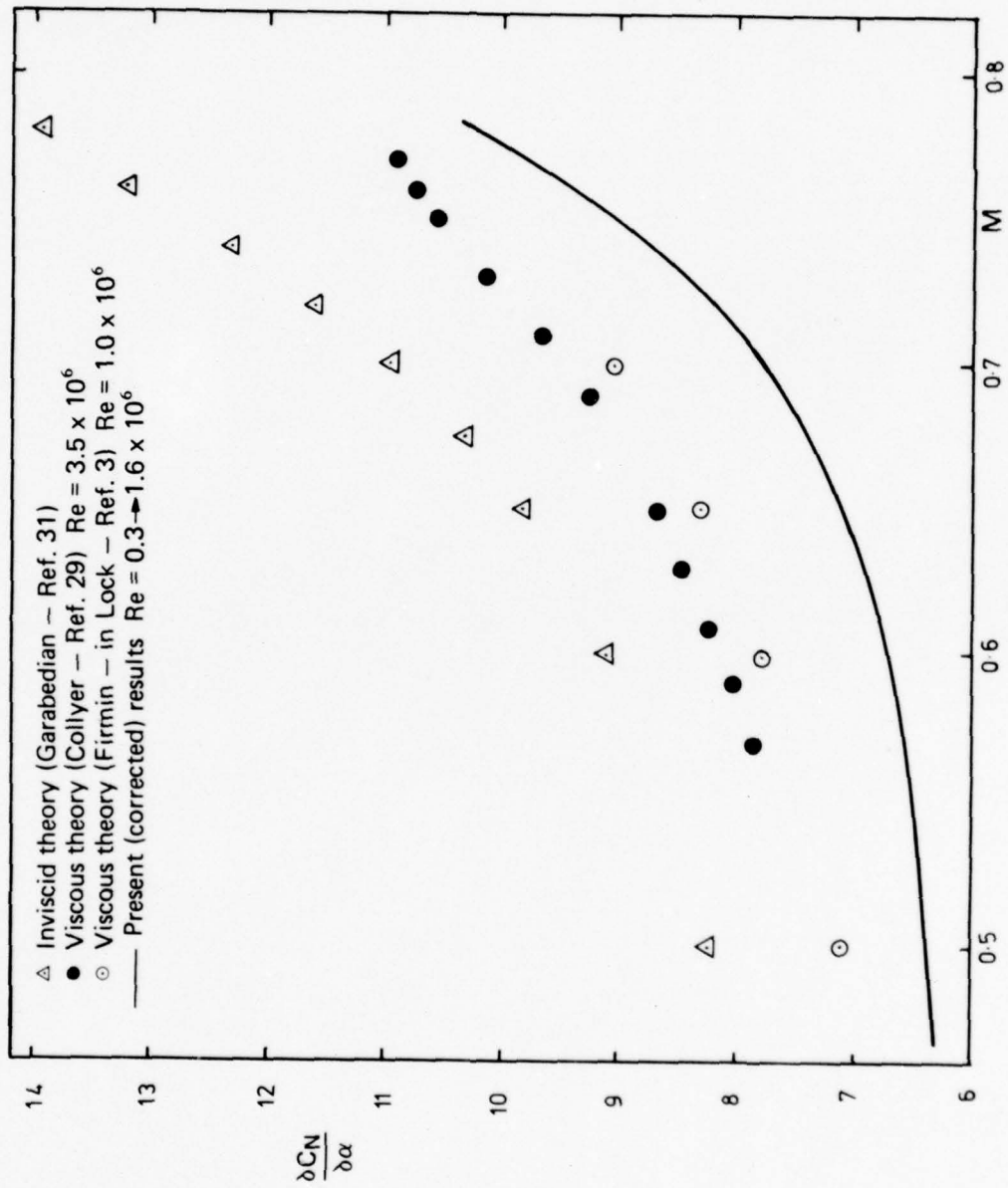


FIG. 35 NACA-0012 LIFT CURVE SLOPE - COMPARISON WITH THEORY

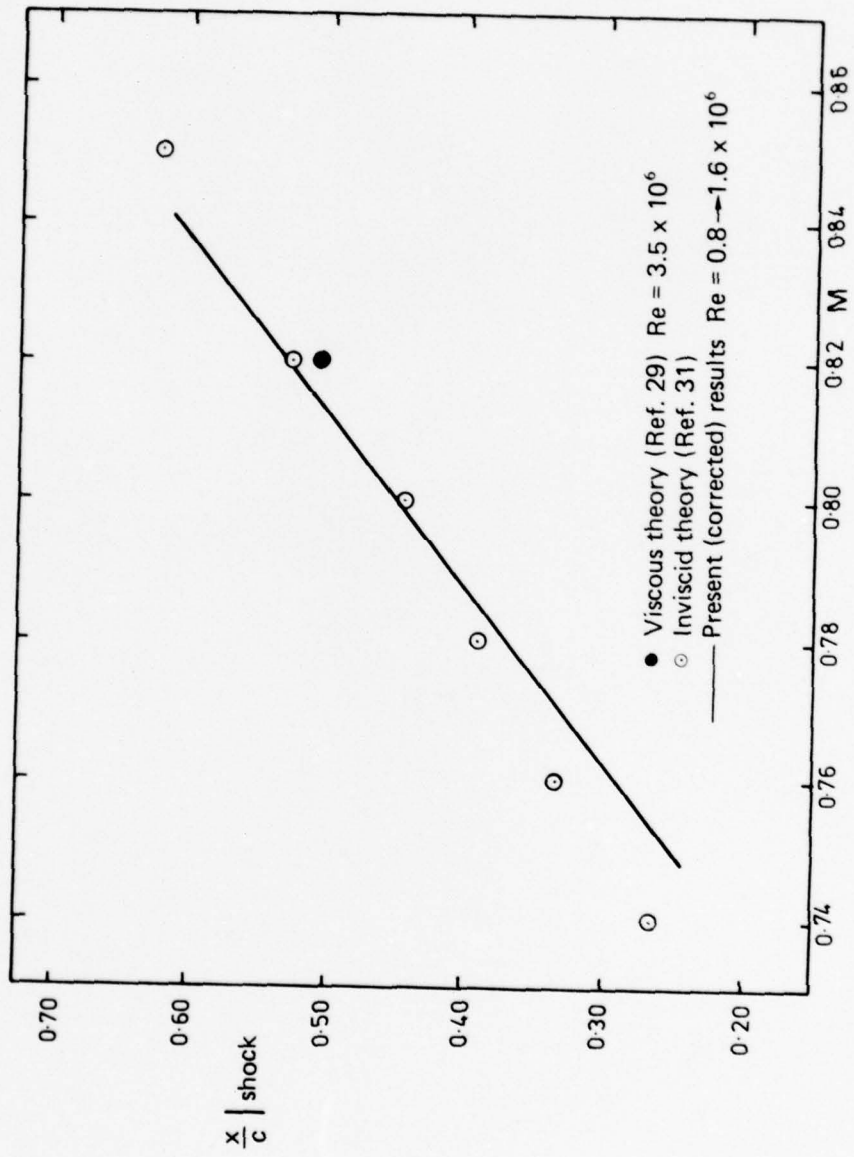
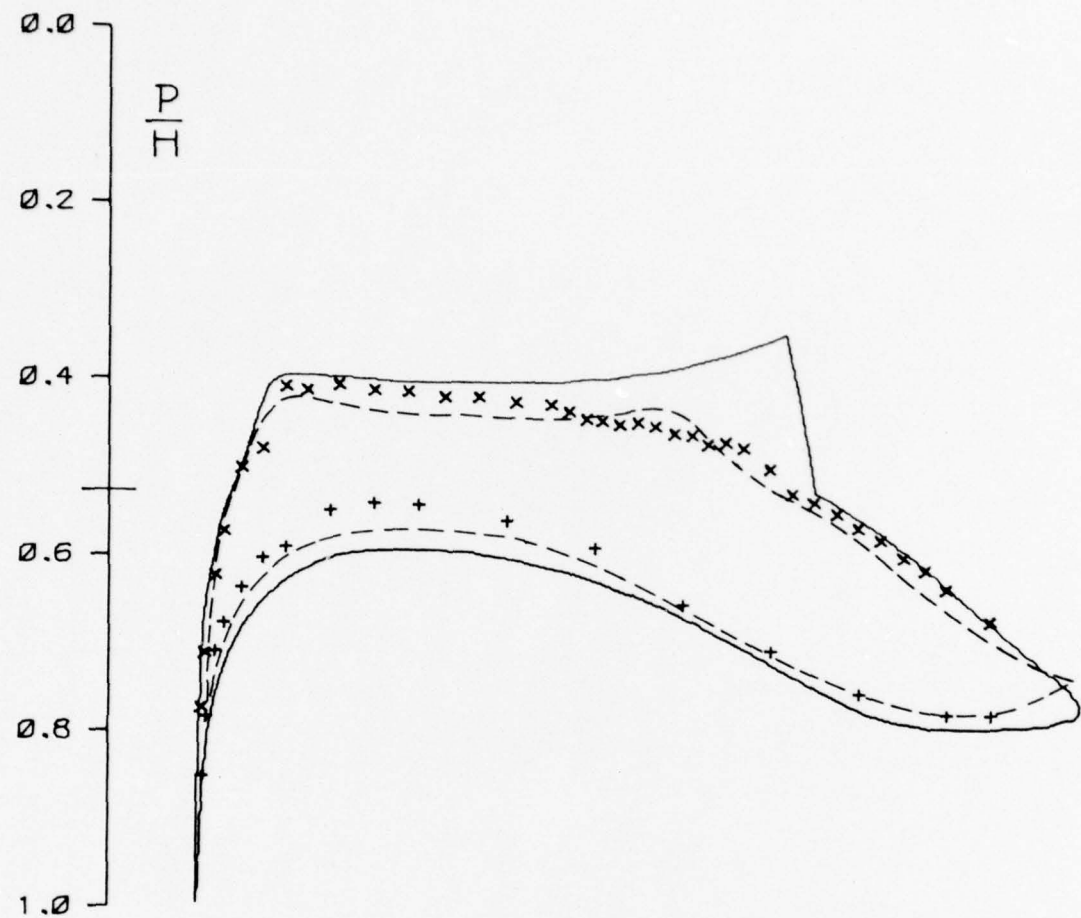
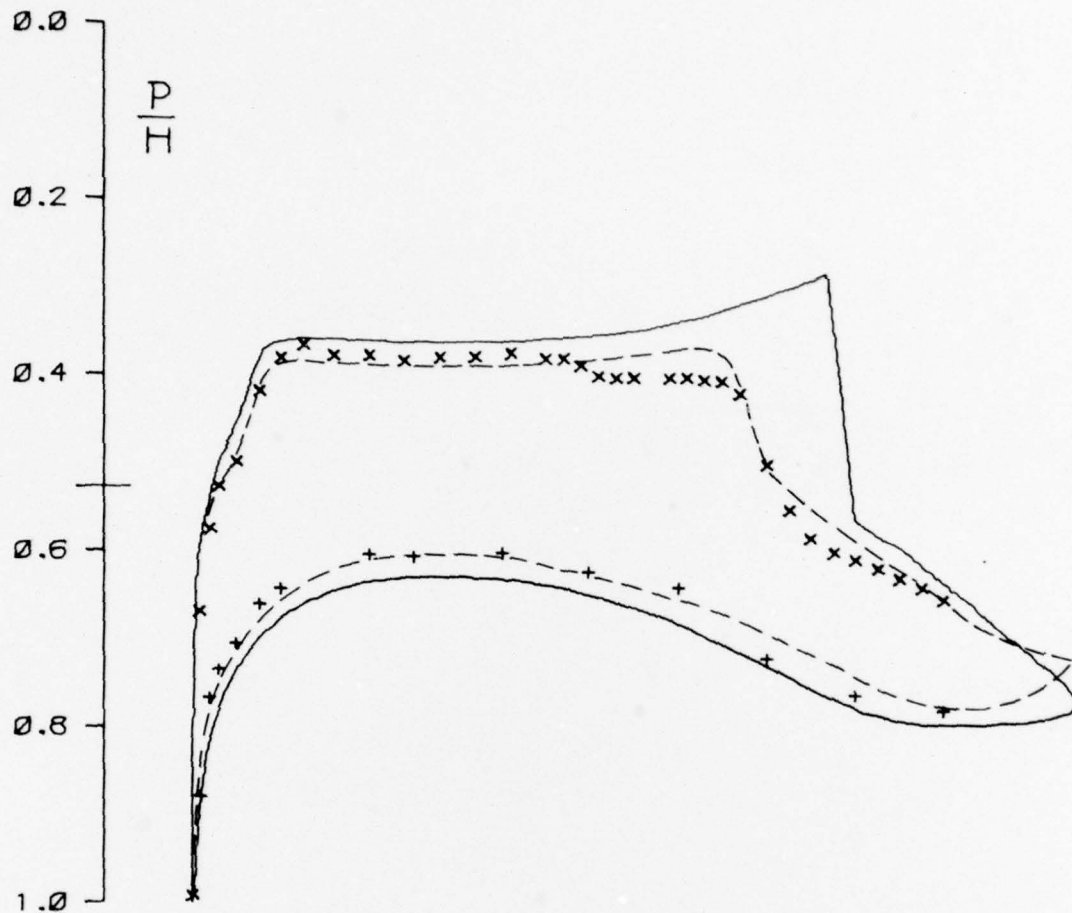


FIG. 36 NACA-0012 SHOCK POSITION - COMPARISON WITH THEORY



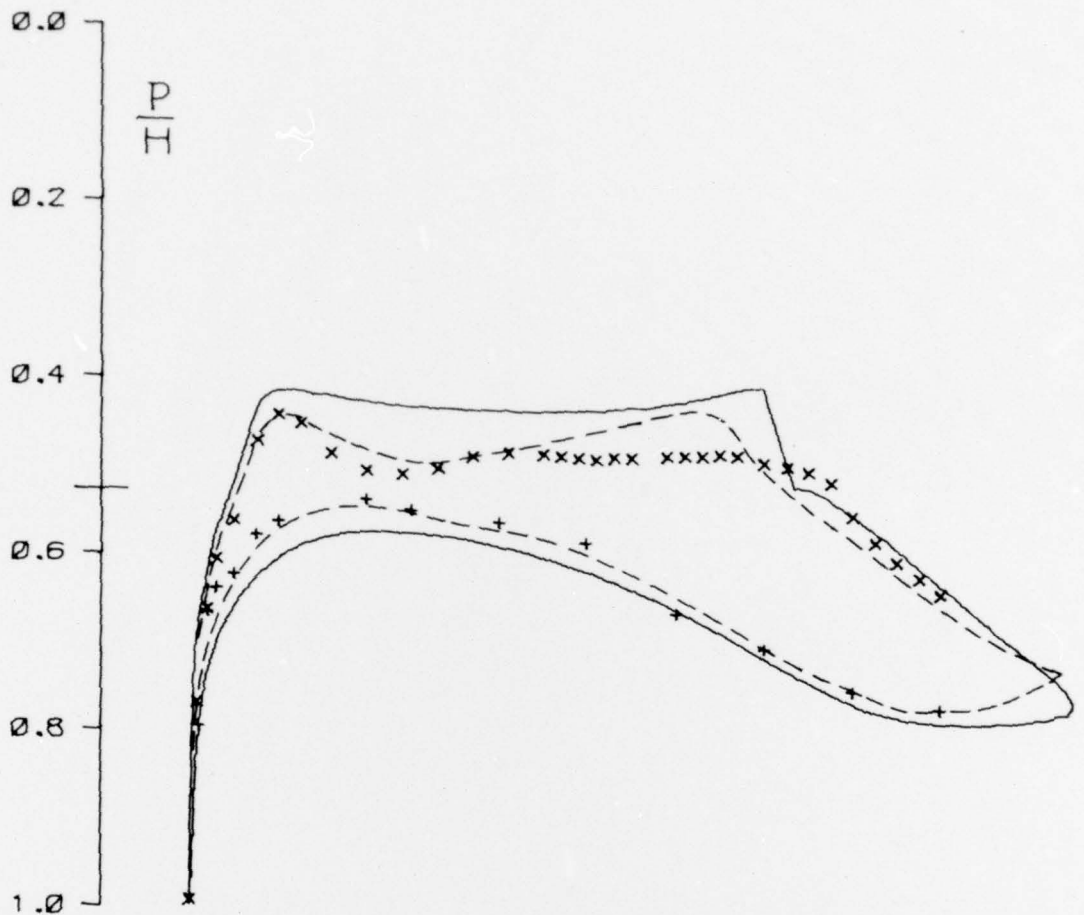
——— INVISCID THEORY (BAUER ET.AL. - REF. 32)  
 M= .760 AL= 0.50 CL= 0.757 CM=-0.171 CD= 0.011  
 - - - VISCOUS THEORY (COLLYER - REF.29)  
 M= .760 AL= 0.50 CN= 0.554 R= 6.000  
 + x EXPERIMENT 203.2MM CHORD SLOTTED WALLS CORRECTED  
 M= .760 AL= 0.50 CN= 0.533 CM=-0.129 R= 1.648

FIG. 37 COMPARISONS OF EXPERIMENTAL AND THEORETICAL PRESSURE  
 DISTRIBUTIONS - BGK-1; M = 0.76  $\alpha$  = 0.5



————— INVISCID THEORY (BAUER ET.AL. - REF.32)  
 ME .758 AL= 1.60 CL= 0.997 CM=-0.204 CD= 0.033  
 - - - - - VISCOUS THEORY (COLLYER - REF. 29)  
 ME .760 AL= 1.60 CN= 0.744 R= 6.000  
 + x EXPERIMENT 101.6MM CHORD SLOTTED WALLS CORRECTED  
 ME .758 AL= 1.59 CN= 0.692 CM=-0.122 R= 0.794

FIG. 38 COMPARISON OF EXPERIMENTAL AND THEORETICAL PRESSURE DISTRIBUTIONS - BGK-1;  $M = 0.76$ ;  $\alpha = 1.5^\circ$



————— INVISCID THEORY (BAUER ET.AL. - REF. 32)  
 M= .758 AL= 0.00 CL= 0.630 CM=-0.155 CD= 0.004  
 - - - - - VISCOUS THEORY (COLLYER - REF. 29)  
 M= .760 AL= 0.00 CN= 0.444 R= 6.000  
 + x EXPERIMENT 101.6MM CHORD SLOTTED WALLS CORRECTED  
 M= .758 AL=-0.06 CN= 0.397 CM=-0.125 R= 0.794

FIG. 39 COMPARISON OF EXPERIMENTAL AND THEORETICAL PRESSURE DISTRIBUTIONS - BGK-1; M = 0.76,  $\alpha = 0^\circ$

but still at the same Mach number we see the typical double shock system predicted by both inviscid and viscous theory and found to some extent in experiment. Also included on these figures are inviscid calculations for the same Mach numbers and angles of incidence. In all cases the agreement between the viscous theory and experiment is better than that of the inviscid theory. Considering the difference in Reynolds number between viscous theory and experiment, the overall agreement is excellent, the theory predicting accurately all the major feature of the pressure distributions. However, lift coefficients are still overestimated by up to 10%, the closest agreement occurring somewhat surprisingly at the experimental design condition, where the difference is less than 5%.

## 6. DISCUSSION

From the comparisons of the previous sections, it is evident that the application of corrections based on classical linear interference theory, with the addition of a semi-empirical formulation of the effects of blockage in the slotted-wall case, produces data which form a self-consistent set, as well as being in general agreement with data from other sources. Several significant points stand out. Firstly, the corrections continue to produce good agreement even when the Mach number is such as to produce significantly supercritical flow over the aerofoil upper surface. Since the basis from which linear theory is derived is certainly not valid under supercritical conditions, this result is somewhat surprising. The present tests do indicate however, that at least up to Mach numbers at which lift coefficients begin to decrease due to shock induced separation on the upper surface and the appearance of a supersonic zone on the lower surface, the application of linear theory still produces quite good results. Secondly, the basic linearized approach to the problem inherent in classical theory, which allows the modelling of the situation by three independent corrections for solid and wake blockage and lift interference, is generally supported. The overall implications of this approach are that if corrections are applied independently to the Mach number and angle of incidence, then the pressure distributions obtained for identical corrected conditions should also agree. (If pressure distributions are compared in the form of pressure coefficients rather than pressure ratios, then care must be taken to correct the pressure coefficients for the effects of blockage on dynamic pressure. It is for this reason that all pressure distributions considered in this report are expressed in the form of pressure ratios.) This has indeed been found to be the case in comparisons between sets of corrected data from the present tests and also in comparisons with corrected data from other sources. This type of comparison is of course only valid so long as the effects of streamline curvature remain small. As noted earlier, the presence of streamline curvature leads to the implication that a warped model should be tested to simulate the uniform flow situation, the degree of warpage being a function of angle of incidence. In the present tests, the maximum correction to lift coefficient due to the effects of streamline curvature amounts to less than 3% in the solid wall case and about 1% for the slotted walls. Thus the streamline curvature effects in the present tests remain small enough not to seriously affect the validity of the corrections, although some differences due to such effects are visible in pressure distributions of the larger (203.2 mm chord) models of both sections. Finally, it is worth noting that the scatter in the agreement of the corrected solid wall results, and in the comparison of corrected results from both solid and slotted wall tests is less than might be expected. As stated previously the errors in measured lift curve slopes are expected to be on the order of  $\pm 2\%$ . The fact that scatter between corrected results is only slightly greater than this level is indeed quite remarkable.

Despite the success of classical linear theory in correcting the present results, its application is not without problems. The major problem area is of course the inability of classical theory to correctly represent the effect of blockage in the slotted wall situation. Its predictions have been seen to underestimate the required corrections to Mach number by up to a factor of five. Several possible mechanisms to explain this anomaly have been investigated. Errors in test section total pressure measurement, which for the present tests was determined from the static pressure in the entrance to the contraction, are possible due to the finite velocity in the contraction. However, the large contraction ratio of the ARL transonic tunnel (27 : 1) minimizes this source of error, the error amounting to less than 0.0003 in Mach number at a Mach number of 0.8. A further possibility is the suggestion by Read *et al.*<sup>39</sup> that the introduction of models with large (greater than 2%) blockage ratios could reduce plenum chamber pressure below the calibrated, empty-

tunnel values at high subsonic Mach numbers. Such an action would have the effect of increasing the Mach number calculated from static pressure in the plenum chamber above that without the model present. Such effects were found by Parker<sup>10</sup> when studying the flow generation properties of a set of slotted walls in the Propulsion Wind Tunnel Facility at the Arnold Engineering Development Centre. The magnitude of this effect, from Parker's measurements, appeared to increase with Mach number, reaching almost 0.01 in Mach number at a Mach number of 0.9. A short investigation was undertaken in the ARL transonic tunnel to discover whether such an effect was the cause of the discrepancy in blockage. Centreline side-wall pressures were measured upstream of the model position for the empty tunnel condition, and with the 203.2 mm chord NACA-0012 model installed in the tunnel at an angle of incidence of 3°. No difference in the relationship between plenum chamber static pressure and upstream test-section-wall pressures was evident between the empty tunnel and model installed cases. During this investigation a check was also made of the possibility of the plenum chamber static pressure varying with position in the plenum chamber due to highly curved flows through the slotted walls. Once again, however, no detectable differences were apparent.

It has been suggested (e.g. see Lock<sup>3</sup>) that unlike the predictions of linear theory, the ratio  $\beta/P$  and hence  $\delta_0$  and  $\delta_1$  will probably be a function of Mach number. The slightly increased amount of scatter towards the high Mach number range in the corrected lift curve slope results of the present tests would tend to support this proposal. However, in this region, where the flow is supercritical, linear theory no longer applies, and allowing  $\beta/P$  to vary with Mach number seems to be simply an artificial attempt to extend the range of validity of linear theory.

As well as being subject to the effects of wind tunnel wall interference, transonic wind tunnel tests on two-dimensional aerofoils are also very sensitive to the magnitude of test Reynolds numbers. The present tests provide a good opportunity for studying Reynolds number effects both in the tests themselves and in comparisons with other data, both experimental and theoretical. Tests in the slotted walls on the 203.2 mm chord models of both sections at the Reynolds number of the 101.6 mm chord models indicated that the effect of this halving of Reynolds number on lift curve slopes was quite small—of the same order as the scatter (about  $\pm 2\%$ ) in the data. The lower Reynolds number data, however, did show a noticeably lower trend, as would be expected. In the corrected data, for both solid and slotted walls, the 101.6 mm chord results, although within the general scatter, do produce noticeably lower values of lift curve slope. This is most noticeably in the NACA-0012 results from the slotted walls shown in Figure 33. Whether this effect is due to the difference in Reynolds numbers, or to an inability of linear theory to correctly account for differences in model size, cannot be determined. It is however, interesting to note that the results of Firmin's<sup>36</sup> theory predict a change in lift curve slope of just under 1.5% for this difference in Reynolds number. As noted earlier, the expected differences in lift curve slope due to significant variations in Reynolds number were not found in comparisons of the present data with other measurements. Again, based on Firmin's theory, the difference in lift curve slope between the lowest ( $1 \times 10^6$ ) and highest ( $40 \times 10^6$ ) Reynolds number data would amount to 11% at a Mach number of 0.7. Since all the available data at Reynolds numbers greater than those of the present tests were obtained on models with aspect ratios less than 1.6, the appearance of three-dimensional effects would seem to be a likely cause of the general lack of lift. It would appear that in their quest for the highest possible Reynolds number, model designers have erred towards aspect ratios which are too small to produce truly two-dimensional data.

Comparisons of viscous theory with the corrected results indicate that these theories have reached a stage where they can predict the overall features of the flow over aerofoils at transonic speeds to a high degree of accuracy. There remains, however, a general tendency for all theories to overestimate lift coefficients, the error amounting to some 10% for the best of the theories. This is even true of the method due to Collyer which has the most complete representation of the physics of the situation, including contributions from wake displacement and curvature effects.

Before completing this discussion of the application of classical interference theory, the effect on the quality of the data of testing in wind tunnels equipped with walls of different open area ratios should be considered. As shown previously, the slotted walls used in the present tests, whose open area ratio of 16.5% was selected primarily on the basis of achieving supersonic operation through diffuser suction, require large corrections for blockage, amounting to about -0.015 in Mach number at  $M = 0.8$ . To obtain blockage free conditions, it has been suggested that

much smaller open-area ratios are required, in the range 2 to 4% for slotted walls. However, the open walls of the present tests do have the advantage of requiring small streamline curvature corrections. As the open-area ratio is decreased the value of  $\delta_1$  ( $-0.05$  for the present walls) will decrease to zero, and then increase again (with opposite sign) towards the closed wall value of  $\pi/2$  ( $+0.13$ ). Tunnels in which the walls have been optimized towards blockage free conditions (for example the  $18'' \times 8''$  ARA tunnel, with an open area ratio of 3.2%) appear to suffer from a larger value of  $\delta_1$ , tending towards the closed wall value ( $+0.11$  for the ARA tunnel). If the effects of blockage can be successfully calculated from linear theory, or computed by empirical means within the overall framework of linear theory as has been done here, the absence of blockage-free conditions would seem to be a small price to pay for the minimization of uncorrectable streamline curvature effects. Taking this approach to its logical conclusion would of course result in the use of walls with open-area ratios arranged such that streamline curvature effects did not exist ( $\delta_1 = 0$ ). In general, such walls would not produce blockage free conditions, but this type of approach may lead to better overall accuracy for two-dimensional aerofoil testing at high subsonic speeds.

## 7. CONCLUSIONS

The results of transonic wind tunnel tests on two-dimensional aerofoils have been analysed with respect to the effects of wind tunnel wall interference. These tests were conducted on two geometrically similar models of each of two aerofoil sections—the NACA-0012 and BGK-1 sections—and covered a range in Mach number from 0.5 to 0.82. Model chords differed by a factor of two, giving model chord to tunnel height ratios of 0.25 and 0.125. In order to examine the validity of classical subsonic linearized wall-interference theory without the complications of the doubtful representation of non-solid wall boundary conditions, the results of tests conducted in test sections fitted with both solid and slotted walls were considered. The results have been corrected using the predictions of classical linear theory. For the solid wall tests, these corrections appear to produce results which are very close to being free of the effects of wall interference. In the case of the slotted wall tests, however, linear theory significantly underestimated the degree of blockage evident in the data. Using the form of the variation of blockage with Mach number suggested by linear theory, and an empirical constant derived from the test data, a satisfactory representation of the blockage correction was obtained. This empirical blockage correction was then combined with the variation of lift interference predicted from linear theory, and the crossflow characteristics ( $\beta/P$ ) of the slotted walls were then obtained by comparison of the slotted wall data with the corrected solid wall data (taken as being free of interference). This procedure led to a value of 0.51 for  $\beta/P$ , and values of lift-interference parameters  $\delta_0$  and  $\delta_1$  of  $-0.16$  and  $-0.05$  respectively.

Comparisons between the sets of corrected data, and with data from other sources, indicated that the correction scheme thus derived did indeed produce results which were largely free of wall interference effects. Such comparisons also verified that the simple independent corrections to Mach number and angle of incidence implied by linear theory, do produce results which represent the same flow conditions. The appearance of streamline curvature effects, which invalidate such independent corrections, was limited to the larger chord (203.2 mm) models, and at all times remained small. The implications for future two-dimensional testing in the slotted wall test section are therefore as follows. To avoid any streamline curvature effects, model chords should be somewhat smaller than those of the larger models tested here. To retain ease of manufacture and to allow installation of sufficient pressure orifices to adequately define the surface pressure distribution, a chord of about 150 mm would appear optimum. The application of the semi-empirical correction scheme derived here should then produce results which are free of wind tunnel wall interference.

In comparing the present corrected results with data from other sources, several interesting features were apparent. Firstly, among most modern tests, especially those conducted at higher Reynolds numbers, there appears to be an unfortunate tendency to sacrifice aspect ratio in the search for the highest possible Reynolds number. This has been taken to such an extent that aspect ratios of little more than unity have become the norm. From comparisons of the present data with other experimental measurements it was evident that many of the higher Reynolds number tests did not show the expected higher values of lift curve slope, and it is likely that the

lack of aspect ratio in these tests is the prime cause. Secondly, comparisons with the latest theoretical methods for calculating the viscous flow around an aerofoil at transonic speeds indicated that such theories are now capable of fairly accurate predictions. Major features of pressure distributions are represented quite well, even in areas expected to be sensitive to small changes in flow conditions. There remains, however, a general tendency to overestimate lift coefficients by about 10%.

## REFERENCES

1. Report of Meeting No. 11 of CAARC, held in Australia, 17-26 September 1973. C.C. 721.
2. Moss, G. F. Report on meeting of Co-ordinators in the Field of Aerodynamics, held in India, 24 November to 4 December 1972. C.C. 704, January 1974.
3. Lock, R. C. A proposal for co-operative aerofoil tests in Commonwealth transonic wind tunnels. C.C. 729, March 1975.
4. Bauer, F., Garabedian, P., and Korn, D. G. Supercritical wing sections. (Lecture notes in economics and mathematical systems, Vol. 66.) Springer-Verlag, Berlin, 1972.
5. Kacprzynski, J. J., Ohman, L. H., Garabedian, P. R., and Korn, D. G. Analysis of the flow past a shockless lifting aerofoil in design and off-design conditions. NRC, NAE Report LR-554, 1971.
6. Kacprzynski, J. J. An experimental analysis and buffet investigation of the shockless lifting aerofoil No. 1. NRC, NAE Report LR-569, 1973.
7. Pollock, N., and Fairlie, B. D. An investigation of supercritical aerofoil BGK-1—Part 1: Near design point tests and comparisons with theory. ARL Report A/144, 1975.
8. Pollock, N., and Fairlie, B. D. An investigation of supercritical aerofoil BGK-1—Part 2: Test Reynolds number requirements and transition fixing. ARL Report A/145, 1975.
9. Fairlie, B. D., and Pollock, N. An investigation of supercritical aerofoil BGK-1—Part 3: Extended subsonic and transonic tests. ARL Report A/146, 1975.
10. Pollock, N., and Fairlie, B. D. Transonic wind tunnel tests on a NACA 0012 aerofoil. ARL Report A/148, 1976.
11. Garner, H. C., Rogers, E. W. E., Acum, W. E. A., and Maskell, E. C. Subsonic wind-tunnel wall corrections. AGARDograph 109, 1966.
12. Berndt, S. B., and Sørensen, H. Flow properties of slotted walls for transonic test sections. AGARD CP-174, 1976.
13. Woods, L. C. On the theory of two-dimensional wind tunnels with porous walls. Proc. Roy. Soc. A, 233, 74, 1955.
14. Fairlie, B. D., and Pollock, N. Transonic wind tunnel tests on a series of two-dimensional aerofoils in a solid wall test section. ARL Aero. Note A/384, 1979.
15. Baldwin, B. S., Turner, J. B., and Knechtal, E. D. Wall interference in wind tunnels with slotted and porous boundaries at subsonic speeds. NACA TN 3176, 1954.
16. Wright, R. H. The effectiveness of the transonic wind-tunnel as a device for minimising tunnel-boundary interference for model tests at transonic speeds. AGARD Rept. 294, 1959.
17. Catherall, D. On the evaluation of wall interference in two-dimensional ventilated wind tunnels by subsonic linear theory. RAE TR76134 1976.
18. Pindzola, M., and Lo, C. F. Boundary interference at subsonic speeds in wind tunnels with ventilated walls. AEDC-TR-69-47, 1969.
19. Davis, D. D., and Moore, D. Analytical study of blockage- and lift-interference corrections for slotted tunnels obtained by the substitution of an equivalent homogeneous boundary for the discrete slots. NACA RM L53E07B, 1953.

20. Barnwell, R. W. Improvements in the slotted-wall boundary condition. Proc. AIAA 9th Aero. Testing Conf., Texas, 1976.
21. Chen, C. F., and Mears, J. W. Experimental and theoretical study of mean boundary conditions at perforated and longitudinally slotted wind tunnel walls. AEDC TR-57-20, 1957.
22. Lo, C. H., and Oliver, R. H. Boundary interference in a rectangular wind tunnel with perforated walls. AEDC TR-70-67, 1970.
23. Monti, R. Wall corrections for airplanes with lift in transonic wind tunnel tests. AGARD Advisory Report No. 36, 1971.
24. Pearcey, H. H., Sinnott, C. S., and Osborne, J. Some effects of wind tunnel interference observed in tests on two-dimensional aerofoils at high subsonic and transonic speeds. AGARD Report 296, 1959.
25. Hammond, B. F. L. Results of tests on aerofoil M.81/5 (BGK-1) in the ARA two-dimensional tunnel. ARA Model Test Note M.81/5, 1978.
25. Ramaswamy, M. A., Krishnamurthy, K., and Ramachandra Sharma. Transonic wind tunnel tests on a supercritical aerofoil. NAL TM AE-TM-24-74, 1974.
26. Dixon, R. C. High Reynolds number investigation of an ONERA model of the NACA 0012 airfoil section. NRC LTR-HA-5X5/0069, 1975.
27. Vidal, R. J., Caltin, P. A., and Chudyk, D. W. Two-dimensional subsonic experiments with an NACA-0012 airfoil. Calspan Rept. No. RK-5070-A-3, 1973.
28. Gregory, N., and Wilby, P. G. NPL 9615 and NACA-0012. A comparison of aerodynamic data. ARC CP No. 1261, 1973.
29. Collyer, M. R. An extension to the method of Garabedian and Korn for the calculation of transonic flow past an aerofoil to include the effects of a boundary layer and wake. RAE TR77104, 1977.
30. Bazin, M., Bernard-Guelle, R., and Ponteziere, J. Critique des techniques d'essais de profils transsoniques. Première partie: Dispositif d'essais industriels à S3MA. L'Aéronautique et L'Astronautique, 31, 1971.  
Deuxième partie: Étude expérimentale des corrections de parois à R1 Ch. L'Aéronautique et L'Astronautique, 32, 1971.
31. Murman, E. M., and Cole, J. D. Calculation of plane steady transonic flow. AIAA J, 9, 114-21, 1971.
32. Bauer, F., Garabedian, P. R., Korn, D. G., and Jameson A. Supercritical wing sections II. Lecture Notes in Economics and Mathematical Systems. Springer-Verlag, 1975.
33. Sells, C. C. L. Plane subcritical flow past a lifting aerofoil. Proc. Roy. Soc. A, 308, 377-401, 1968.
34. Bavitz, P. C. An analysis method for two-dimensional transonic viscous flow. NASA TN D-7718, 1975.
35. Bauer, F., and Garabedian, P. R. Computer simulations of shock wave boundary-layer interactions. Comm. Pure and App. Maths, 36, 659-65, 1973.
36. Firmin, M. C. P. Calculation of the pressure distribution, lift and drag on aerofoils at sub-critical conditions. Part I: Interim method. RAE TR72235, 1973.
37. Bailey, F. R. On the computation of two- and three-dimensional steady transonic flows by relaxation methods. Prog. in Num. Fluid Dyn., von Karman Inst. for Fluid Dyn., Lecture Series 63, 1974.
38. Murman, E. M. Analysis of embedded shock waves calculated by relaxation methods. Proc. AIAA Comp. Fluid Dyn. Conf., Palm Springs, 1973.

39. Reed, T. D., Pope, T. C., and Cooksey, J. M. Calibration of transonic and supersonic wind tunnels. NASA-CR-2920, 1977.
40. Parker, R. L. Flow generation properties of five transonic wind tunnel test section wall configurations. AEDC-TR-75-73, 1975.

**DOCUMENT CONTROL DATA SHEET**

Security classification of this page: Unclassified

- |  |  |
|--|--|
| 1. Document Numbers<br>(a) AR Number:<br>AR-001-596<br>(b) Document Series and Number:<br>Aerodynamics Report 151<br>(c) Report Number:<br>ARL-Aero-Report-151 | 2. Security classification<br>(a) Complete document:<br>Unclassified<br>(b) Title in isolation:<br>Unclassified<br>(c) Summary in isolation:<br>Unclassified |
|--|--|

3. Title: EVALUATION OF WALL INTERFERENCE EFFECTS IN A TWO-DIMENSIONAL TRANSONIC WIND TUNNEL BY SUBSONIC LINEAR THEORY

- |   |  |
|---|--|
| 4. Personal Author(s):<br>B. D. Fairlie<br>N. Pollock | 5. Document Date:<br>Written May 1978<br>Published February 1979 |
|---|--|

6. Type of Report and Period Covered:

- |   |   |
|---|---|
| 7. Corporate Author(s):<br>Aeronautical Research Laboratories | 8. Reference Numbers<br>(a) Task:<br>(b) Sponsoring Agency: |
| 9. Cost Code: 54 7710   |   |

- |  |  |
|--|--|
| 10. Imprint:<br>Aeronautical Research Laboratories,<br>Melbourne | 11. Computer Program(s)<br>(Title(s) and language(s)): |
|--|--|

12. Release Limitations (of the document): Approved for public release

12-0. Overseas:	N.O.	P.R.	I	A	B	C	D	E
-----------------	------	------	---	---	---	---	---	---

13. Announcement Limitations (of the information on this page): No limitation

- |  |   |                                   |
|--|---|-----------------------------------|
| 14. Descriptors:<br>Airfoils<br>Transonic flow<br>Two dimensional flow | Linear theory<br>Wind tunnel tests<br>Wall interference | 15. Cosati Codes:<br>2004<br>0103 |
|--|---|-----------------------------------|

16. *ABSTRACT*

*Results of transonic wind tunnel tests on two-dimensional aerofoils are analysed with respect to the effects of wind tunnel wall interference. The tests were conducted on two geometrically similar models of each of two aerofoil sections—the NACA 0012 and the BGK-1 sections—and covered a range of Mach numbers from 0.85 to 0.82 with model chord to tunnel height ratios of 0.125 and 0.25. Results from measurements on all models in both solid- and slotted-wall test sections are corrected for wind tunnel wall interference effects by the application of classical linearized theory. For the solid wall results, these corrections appear to produce data which are very close to being free of the effects of interference. In the case of slotted walls however, linear theory is found to significantly underestimate the magnitude of blockage interference. The introduction of an empirical blockage correction, when combined with the linear theory representation of lift-interference, enables the cross-flow characteristics of the slotted walls to be determined, and leads to a successful correction scheme for the slotted wall results. Extensive comparisons with data from other sources, both experimental and theoretical, provide further verification that the corrected results are indeed closely interference free.*

## DISTRIBUTION LIST

Copy No.

### AUSTRALIA

#### Department of Defence

##### Central Office

Chief Defence Scientist	1
Deputy Chief Defence Scientist	2
Superintendent, Science and Technology Programs	3
Defence Library	4
Joint Intelligence Organization	5
Assistant Secretary, DISB	6-22
Australian Defence Science and Technology Representative (UK)	23
Counsellor, Defence Science (USA)	24

##### Aeronautical Research Laboratories

Chief Superintendent	25
Superintendent, Aerodynamics Division	26
Divisional File, Aerodynamics Division	27
Authors: N. Pollock	28
B. D. Fairlie	29
Transonic Wind Tunnel Group	30-35
Library	36

##### Materials Research Laboratories

Library	37
---------	----

##### Defence Research Centre, Salisbury

Library	38
---------	----

##### Engineering Development Establishment

Library	39
---------	----

##### RAN Research Laboratory

Library	40
---------	----

#### Department of Productivity

##### Government Aircraft Factories

Library	41
---------	----

#### Statutory, State Authorities and Industry

CSIRO Mechanical Engineering Division (Chief)	42
SEC Herman Research Laboratory (Librarian) Victoria	43
Commonwealth Aircraft Corporation (Manager of Engineering)	44
Hawker de Havilland Pty Ltd (Librarian), Bankstown	45
Hawker de Havilland Pty Ltd (Manager), Lidcome	46

#### Universities and Colleges

Adelaide	Barr Smith Library	47
	Professor of Mechanical Engineering	48
Australian National	Library	49
Flinders	Library	50

James Cook	Library	51
La Trobe	Library	52
Melbourne	Engineering Library	53
	Professor of Mechanical Engineering	54
	Professor P. N. Joubert, Mechanical Engineering	55
Monash	Library	56
Newcastle	Library	57
New England	Library	58
New South Wales	Physical Sciences Library	59
	Professor R. A. A. Bryant, Mechanical and Industrial Engineering	60
Queensland	Library	61
Sydney	Professor G. A. Bird, Aeronautical Engineering	62
	Professor J. W. Roderick, Mechanical Engineering	63
	Professor R. I. Tanner, Mechanical Engineering	64
Tasmania	Engineering Library	65
	Professor A. R. Oliver, Civil and Mechanical Engineering	66
Western Australia	Library	67
	Professor Allen-Williams, Mechanical Engineering	68
RMIT	Library	69
	Mr. H. Millicer, Aeronautical Engineering	70
	Mr. Pugh, Mechanical Engineering	71
<b>CANADA</b>		
	NRC National Aeronautics Establishment Library	72
<b>Universities</b>		
	McGill Library	73
	Toronto Institute of Aerophysics	74
<b>FRANCE</b>		
	AGARD Library	75
	ONERA Library	76
	Service de Documentation, Technique de l'Aéronautique	77
<b>GERMANY</b>		
	ZLDI	78
<b>INDIA</b>		
	Defence Ministry, Aero Development Establishment, Library	79
	Hindustan Aeronautics Ltd., Library	80
	Indian Institute of Science, Library	81
	Indian Institute of Technology, Library	82
	National Aeronautical Laboratory (Director)	83
<b>ISRAEL</b>		
	Technion—Israel Institute of Technology (Professor J. Singer)	84
<b>ITALY</b>		
	Associazione Italiana di Aeronautica e Astronautica (Professor A. Evla)	85
<b>JAPAN</b>		
	National Aerospace Laboratory, Library	86
<b>Universities</b>		
	Tohoku (Sendai) Library	87
	Tokyo Institute of Space and Aerospace	88

**NETHERLANDS**

- Central Organization for Applied Science Research in the Netherlands TNO, Library 89  
National Aerospace Laboratory (NLR), Library 90

**NEW ZEALAND**

- Air Department, RNZAF Aero Documents Section 91

**Universities**

- Canterbury Library 92  
Professor D. Stevenson, Mechanical Engineering 93  
Mr. F. Fahy, Mechanical Engineering 94  
Mr. J. Stott, Chemical Engineering 95

**SWEDEN**

- Aeronautical Research Institute 96  
Chalmers Institute of Technology, Library 97  
Kungl. Tekniska Hogskolens 98  
SAAB, Library 99

**SWITZERLAND**

- Institute of Aerodynamics (Professor J. Ackeret) 100

**UNITED KINGDOM**

- Aeronautical Research Council, NPL (Secretary) 101  
CAARC NPL (Secretary) 102  
Royal Aircraft Establishment Library, Farnborough 103  
Dr. R. C. Lock, RAE, Farnborough 104  
Royal Aircraft Establishment Library, Bedford 105  
National Physical Laboratories Aero Division (Superintendent) 106  
British Library, Science Reference Library 107  
British Library, Lending Division 108  
Engineering Sciences Data Unit Ltd. (Mr. R. H. Blockley) 109  
Aircraft Research Association Library 110  
Science Museum Library 112  
Hawker Siddeley Aviation Ltd., Brough 113  
Hawker Siddeley Aviation Ltd., Greengate 114  
Hawker Siddeley Aviation Ltd., Kingston-upon-Thames 115  
Hawker Siddeley Dynamics Ltd., Hatfield 116  
British Aircraft Corporation (Holdings) Ltd., Commercial Aviation Division 117  
British Aircraft Corporation (Holdings) Ltd., Military Aircraft Division 118  
British Hovercraft Corporation Ltd. (East Cowes) 119  
Short Brothers 120  
Westland Helicopters Ltd. 121

**Universities and Colleges**

- Bristol Library, Engineering Department 122  
Professor L. Howarth, Engineering Department 123  
Cambridge Library, Engineering Department 124  
Liverpool Professor J. H. Preston, Fluid Mechanics Department 125  
London Professor A. D. Young, Queen's College 126  
Nottingham Library 127  
Southampton Library 128  
Strathclyde Library 129  
Cranfield Institute of Technology Library 130  
Imperial College Professor of Mechanical Engineering 131  
Mr. P. Bradshaw, Department of Aeronautics 132

**UNITED STATES OF AMERICA**

NASA Scientific and Technical Information Facility	133
Sandia Group (Research Organization)	134
American Institute of Aeronautics and Astronautics	135
Applied Mechanics Review	136
Chemical Abstracts	137
The John Crerar Library	138
United Technologies Corporation, Fluid Dynamics Laboratories	139
Battelle Memorial Institute, Library	140
Calspan Corporation	141

**Universities and Colleges**

California	Dr. M. Holt, Department of Aero Sciences	142
Cornell	Library	143
Florida	Mark H. Clarkson, Department of Aeronautical Engineering	144
Harvard	Professor A. F. Carrier, Division of Engineering and Applied Mathematics	145
Johns Hopkins	Professor S. Corrsin, Department of Mechanical Engineering	146
Stanford	Library, Department of Aeronautics	147
Wisconsin	Memorial Library, Serials Department	148
Brooklyn Institute of Polytechnology	Library, Aeronautical Laboratories	149
California Institute of Technology	Library, Guggenheim Aeronautical Laboratories	150
Massachusetts Institute of Technology	Library	151

Spares

152-161